The Canadian Journal of Chemical Engineering

formerly

CANADIAN JOURNAL OF TECHNOLOGY

THE UNIVERSITY OF MICHIGAN
OCT 1
ENGINEERING LIBRARY

CONTENTS

Evaporation of Stationary Droplets in High Temperature Surroundings — *T. W. Hoffman, W. H. Gauvin* — **129**

Pressure Drop of Single Phase Flow Through Raschig Ring Type Tower Packings: Effect of Hole Size — *Liang-tseng Fan* — **138**

Fundamental Aspects of Solids-Gas Flow Part IV: The Effects of Particle Rotation, Roughness and Shape — *L. B. Torobin, W. H. Gauvin* — **142**

Graphical-Numerical Determination of Variable Diffusion Coefficient in Solids — *Raymond C. Hall* — **154**

Concentration Distribution in Two-Phase Pipe Flow — *S. L. Soo, J. A. Regalbuto* — **160**

Industrial Section

The Corrosion Behavior of Aluminum in Natural Waters — *Hugh P. Godard* — **167**

Published by
THE CHEMICAL INSTITUTE OF CANADA
OTTAWA CANADA

Photograph taken at C-I-L Central Research Laboratory, McMasterville, Que.

Plastics Detective

This photograph shows the High Shear Viscometer, designed and built at our Central Research Laboratory, used to investigate factors involved in complex flow behaviour of molten thermo-plastics during commercial processing.

Information on this newly developed pressure-driven capillary Viscometer has been made available to industry by C-I-L, and many industrial laboratories in the United States, England, India and Australia have built identical machines.

Such C-I-L research contributes to higher standards of performance in the plastics industry, to new and better plastics products and—through better technical service—to greater success in the application of these new materials to modern living.

C-I-L **CANADIAN INDUSTRIES LIMITED**

Serving Canadians Through Chemistry

Agricultural Chemicals • Ammunition • Coated Fabrics — Industrial Chemicals • Commercial Explosives • Paints • Plastics • Textile Fibres

The Canadian Journal of Chemical Engineering

formerly

Canadian Journal of Technology

Published by The Chemical Institute of Canada

VOLUME 38 | OCTOBER, 1960 | NUMBER 5

Editor
A. Cholette
Faculty of Science, Laval University
Quebec, Que.

Managing Editor
T. H. G. Michael

Publishing Editor
D. W. Emmerson

Assistant Publishing Editors
R. G. Watson
R. N. Callaghan

Circulation Manager
M. M. Lockey

EDITORIAL BOARD

Chairman
W. M. CAMPBELL, Atomic Energy of Canada Limited, Chalk River, Ont.

P. W. BLAYLOCK, Shawinigan Chemicals Limited, Montreal, Que.

L. D. DOUGAN, Polymer Corp. Limited, Sarnia, Ont.

F. A. FORWARD, University of British Columbia, Vancouver, B.C.

J. W. HODGINS, McMaster University, Hamilton, Ont.

A. I. JOHNSON, University of Toronto, Toronto, Ont.

LEO MARION, National Research Council, Ottawa, Ont.

R. R. McLAUGHLIN, University of Toronto, Toronto, Ont.

G. L. OSBERG, National Research Council, Ottawa, Ont.

A. C. PLEWES, Queen's University, Kingston, Ont.

J. H. SHIPLEY, Canadian Industries Limited, Montreal, Que.

H. R. L. STREIGHT, Du Pont of Canada Limited, Montreal, Que.

EX-OFFICIO

W. N. HALL, President, The Chemical Institute of Canada.

A. A. SHEPPARD, Chairman of the Board of Directors.

B. A. B. CLARK, Director of Publications.

Authorized as second class mail, Post Office Department, Ottawa. Printed in Canada

Manuscripts for publication should be submitted to the Editor: Dr. A. Cholette, Faculty of Science, Laval University, Boulevard de l'Entente, Quebec, Que. (Instructions to authors are on the next page).

Editorial, Production and Circulation Offices: 48 Rideau Street, Ottawa 2, Ont.

Advertising Office: C. N. McCuaig, manager of advertising sales, *The Canadian Journal of Chemical Engineering*, Room 601, 217 Bay Street, Toronto, Ont. Telephone—EMpire 3-3871.

Plates and Advertising Copy: Send to *The Canadian Journal of Chemical Engineering*, 48 Rideau Street, Ottawa 2, Ont.

Subscription Rates: In Canada—$6.00 per year and $1.25 per single copy; U.S. and U.K.—$7.00, Foreign—$7.50.

Change of Address: Advise Circulation Department in advance of change of address, providing old as well as new address. Enclose address label if possible.

The Canadian Journal of Chemical Engineering is published by The Chemical Institute of Canada every two months.

Unless it is specifically stated to the contrary, the Institute assumes no responsibility for the statements and opinions expressed in *The Canadian Journal of Chemical Engineering*. Views expressed in the editorials do not necessarily represent the official position of the Institute.

The Canadian Journal of Chemical Engineering

INSTRUCTIONS TO AUTHORS

Manuscript Requirements for Articles

1. The manuscript should be in English or French.
2. The original and two copies of the manuscript should be supplied. These are to be on 8½ x 11 inch sheets, typewritten, and double spaced. Each page should be numbered.
3. Symbols should conform to American Standards Association. An abridged set of acceptable symbols is found in the third edition of Perry's Chemical Engineers' Handbook. Greek letters and subscripts and superscripts should be carefully made.
4. Abstracts of not more than 200 words in English indicating the scope of the work and the principal findings should accompany all technical papers.
5. References should be listed in the order in which they occur in the paper, after the text, using the form shown here: "Othmer, D. F., Jacobs, Jr., J. J., and Levy, J. F., Ind. Eng. Chem. **34**, 286 (1942). Abbreviations of journal names should conform to the "List of Periodicals Abstracted by Chemical Abstracts". Abbreviations of the common journals are to be found in Perry's Handbook also. All references should be carefully checked with the original article.
6. Tables should be numbered in Arabic numerals. They should have brief descriptive titles and should be appended to the paper. Column headings should be brief. Tables should contain a minimum of descriptive material.
7. All figures should be numbered from 1 up, in Arabic numerals. Drawings should be carefully made with India ink on white drawing paper or tracing linen. All lines should be of sufficient thickness to reproduce well, especially if the figure is to be reduced. Letters and numerals should be carefully and neatly made, with a stencil. Generally speaking, originals should not be more than twice the size of the desired reproduction; final engravings being 3¼ in. or 7 in. wide depending on whether one column or two is used.
8. Photographs should be made on glossy paper with strong contrasts. Photographs or groups of photographs should not be larger than three times the size of the desired reproduction.
9. All tables and figures should be referred to in the text.

Submission of Manuscripts

1. The three copies of the manuscript, including figures and tables, should be sent directly to:
   DR. A. CHOLETTE, editor,
   The Canadian Journal of Chemical Engineering,
   Faculty of Science, Laval University,
   Boulevard de l'Entente,
   Quebec, Que.
2. The authors addresses and titles should be submitted with the manuscript.
3. The author may suggest names of reviewers for his article, but the selection of the reviewers will be the responsibility of the editor. Each paper or article is to be reviewed by two chemical engineers familiar with the topic. Reviewers will remain anonymous.
4. All correspondence regarding reviews should be directed to the editor.

Reprints

1. At least 50 free "tear sheets" of each paper will be supplied.
2. Additional reprints may be purchased at cost. An estimated cost of reprints, with an attached order form, will be sent to the author with the galley proofs.
3. Orders for reprints must be made before the paper has appeared in the Journal.

Communications, Letters and Notes to the Editor

Short papers, as described below, will be considered for publication in this Journal. Their total length should not exceed 600 words, or its equivalent.

Communications

A communication is a prompt preliminary report of observations made which are judged to be sufficiently important to warrant expedited publication. It usually calls for a more expanded paper in which the original matter is republished with more details.

Letters

A letter consists of comments or remarks submitted by readers or authors in connection with previously published material. It may deal with various forms of discussion arising out of a publication or it may simply report and correct inadvertent errors.

Notes

A note is a short paper which describes a piece of work not sufficiently important or complete to make it worth a full article. It may refer to a study or piece of research which, while it is not finished and may not be finished, offers interesting aspects or facts. As in the case of an article a note is a final publication.

* * *

Evaporation of Stationary Droplets in High Temperature Surroundings[1]

T. W. HOFFMAN[2] and W. H. GAUVIN[3]

An experimental study of the rate of evaporation of stationary droplets of water, methanol, cumene, pentane and benzene was carried out in an electrically-heated 9-inch stainless steel sphere. The gaseous environment consisted of the superheated vapor of the liquid under investigation and, in all cases, the wall and gas temperatures were the same. Drop diameters ranged from 0.4 to 1.4 mm., and temperatures from 100°C. to 550°C.

The evaporation rate of stationary droplets in high temperature surroundings does not appear to be governed by the rate of heat transfer by natural convection, since no dependency of the Nusselt Number on the Grashof Number was found. Attempts to correlate the results on the basis of Godsave's model (conduction across the boundary layer controlling) or Spalding's modified approach to the latter were equally unsuccessful. The experimental evaporation rates could, however, be very satisfactorily correlated in terms of Spalding's Transfer Number B.

The correlation obtained indicates that the mechanism of the evaporation process is governed by the effect of the evolved vapors on the boundary layer flow.

On a fait une étude expérimentale du taux d'évaporation de gouttelettes stationnaires d'eau, de méthanol, de cuméne, de pentane et de benzène dans une sphère d'acier inoxydable de 9″ chauffée à l'électricité. L'enveloppe gazeuse autour des gouttelettes consistait en vapeur surchauffée du liquide étudié; les températures de la paroi et du gaz étaient les mêmes dans tous les cas. Les diamètres des gouttes ont varié de 0.4 à 1.4 mm, et les températures de 100°C à 550°C.

Il ne semble pas que le taux d'évaporation de gouttelettes stationnaires dans un milieu à haute température soit régi par le taux de transport de chaleur par convection naturelle puisque le nombre de Nusselt ne dépend aucunement du nombre de Grashof. Il a été impossible également d'établir une corrélation entre les résultats, en utilisant soit le modèle de Godsave (où la conduction à travers la couche limite est le facteur principal) ou même l'approche modifiée proposée par Spalding. Les auteurs ont obtenu cependant une bonne corrélation des taux d'évaporation expérimentaux en se servant du nombre de transport de Spalding, B.

On obtient une corrélation indiquant que le mécanisme de l'évaporation est contrôlé par l'effet des vapeurs produites sur l'écoulement à l'intérieur de la couche limite.

The evaporation of liquid droplets in high temperature surroundings is important in an increasing number of processes involving the use of sprays, such as cyclone evaporation, spray drying, liquid fuel combustion and in operations carried out by the Atomized Suspension Technique.

The mass transfer from liquid and solid spheres has been extensively investigated in studies which, in the main, fall into two broad classes:

(1) mass transfer from stationary liquid droplets in an atmosphere, the temperature of which is only moderately higher than that of the droplet[1,2,3,4,5].

(2) mass transfer from liquid and solid spheres in a velocity field, i.e. under forced convection conditions[6,7,8,9,10,11,12].

Most of these investigations were concerned with low transfer rates. Recently, a marked interest has developed in the burning of small liquid droplets[13,14,15,16,17,18,19,20], in which it has been shown that the combustion rate depends on the rate of evaporation of the droplets.

Theoretical calculation of the rate of heat transfer by conduction to a sphere immersed in an infinite stagnant fluid environment predicts that the Nusselt number, (hD/k_f), should be equal to 2.0. When a temperature difference exists between the sphere and the fluid, natural convection effects arise by virtue of the varying buoyancy forces around the body, and the heat transfer rate is increased accordingly. Moreover, any forced motion of the fluid past the sphere further increases the Nusselt number above the minimum value.

In an analysis of the convective heat transfer problem, the usual procedure[21,22] is to consider the equations which govern the transfer of momentum, heat and mass in the boundary layer. These equations, known as the Prandtl boundary layer equations, point to the essential feature of free convection systems, in that the distribution of temperature and velocity are interdependent. In such systems, the velocity of the fluid is due entirely to the action of buoyancy forces arising from variations in density or temperature. The non-linearity of the equations has made direct solution of the temperature and velocity fields impossible. It is

[1]*Manuscript received January 7; accepted April 27, 1960.*
[2]*Present address: Department of Chemical Engineering, McMaster University, Hamilton, Ont.*
[3]*Department of Chemical Engineering, McGill University and Pulp and Paper Research Institute of Canada, Montreal, Que.*
Based on a paper presented to the C.I.C. Chemical Engineering Conference, Hamilton, Ont., November 8-11, 1959.

important to realize that the velocity and temperature gradients in the boundary layer are modified as soon as relative motion between the body and the surrounding fluid is established.

Although mathematically intractable, the boundary layer equations have been used to derive the dynamic similarity relationships existing between two different systems and have thereby allowed a prediction of the dimensionless groups associated with these problems[22,23].

Ranz and Marshall[9] made an extensive study of the rate of heat and mass transfer from stationary liquid drops under forced convection, and proposed the following correlations:

$$Nu = 2.0 + 0.60\,(\mathrm{Re})^{1/2}\,(\mathrm{Pr})^{1/3} \quad \ldots\ldots(1)$$

$$Nu' = 2.0 + 0.60\,(\mathrm{Re})^{1/2}\,(\mathrm{Sc})^{1/3} \quad \ldots\ldots(2)$$

In his classic paper, Froessling[6] presented an approximate solution for the Navier-Stokes equations which gave an expression for Nu′ of identical form, but with a coefficient of 0.552, instead of 0.600. From dynamic similarity reasoning, Ranz and Marshall extended these correlations to include the natural convection case:

$$Nu = 2.0 + 0.60\,(\mathrm{Gr})^{1/4}\,(\mathrm{Pr})^{1/3} \quad \ldots\ldots(3)$$

$$Nu' = 2.0 + 0.60\,(\mathrm{Gr})^{1/4}\,(\mathrm{Sc})^{1/3} \quad \ldots\ldots(4)$$

Inherent in the derivation of Equations (3) and (4) is the assumption that material transfer did not affect the natural convection phenomena; these two equations have so far received little experimental confirmation.

Mathers et al[21] assumed that the velocity normal to the surface was zero and neglected the inertia terms in the Navier-Stokes equations. They then proceeded to solve the four boundary layer equations on an analogue computer and thereby showed that mass transfer augmented the density gradients around a body. Their experimental work with spheres at very low mass transfer rates provided excellent experimental evidence for their calculations.

Clearly, the analysis of the effect of mass transfer on the hydrodynamic flow pattern around an evaporating droplet is probably more complex than Ackermann's simple treatment would suggest[24]. For the case of appreciable mass transfer in a free convection field, the velocity normal to the surface may be of the same magnitude as the fluid velocity in the boundary layer. The momentum associated with this mass will have to be taken into account when one attempts a solution of the momentum equation. This suggests that an additional boundary condition:

$$\rho_g v_w = D_v \frac{dc}{dy} \qquad \text{at } y = o \quad \ldots\ldots(5)$$

must be considered.

To circumvent some of the mathematical difficulties associated with the differential equation, velocity, concentration and temperature profiles in the boundary layer have been approximated by various polynomial expansions in terms of the boundary layer thickness[23,25,26], thus permitting integration of the equations, typical of which are the integral forms presented by Schlichting[23]. In analyzing the simultaneous heat and mass transfer from a vertical wall with free convection, Spalding[27] and Somers[26] followed this procedure and considered Equation (5) as one of the boundary conditions. Spalding's *a priori* solutions show that the boundary layer becomes thicker as greater mass transfer occurs, thereby reducing the rate of heat transfer from the surface.

Spalding[27] also pointed out that most analyses of convective heat transfer assume that:

$$1 - \frac{T_\infty}{T} = \frac{T}{T_\infty} - 1 \quad \ldots\ldots(6)$$

and are therefore applicable only to those cases where $(T_\infty - T)$ is small. This assumption may lead to an over-estimation of the buoyancy forces when the temperature differences are large. In his own analysis, he considered the buoyancy forces to be at a maximum throughout the boundary layer (i.e. $\triangle T/T_\infty = 1$), although this force ranges from zero at the outer edge of the boundary layer to its highest value at the transfer surface.

Godsave[15], in his treatment of the rate of combustion of fuel drops, has shown that, at high evaporation rates, the relatively cold vapors leaving the drop can seriously reduce the heat transfer rate at the drop surface. This same analysis has been extended or presented in a slightly different form by Goldsmith and Penner[16], Marshall[28], Ranz[29], Sleicher and Churchill[30] and Spalding[31]. Starting with the diffusion equation obtained from a material balance on the diffusing component[28] and assuming radial flow of vapor only (convection effects are considered negligible), the evaporation rate $(dm/d\theta)$ can be predicted from the expression:

$$(dm/d\theta) = ln\,(1 + c_p\Delta T/\lambda') \,/\, (c_p/4\pi k_f)\,(1/r_d - 1/r_b) \quad \ldots\ldots(7)$$

where $$\lambda' = \lambda - [q_R/(dm/d\theta)]$$

and r_b is the effective radius of the so-called stagnant film surrounding the drop. This analysis ignores convection effects and attributes all transfer to conduction, much in the same way as Langmuir[32] did in his pioneer work on this subject. Convection is considered only to reduce r_b.

From this equation, the effect of evaporation rate on heat transfer to droplets is shown to depend on the magnitude of Spalding's Transfer Number $B' = (c_p\triangle T/\lambda')$. In this analysis, subject to the above limitations, it is shown that the true Nusselt number Nu_T, for pure heat transfer (that is, in the absence of evaporation), should be modified to yield the actual Nusselt number, Nu_A, for the case of simultaneous heat and mass transfer, as follows:

$$Nu_A/Nu_T = E(1/r_d - 1/r_b)/(e^{E(1/r_d - 1/r_b)} - 1) \quad \ldots\ldots(8)$$

where $E = (dm/d\theta)\,c_p/4\pi k_f$

By combining Equations (7) and (8):

$$Nu_A = \frac{ln\,(1 + B')}{B'}\,Nu_T \quad \ldots\ldots(9)$$

and the actual Nusselt number yields the actual rate of heat transfer that is available for evaporation at the droplet surface. Equation (9) has not been experimentally verified and the problem of selecting a proper temperature at which to evaluate the gas properties remains unsolved.

The purpose of the present study was to investigate some of the problems associated with the simultaneous transfer of heat and mass at high temperatures.

EXPERIMENTAL

Equipment

The present investigation involved measurement of the evaporation rates of liquid droplets (0.4 to 1.4-mm. in diameter) suspended on thin glass fibres at the centre of a heated 9-in. I.D. stainless steel sphere with a 3/8-in. wall. The sphere, shown in Figures 1 and 2 was made up of two hemispheres and was designed to operate at temperatures up to 1500°F. and pressures up to 10 atmospheres.

The drop-injection and holder assembly, shown in Figure 1 and 2, was fitted into a 1 1/2-in. diameter port at the top of the sphere. The blanked-off end of a 1/2-in. tube was drilled to make a centered 1/16-in. diameter hole, through which the hypodermic needle feed system could be inserted. Guides were provided in the 1/2-in. tube, so that the hypodermic needle could be quickly inserted or removed. For atmospheric pressure operation, a slip seal was provided at the outermost point to prevent the entry of outside air.

A fine glass filament, approximately 70 microns in diameter, was secured to the bottom of the 1/2-in. tube, so that its end was in line with the 1/16-in. diameter hole and at a distance of

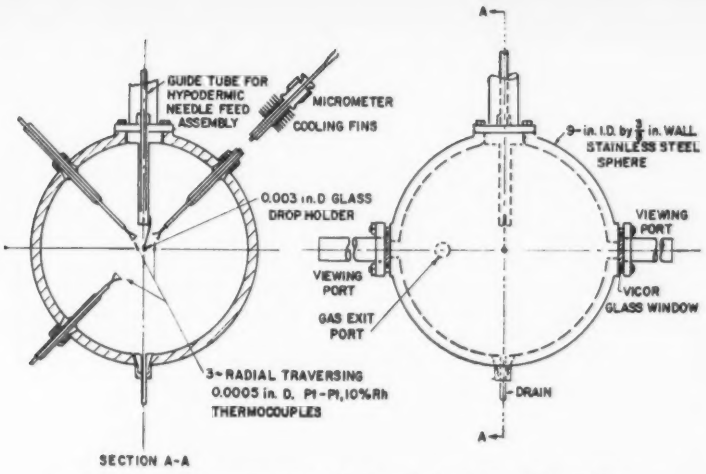

Figure 1—Diagrammatic sketch of the 9-in. I.D. sphere assembly.

approximately 3/4-in. below it. A very small ball (diameter approximately 200 to 250 microns) made up of a 3/8-in. length of 0.0005-in. platinum, 10% rhodium wire, was fused to the end of the glass fibre to provide the necessary surface area to hold the droplet. When holding a drop, this ball was located in the uppermost part of the drop. No measurements of drop diameter were made when the drop diameter was less than twice the size of the ball.

Three 0.0005-in. platinum-platinum, 10% rhodium thermocouples were provided for measuring droplet and gas temperatures. The 0.0005-in. wires were fused to 0.005-in. diameter wire of the same material, which in turn were insulated by enclosing them in small glass tubes. These lead wires were conducted out of the sphere through a 1/8-in. diameter, thin-walled stainless steel tube, and this complete assembly was inserted into another fixed 5/16-in. tube (Figure 1). The thermocouples could be moved by a screwed micrometer arrangement remote from the sphere, so that the thermocouple could traverse the gas atmosphere surrounding the drop or be inserted into the drop itself. One micrometer had a large pitch thread, so that it could be moved quickly in and out of the drop. The wall temperature of the sphere was measured by three chromel-alumel thermocouples welded to the outside surface.

The sphere assembly was housed in a 16-in. × 16-in. × 12-in. deep stainless steel box, the inside surface of which was equipped with nichrome wire heaters. The power to each of the two separate electrical heater circuits in the top and bottom of the box was controlled by Powerstat transformers. The final temperature control was effected by a Minneapolis-Honeywell Pyrovane proportional controller. The whole assembly was insulated with 6 inches of vermiculite.

The details of the optical bench and photography set-up are shown in Figure 2. It consisted of a telescope, a light-splitter and a variable speed Bolex motion picture camera. Shadow photographs of the evaporating droplets were obtained by projecting a low power light from the side opposite to the camera. For the lower temperature runs, a 35-mm. camera was used, and in both cases the camera lens was removed. The 16-mm. and 35-mm. cameras gave a magnification of approximately 1.5x and 3x respectively.

Procedure

The complete apparatus was maintained at the desired temperature for about two hours prior to a run. During this time adjustments were made to the heater circuits, so that uniform temperature conditions existed in all parts of the sphere. The sphere was then purged of the entrapped air by injecting approximately 75-cc. of the liquid under study. About half an hour was

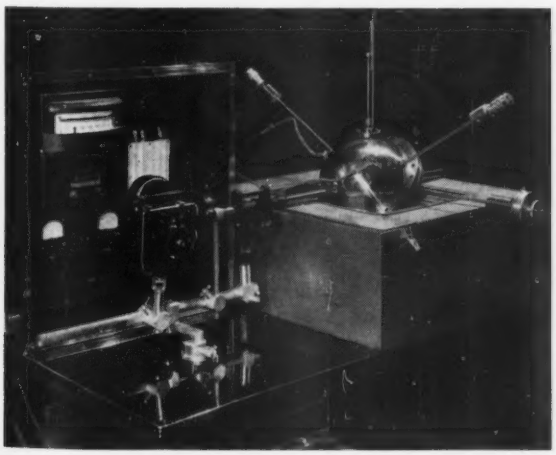

Figure 2—Photograph showing the entire experimental apparatus, without the upper heater box and insulation.

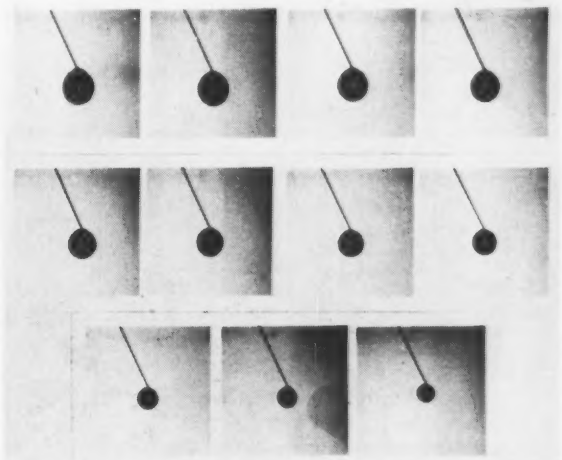

Figure 3—A sequence of photographs in the evaporation of a water droplet showing the relative sphericity at various drop sizes.

allowed for the temperature to reach steady conditions, at which time all gas thermocouples registered the same temperature as the wall.

The hypodermic needle was inserted to a position such that when a drop was formed at the tip, the latter contained the end of the drop holder. The generation of vapor in the feed tube caused the drop to increase slowly in size, until it separated from the needle. The drop usually remained on the drop holder. The needle was then removed and the camera started immediately. Some difficulty was experienced with this technique at the highest temperatures, in which case, after two drops had failed to be retained by the holder, the system was allowed to equilibrate before proceeding again. Before evaporation measurements were made, a drop was placed on the holder and its temperature recorded. If this temperature was more than 0.5°C. below the boiling point, the system was purged again. In most cases, the temperature was within 0.1°C. of the boiling point, and at the highest temperature (~ 600°C.) any slight increase in temperature above the boiling point could not be detected.

Prior to heating the apparatus, the actual magnification on the film was measured by photographing an accurately measured 1.6500-mm. stainless steel hypodermic needle inserted through the injection hole. The camera speed was measured by photographing an electric clock which was equipped with a sweep second hand.

The photographic negatives were mounted on glass microscope slides and the droplet diameter was measured on a Nikon Shadowgraph projection microscope, with an additional magnification of 50x. The larger droplets were slightly elliptical in shape (eccentricity $(a/b) = 1.08$ max.); they were therefore treated as prolate ellipsoids. The diameter of the sphere equal to the volume of this ellipsoid is given by:

$$D = (ab^2)^{1/3} \quad \ldots\ldots\ldots\ldots\ldots\ldots\ldots\ldots (10)$$

With these small eccentricities, this diameter is essentially the same as that of a sphere with the same surface area as the droplet. A sequence of droplet photos shown in Figure 3 indicates the high degree of sphericity of the droplets over the range of diameters measured.

Some experiments were performed with the thermocouple at a fixed position in the boundary layer surrounding the drop. This temperature was observed to increase as the droplet decreased in size. Since these measurements indicated a very thin boundary layer thickness (ca. three times the drop radius), very large temperature gradients existed near the drop. Even with these fine wires, therefore, considerable heat must have been conducted along the wires to the thermocouple weld. Moreover, since the wires extended through an unknown temperature field, correction of the observed temperature could not be made; these observations were therefore considered as approximate only.

Materials Investigated

Essentially pure water was obtained by passing once-distilled water through an ion exchange column. Benzene, cumene, methyl alcohol and n-pentane were also studied; all four liquids were spectroscopic grade supplied by Eastman Kodak Co.; they were kept under desiccant when not in use. It was found necessary to remove most of the dissolved gases from the liquid under test prior to a run, to remove the possibility of internal boiling during the evaporation studies. Simpson[33] has shown that internal boiling can result through focussing of radiation inside the droplet by refraction effects.

The use of a one-component system alleviated some of the difficulties associated with choosing correct properties of the vapor phase surrounding the drop. The liquid density and boiling point data were obtained from International Critical Tables[34]. The vapor properties at the higher temperatures presented a more serious problem. Only the properties of steam have been measured with any precision by Keyes[35]. The thermal conductivity data for the organic vapors were obtained by extrapolating the data reported by Vines[36] and Vines and Bennett[37] on a log-log plot. The specific heat data of Montgomery and De Vries[38] and De Vries and Collins[39] for benzene and methanol respectively were used in the extrapolation to the required higher temperatures.

Results

It was found that the experimental data could be represented by straight lines on a plot of (diameter)^2-versus-time. A typical plot (for water at high temperatures) is shown in Figure 4. For water droplets above 500°C., a slight decrease in slope was observed (less than 6% from an initial drop diameter of 1.40-mm. to a final diameter of 0.50-mm.). At any one temperature, at least three measurements of evaporation rate were made at any given time. Some of these observations were repeated with different drop holders. The measurements indicated that data were reproducible to ± 5% and in most cases complete reproducibility was obtained.

The evaporation rate at any drop size was found from the slope of the D^2-versus-θ plot, by means of the relationship:

$$(dm/d\theta) = (\pi/6)\rho_L [d(D)^3/d\theta] = (\pi/4)\rho_L D [d(D)^2/d\theta] \quad \ldots\ldots (11)$$

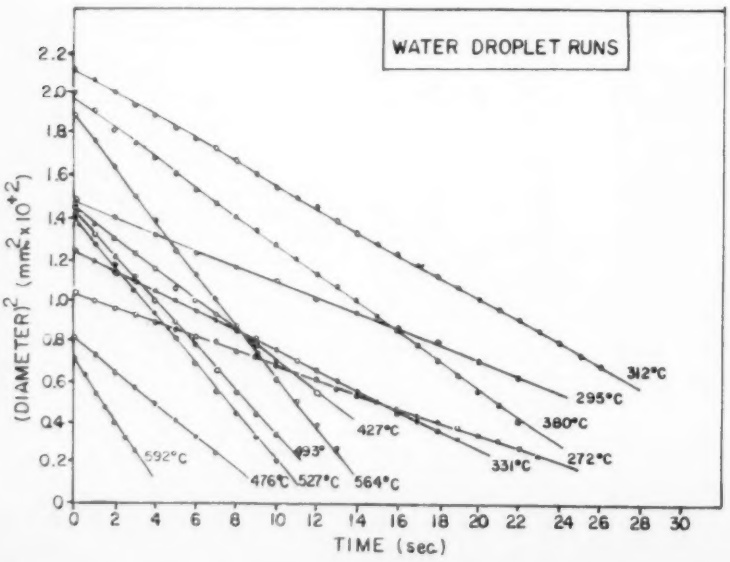

Figure 4—Measured variation of (diameter)^2 with time, for water droplets at high temperatures.

The evaporation rate data for 0.70-mm. and 1.0-mm. diameter drops are given in Table 1* and the results for water are plotted in Figure 5. The data of Kobayasi[17] and Nishiwaki[20] for water droplets evaporating in a high temperature air environment are shown by the broken-line curves.

Treatment and Discussion of Data

The total interfacial heat flux from the gas to the droplet can be determined from the following energy balance:

$$\lambda\,(dm/d\theta) - q_R - q_k = k_f\,A\,(dT/dr)_s = h_A\,A\Delta T \quad \ldots\ldots\ldots\ldots (12)$$

The heat conducted along the support-rod cannot be calculated to any degree of accuracy. As a result of the small thermal conductivity and small diameter of the glass fibre, the heat conducted into the drop through the holder will be very small. An approximate calculation, similar to that used for conduction along thermometer wells[40] showed this heat flux to be less than 2% of the total evaporative heat requirements at the worst condition. It was therefore ignored.

Since in this work the droplets were suspended in a gaseous atmosphere which was at the same temperature as that of the walls, some of the thermal radiation emitted by the gas was absorbed in the relatively colder boundary layer. An estimate of the magnitude of this absorption (by means of a method which will be discussed in a subsequent paper) showed it to be very small. Therefore the thermal radiation received by the droplet will be essentially the same as that which it would receive if it were in a non-absorbing medium. Since the area of the radiating surfaces surrounding the droplet is very much larger than that of the droplet itself, data on the emissivities of these surfaces are not required. Hence the radiation absorbed by the droplet is given by:

$$q_R = \alpha_p \sigma A (T_w^4 - T_d^4) \quad \ldots\ldots\ldots\ldots\ldots\ldots (13)$$

Absorptivity or complete spectral transmissivity data for the various liquids were not available at the time of this study. The method for determining the absorptivity of a droplet has been discussed elsewhere[33,41], and can be shown to depend on drop size and source temperature.

Water is decidedly opaque to thermal radiation and an absorptivity as high as 0.95 has been reported[42]. The measurements of Brown[43] on water films 0.05-mm. thick indicated slightly lower values. Use of an absorptivity equal to 0.90 for all temperatures and drop sizes will therefore not lead to appreciable error. A realistic absorptivity could not be assigned to the organic liquid droplets and therefore all these results were calculated twice, on the basis of $\alpha_p = 0$ and 1.0 respectively, to show the effect of this parameter.

From Equation (12):

$$Nu_A = h_A D/k_f = (dm/d\theta)\,(c_p)/(\pi D k_f B') \quad \ldots\ldots\ldots\ldots (14)$$

where

$$B' = (c_p \Delta T)/[\lambda - q_R/(dm/d\theta)] \quad \ldots\ldots\ldots\ldots (15)$$

Combining Equations (9) and (14):

$$Nu_T = (dm/d\theta)\,(c_p)/(\pi D k_f)\,ln\,(1 + B') \quad \ldots\ldots\ldots\ldots (16)$$

Thus the Nusselt numbers were calculated directly from the experimental data. The gas properties were evaluated at the average film temperature.

It is interesting to note that, since, for a given liquid and at a given temperature:

$$d(D)^2/d\theta = \text{constant},$$

the evaporative rate is directly proportional to the droplet diameter, as Equation (11) shows. However, the Nusselt number for heat transfer by natural convection is known to depend on (Gr)^n, where Ranz and Marshall[9] suggest $n = 0.25$, as in Equation (3) while Kyte et al [44] report $n = 0.37$. One would therefore expect the evaporation rate under these conditions to be a function of D^{3n+1}. However, the observations of this study imply that $n = 0$; this non-dependence on the Grashof number becomes immediately obvious if one attempts to plot the Nusselt number (true or actual) against the Grashof number.

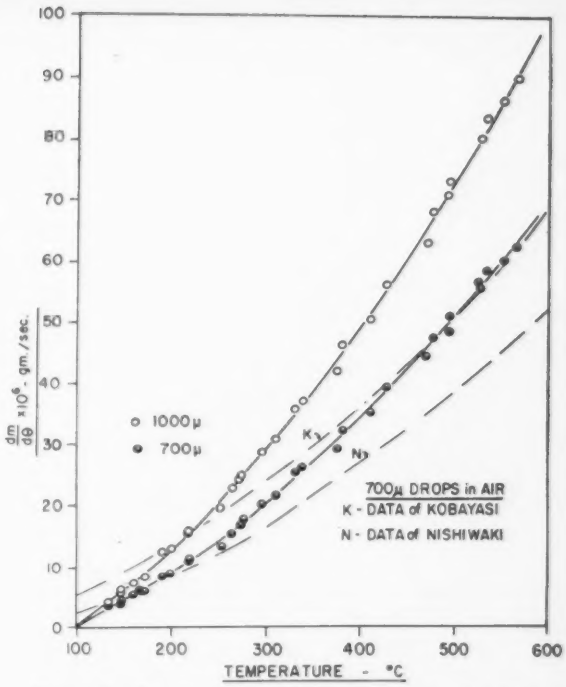

Figure 5—Evaporation rate data for water droplets.

The use of $[(T_\infty - T_d)/T_\infty]^*$ in the Grashof number may not satisfactorily account for the buoyancy forces at these temperatures. This ratio was therefore set equal to unity throughout the boundary layer when the values of Gr were calculated, in accordance with the suggestion of Spalding[31].

An attempt to correlate the experimental results by means of Spalding's method[31] is shown in Figure 6. These plots show that a straight line satisfactorily represents the data for each liquid investigated at any chosen value of droplet absorptivity. Since the lines are nearly parallel, one is tempted to try to bring all the data together through the use of an appropriate exponent on the Temperature Number. However, the data at other drop diameters would then not correlate with these results, since the ordinate is a function of $D^{-0.75}$, and the abscissa contains a radiation term which increases as D^2 increases. In addition, α_p is expected to increase with droplet diameter. The foregoing plots seem to indicate that the buoyancy forces are not represented by the Grashof or Gravity number. In addition, the direct dependence of evaporation rate on drop diameter suggests that the radiant heat transfer contribution may not be separable from the heat transferred by convection and conduction. That is to say, that the overall phenomenon depends only on the total heat absorbed by the droplet, no matter how this heat is transferred. Accordingly, the gravity term and radiant energy "correction" to the latent heat of vapourization were eliminated

*Table 1 of this paper has been deposited as Document No. 6388 with the ADI Auxiliary Publications Project, Photoduplication Service, Library of Congress, Washington 25, D.C. A copy may be obtained by citing the Document No. and by remitting $1.25 for photoprints, or $1.25 for 35 mm. microfilm. Advance payment is required. Make cheques or money orders payable to: Chief, Photoduplication Service, Library of Congress.

*This ratio is defined as a Temperature number and was first used by Nusselt[45] and later by Hermann[46]. The Grashof number was expressed in two parts, a Gravity number $G = D^3\rho^2/\mu^2$ and a Temperature number $T\epsilon = \Delta T/T_\infty$. This was suggested, so that an exponent on $T\epsilon$ would allow for the variation of gas properties with temperature.

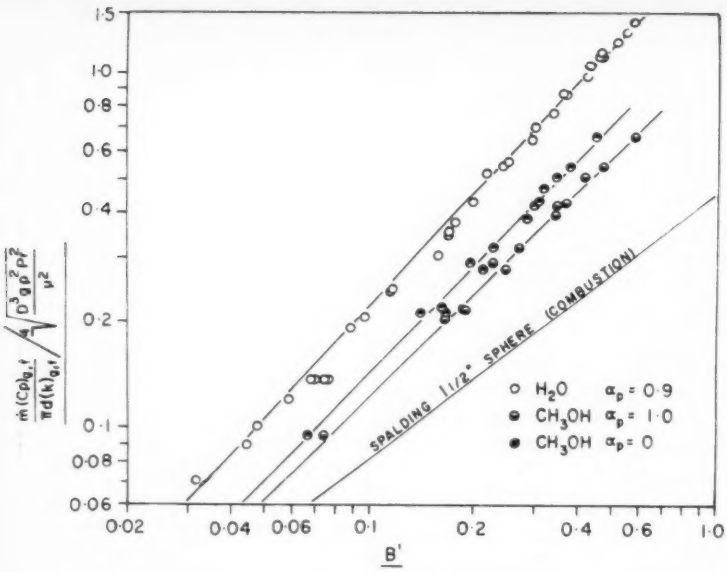

Figure 6—Comparison of experimental results with Spalding's correlation for free convection phenomena arising in combustion of liquids on a 1½-in. spherical burner [31].

from the Spalding correlation and $(dm/d\theta)(c_p)/(\pi Dk_f)$ was plotted against $B = c_p \Delta T/\lambda$, as shown in Figure 7. All the data satisfactorily correlate along a single straight line of equation:

$$[(dm/d\theta)\,(c_p)/(\pi Dk_f)]\,(\mathrm{Pr})^{-1/3} = 3.2\,B^{0.97} \quad \ldots\ldots\ldots (17)$$

The Prandtl number was included in the correlation in an attempt to account for the viscosity effects and hence the difference between the velocity and temperature profiles in the boundary layer of the various liquid droplets investigated. The exponent is consistent with that suggested by Pohlhausen's[47] mathematical treatment of heat transfer phenomena.

This equation was obtained by a least-squares analysis using the water droplet data only, since it was felt that the physical property data are more reliable in this case. The fact that the organic liquid data are slightly lower may possibly be accounted for as follows:

(1) Radiation effects. At any given value of B, the radiant heat transfer to the water droplets is much higher than that for the organic liquid droplets.

(2) Unreliable transport properties for the organic vapors. The transport properties of steam have been measured with high precision[35], whereas those for organic vapors had to be found by extrapolating low temperature data of unknown accuracy.

Kobayasi's data[17] for evaporation of droplets in an air atmosphere can be predicted from the correlation given in Equation (17), which lends additional support to its validity. These data are shown on Figure 7 as well. Although Kobayasi's experiments were conducted in an air atmosphere, the transport properties of the pure evolved vapors were used throughout in the calculations. This was suggested by the Schlieren photographs of Nishiwaki[20], which clearly show that the droplets are completely surrounded by a downward-flowing shell of evolved vapor. The one point which lies very much above the correlating curve on Figure 7 refers to a benzene drop evaporating in a 100°C. air atmosphere. At this temperature, it may be predicted that the concentration of air diffusing into the vapor boundary layer will be relatively high and the transport properties may therefore very well be intermediate between those

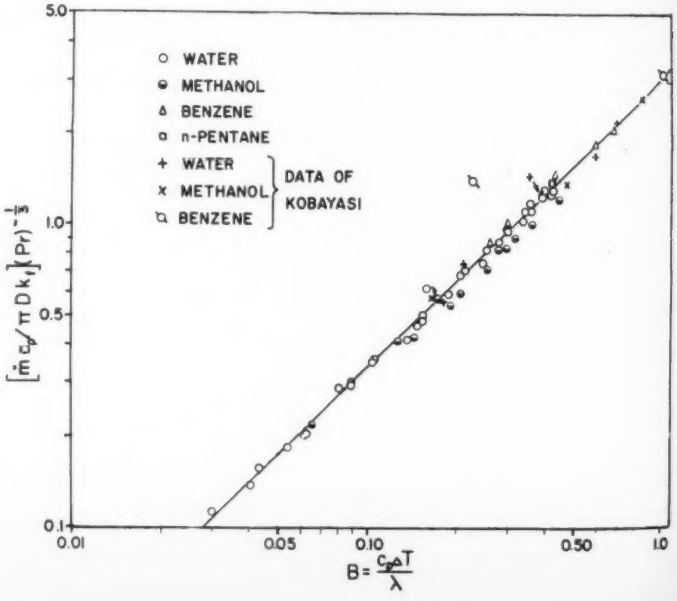

Figure 7—Correlation of all experimental data. The experimental results of Kobayasi [17] are also shown.

of benzene vapor on the one hand and air on the other.

It would be instructive to calculate the approximate magnitude of the effective boundary layer thickness and how it changes with temperature, using a very simplified model consisting of a spherical symmetrical model. If a vapor shell of thickness dr and temperature T at a distance r from the centre of the sphere ($r_d < r < r_b$) is considered, the following energy balance can be established:

$$4\pi r^2 k(dT/dr) = (dm/d\theta)\lambda - q_R + (dm/d\theta)\int_{T_d}^{T} c_p dT \quad \ldots\ldots(18)$$

This expression neglects radiation absorbed by the boundary layer since — as mentioned earlier — it can be shown that such absorption is quite small at atmospheric pressure[41]. For water vapor the specific heat can be considered constant with temperature, and the thermal conductivity variation with temperature can be approximated by a straight line of the form:

$$k = k_o + \gamma t \quad \ldots\ldots(19)$$

where $k_o = 37.5 \times 10^{-6}$ (cal.)/(sec.)(cm.)(°C.) and $\gamma = 19.5 \times 10^{-8}$ (cal.)/(sec.)(cm.)(°C.)^2.

Equation (18) can be integrated over the temperature limits T_d to T_b to yield:

$$(1/r_d - 1/r_b) = [4\pi k_o \ln(1 + c_p\Delta T/\lambda')]/c_p(dm/d\theta) + \frac{(4\pi\gamma\lambda')}{(c_p^2)(dm/d\theta)}\{\ln(1 + c_p\Delta T/\lambda') - [c_p\Delta T/(\lambda' + c_p\Delta T)]\} \quad \ldots\ldots(20)$$

The values of $(dm/d\theta)$ for 700-micron water drops at various temperatures were taken from Figure 5 and the calculated ratios (r_b/r_d) are shown in Table 2 for $\alpha_p = 0$ and $\alpha_p = 0.90$.

Although the values of (r_b/r_d) and of the effective boundary layer thickness $(r_b - r_d)$ calculated from Equation (20) are probably of the right order of magnitude, as indicated by Nishiwaki's Schlieren photographs[20], this equation predicts that the boundary layer will become thinner as the temperature — and hence the rate of evaporation — increases, which is difficult to reconcile with the greater radial velocity imposed by the higher vapor evolution. From Kumagai's application of classical hydrodynamics to the problem of a burning fuel droplet, considered as a point source of vapor in a uniform velocity field[18], the role played by the radial vapor velocity in the determination of the boundary layer thickness was clearly implied. It must be remembered, however, that at higher temperatures, the addition of cold vapor and the sensible heat requirements of this vapor is greater, and this in turn imposes a relatively larger heat load at every point in the boundary layer. Thus the relative temperature at any point will be lower than that for a similar drop at lower temperatures. As a consequence of these increased downward forces, the free convection velocity will be greater and the boundary layer thickness will be affected accordingly.

Since, at any given gas temperature, the rate of evaporation is proportional to the diameter, the vapor velocity measured at the drop surface is inversely proportional to its diameter. This suggests that the momentum of the vapor at the drop surface remains the same at all drop diameters. Equation (26) predicts that for any given ambient temperature, the ratio r_b/r_o remains constant when $\alpha_p = 0$; this calculated ratio decreases as the droplet diameter decreases when radiation is absorbed by the droplet.

These results can only be suggested from the symmetrical model. The actual interaction of vapor momentum and cooling effects requires experimental observation by Schlieren or interferometric optical techniques.

TABLE 2

EFFECTIVE BOUNDARY LAYER THICKNESS AROUND A 700-MICRON DIAMETER WATER DROPLET

T_G °C.	$dm/d\theta \times 10^6$ (Fig. 5) gm./sec. $D = 700\mu$	$\alpha_p = 0$		$\alpha_p = 0.90$	
		r_b microns	r_b/r_d	r_b microns	r_b/r_d
150	4.40	817	3.22	875	2.50
200	9.30	806	2.31	929	2.65
250	14.40	802	2.29	800	2.80
300	20.40	778	2.22	960	2.74
350	27.00	743	2.12	925	2.64
400	34.40	712	2.03	900	2.55
450	42.70	685	1.96	862	2.46
500	51.20	670	1.92	833	2.30
550	60.50	650	1.86	813	2.32
600	70.50	625	1.79	790	2.26

CONCLUSIONS

The evaporation rate of stationary droplets in high temperature surroundings does not appear to be governed by the rate of heat transfer by natural convection, since no dependency of the Nusselt number on the Grashof number was found. Attempts to correlate the results on the basis of Godsave's model (conduction across the boundary layer controlling) or Spalding's approach were equally unsuccessful.

On the other hand, the evaporation rates appear to be very satisfactorily predicted by the expression:

$$[(dm/d\theta)(c_p)/(\pi D k_f)](\mathrm{Pr})^{-1/3} = 3.2\,B^{0.97} \quad \ldots\ldots(17)^*$$

over the range $0.03 < B < 1.0$. The accuracy of this expression is quite encouraging, particularly in view of the uncertainties concerning the physical properties of the vapors of benzene, methanol, cumene and pentane. Since, in the evaporation range studied, the boundary layer consists essentially of the evolved vapors, the values of c_p and k for the latter at the arithmetic average film temperature should be used.

It should be noted that since:

$$(dm/d\theta)\lambda - q_R = h_A A\Delta T \quad \ldots\ldots(12)$$

and hence $$Nu_A = h_A D/k_f = (dm/d\theta)(c_p)/(\pi D k_f B') \quad \ldots\ldots(21)$$

where $$B' = (c_p\Delta T)/[\lambda - (q_R)/(dm/d\theta)]$$

an alternative expression for the proposed correlation is:

$$B' Nu_A (\mathrm{Pr})^{-1/3} = 3.2\,B^{0.97} \quad \ldots\ldots(22)$$

It must be remembered that this equation can only be considered valid when the gas and the containing walls are at the same temperature.

It is highly significant that the two forms of the correlation involve either the total evaporation rate — as shown by Equation (17) — or the total heat transferred (convection and radiation) — as shown by Equation (22) — rather than the individual transfer coefficient or Nusselt numbers (Nu or Nu′) as in most previously published expressions. Since the mass rate of vapor evolution depends obviously on the evaporation rate, the inference may be drawn that the proposed correlation relates the vapor flow in the boundary layer to the system conditions expressed by the Transfer number B. Although the buoyancy effects which undoubtedly exist in the boundary layer could not be accounted for in the conventional way, that is, by means of the Grashof number, a marked downward flow of cold evolved vapor will be established around the droplets, which will in turn determine the temperature, density and velocity profiles in the boundary layer. The magnitude of these profiles will be dictated by the evaporation rate, which may be thought of as the controlling factor, although they are obviously interdependent.

If the proposed mechanism is correct, it might be predicted that the correlation should break down if high rates of evaporation are produced in cold surroundings, that is, under conditions where strong convective currents cannot be produced as a result

of large temperature differences. Such an experimental situation was investigated by Diederichsen and Hall[13], who focussed the radiations from a carbon arc onto water droplets in still air, through a large condenser lens. The life-time of 700-micron drops varied from 40 to 100 seconds, depending on the radiant energy level. The rate of evaporation was found to be directly proportional to the square of the drop diameter, whereas a dependence on the first power of the diameter was found in the present study.

The present experimental data might be criticized on the grounds that they were obtained under unsteady state conditions, that is with the droplet diameter continuously decreasing, and that the recession of the boundary might have an effect on the results. In his analysis of a vapor bubble — liquid boundary, Forster[48] has pointed out, however, that the relative position of the fluid particles is not changed by the radial motion of the spherical boundary, and that the heat transfer at the boundary should not be affected by additional convective effects.

The experimental data and the correlating equation indicate that the phenomena occurring at these drop-sizes will continue to appear, even when the drop diameter is very small. Normally, natural convection effects disappear as the Grashof number or the size of the body becomes very small. Further experimental investigations on the evaporation of very small droplets are required. It may well be that the existence of a relative velocity resulting from free-fall of the droplet, or turbulence effects, will affect the boundary layer phenomena around the droplet and the resulting heat transfer in a forced-flow or turbulent field may be less than that reported here, as other studies have indicated[49]. Moreover, such effects probably alter the evaporation rate of water droplets at low temperatures and very low Reynolds numbers, as reported by Kinzer and Gunn[11]. These aspects will also require further study.

It is interesting to note that the group $[(dm/d\theta)\ (c_p)/\pi Dk_f)]$ which appears on the left-hand side of Equation (17) happens to be the Peclet number for the evolved vapor, being the product of the Reynolds number at the drop surface in a radial direction, and the Prandtl number. This particular Reynolds number arises from the momentum balance equation in the radial direction. This indicates that this balance cannot be neglected and emphasizes once more the importance of the radial flow.

Acknowledgements

Assistance from the Pulp and Paper Research Institute in the form of an equipment grant and of financial support to T. W. Hoffman is gratefully acknowledged. Recognition is due also to K. Webb and A. Lapointe for their valuable help in the design and fabrication of the experimental apparatus.

Nomenclature

Roman Symbols

a = major axis of an ellipsoid.
A = surface area of droplet, cm.²
b = minor axis of an ellipsoid.
B = Transfer number: $c_p\Delta T/\lambda$ (radiation not included), dimensionless.
B' = Transfer number: $c_p\Delta T/[\lambda - (q_R)/(dm/d\theta)]$, (radiation included), dimensionless.
c_p = heat capacity of gas, (cal.)/(gm.) (°C.).
dc/dy = concentration gradient normal to surface, (g./cm.³)/cm.
D = droplet diameter, cm.
D_v = mass diffusion coefficient, cm.²/sec.
E = defined by equation (13).
g = acceleration due to gravity, cm./(sec.)².
Gr = Grashof number: $(D^3g\rho^2\beta\Delta T)/(\mu^2)$.
h = heat transfer coefficient, (cal.)/(sec.) (cm.²) (°C.).
h_A = actual heat transfer coefficient at the drop surface.
k'_s = mass transfer coefficient, cm./sec.
k_f = thermal conductivity of the gas evaluated at the average film temperature, (cal.)/(sec.) (cm.) (°C.).
m = mass, gm.
$\dot{m}$ = evaporation rate, $(dm/d\theta)$, gm./sec.
Nu = Nusselt number for heat transfer: hD/k., dimensionless.
Nu_A = actual Nusselt number.
Nu_T = true Nusselt number.
Nu' = Nusselt number for mass transfer: k'_sD/D_v, dimensionless.
Pr = Prandtl number: $c_p\mu/k_f$, dimensionless.
q_R = radiant heat transfer rate to drop, cal./sec.
q_k = conduction heat transfer rate along drop holder, cal./sec.
r_d = radius of droplet, cm.
r_b = radius of effective spherical boundary layer, cm.
Re = Reynolds number: $DV\rho/\mu$, dimensionless.
Sc = Schmidt number: $\mu/\rho D_v$, dimensionless.
T = absolute temperature, °K. T_d: at droplet surface; T_w: at the wall; T_∞: temperature of the gas at infinite distance from the heat-receiving surface.
Te = Temperature number: $\Delta T/T_\infty$, dimensionless.
v_w = velocity of vapor normal to and at the evaporating surface; cm./sec.
V = stream velocity, cm./sec.

Greek Symbols

α_p = absorptivity of drop, dimensionless.
β = volumetric coefficient of thermal expansion, °K.$^{-1}$.
γ = defined in Equation (19).
θ = time, sec.
λ = latent heat of vaporization, cal./gm.
λ' = $\lambda - [q_R/(dm/d\theta)]$, cal./gm.
μ = absolute viscosity, gm./(cm.) (sec.).
ρ = density, gm./cm.³; ρ_g: of gas; ρ_L: of liquid.
σ = Stefan-Boltsmann constant: 1.355×10^{-12} (cal.)/(sec.) (cm.²) (°K.⁴).

References

(1) Birks, J., and Bradley, R. S., Proc. Roy. Soc. **A 198:** 226 (1949).
(2) Bradley, R. S., Evans, N. G., and Whytlaw-Gray, R., Proc. Roy. Soc. **A 186:** 368 (1946).
(3) Bradley, R. S., and Shelland, A. D., Proc. Roy. Soc. **A 198:** 239 (1949).
(4) Moncheck, L., and Reiss, H., J. Chem. Phys. **22:** 831 (1954).
(5) Topley, B., and Whytlaw-Gray, R., Phil. Mag. **4:** 873 (1927).
(6) Froessling, N., Gerlands Beitr. Geophys., **52:** 170 (1938).
(7) Hsu, N. T., Sato, K., and Sage, B. H., Ind. Eng. Chem. **46:** 870 (1954).
(8) Ingebo, R. D., Chem. Eng. Prog. **48:** 403 (1952).
(9) Ranz, W. E., and Marshall, W. R., Jr., Chem. Eng. Prog. **48:** 141, 173 (1952).
(10) Mirsky, W., Ph.D. Thesis, Univ. of Mich. (1956).
(11) Kinzer, G. D., and Gunn, R. J., J. Meterorol. **8:** 71 (1951).
(12) Maisel, D. S., and Sherwood, T. K., Chem. Eng. Prog. **46:** 131 (1950).
(13) Diederichsen, J., and Hall, A. R., Fourth Symposium (International Symposium on Combustion), p. 837, The Williams and Wilkins Co., Baltimore (1953).
(14) Fourth Symposium (International) on Combustion, pp. 818-865, The Williams and Wilkins Co., Baltimore (1953), also Fifth Symposium (International) on Combustion, pp. 101-158, Reinhold Publ. Corp., New York (1955).
(15) Godsave, G. A. E., Report No. R66, N.G.T.E. (England) March (1950), Report No. R87, N.G.T.E. (England) April (1951), Report No. R88, N.G.T.E. (England) August (1952), Report No. R125, N.G.T.E. (England) October (1952).
(16) Goldsmith, M., and Penner, S. S., Jet Prop. **24:** 245 (1954).
(17) Kobayasi, K., Trans. J.S.M.E., **20,** 100:826, 831 (1954).
(18) Kumagai, S., and Kimura, I., Sc. of Mach. **3:** 431 (1951).
(19) idem ibid., **4:** 337 (1952).
(20) Nishiwaki, N., Fifth Symposium (International) on Combustion, p. 148, Reinhold Publ. Corp., New York (1955).
(21) Mathers, W. G., Madden, A. J. Jr., and Piret, E. L., Ind. Eng. Chem. **49:** 961 (1957).
(22) Schlichting, H., "Boundary Layer Theory" (Translated by J. Kestin), McGraw-Hill Co. Inc., New York (1955).
(23) Jakob, M., "Heat Transfer", Vol 1, Chap. 23, John Wiley and Son, New York (1950).
(24) Ackermann, G., VDI. – Forschungsheft No. 382 (1937).
(25) Perry, J. H., "Chemical Engineers' Handbook", 3rd edit., McGraw-Hill Co. Inc. (1950).
(26) Somers, E. V., J. App. Mech. **23:** 295 (1956).
(27) Spalding, D. B., Proc. Roy. Soc., **A 221:** 78 (1954).
(28) Marshall, W. R. Jr., Chem. Can. **7:** 37 (1955).
(29) Ranz, W. E., Trans. A.S.M.E. **78:** 909 (1956).

(30) Sleicher, C. A. Jr., and Churchill, S. W., Ind. Eng. Chem., **48**: 1819 (1956).
(31) Spalding, D. B., Fourth Symposium (International) on Combustion, p. 847, The Williams and Wilkins Co., Baltimore (1953).
(32) Langmuir, I., Phys. Rev. **34**: 401 (1912).
(33) Simpson, H. C., Sc.D. Thesis, M.I.T. (1954).
(34) "International Critical Tables", McGraw-Hill Co. Inc., New York (1928).
(35) Keyes, F. G., Trans. A.S.M.E., **73**: 589 (1951).
(36) Vines, R. G., Australian J. Chem. **6**: 1 (1953).
(37) Vines, R. G., and Bennett, L. A., J. Chem. Phys., **22**: 360 (1954).
(38) Montgomery, J. B., and De Vries, T., J. Am. Chem. Soc. **64**: 2375 (1942).
(39) De Vries T., and Collins, B. T., J. Am. Chem. Soc. **63**: 1343 (1941).
(40) Marshall, W. R. Jr., and Pigford, R. L., "Differential Equations for Chemical Engineers", p. 38, Univ. of Delaware, (1947).
(41) Hoffman, T. W., Ph.D. Thesis, McGill University (1959).
(42) McAdams, W. H., "Heat Transmission", McGraw-Hill Co. Inc., New York (1954).
(43) Brown, S. L., Phys. Rev., **21(2)**: 103 (1923).
(44) Kyte, J. R., Madden, A. J., Jr. and Piret, E. L., Chem. Eng. Prog., **49**: 653 (1953).
(45) Nusselt, W., Cesundheits – Ing., **38**: 477, 490 (1915).
(46) Hermann, R., VDI – Forschungsheft No. 379 (1936).
(47) Pohlhausen, E., ZAMM, **1**: 115 (1921).
(48) Forster, H. K., A.I.Ch.E. Journ., **3**: 535 (1957).
(49) Dlouhy, J., and Gauvin, W. H., A.I.Ch.E. Journ., **6**: 29 (1960).

★ ★ ★

Pressure Drop of Single Phase Flow Through Raschig Ring Type Tower Packings: Effect of Hole Size[1]

LIANG-TSENG FAN[2]

The effects of hole size of the cylindrical tower packing on pressure drop of single phase flow were investigated. It was shown that the hole size had a profound effect on the correlation of pressure drop data. This was attributed to the difference in the characteristics of the spaces inside and outside the packing units and to the interlocking of the packing units in the beds.

A large variety of materials has been employed for tower packing in chemical and process industries. The Raschig ring, which is a hollow cylinder whose length is usually equal to its diameter[1], is still one of the most common types of tower packings[1,2].

Some of the major requirements of a tower packing are[1]:

1. High effective contact surface area per unit volume of tower packing.
2. High voidage and low pressure drop.
3. Low weight per unit volume.
4. Random packing arrangement, leading to uniform flow distribution.
5. Durability and low cost.

The hole in the Raschig ring is provided to meet the first four requirements of tower packing mentioned above. Durability is the main limiting factor for hole size which can be made in the Raschig rings.

The pressure drops of a single phase flow through a bed packed with Raschig rings have been investigated frequently, and the results of such investigations have been included in several of the generalized correlations of the packed bed pressure drops[3,4,5,6,7,8].

In all of the previous studies, Raschig rings employed were mostly commercial products, and consequently, the use of various sizes of Raschig rings caused simultaneous changes of the outside diameter of the packing, diameter of the hole and their ratios. It is, therefore, difficult to separate or distinquish the effects of hole size on the performance of the column packed with Raschig rings from the results of previous investigations. The purpose of this investigation was to study the effects of hole size on the pressure drop of a single phase flow. In order to achieve this purpose, specially manufactured clay cylinders with the same external dimensions but with different sizes of holes were employed, and all the variables of the experiment except the fluid flow rate were fixed.

Packing Material and Experimental Apparatus

The characteristics of clay packing units employed are tabulated in Table 1.

Table 1

Characteristics of Packing Units

Packing	Solid	Small Hole	Large Hole
Outside diameter, in.	3/4	3/4	3/4
Height, in.	3/4	3/4	3/4
Diameter of hole, in.	0	0.197	0.394
Volume, cu. ft. $\times 10^4$	1.91	1.78	1.38
Surface area, sq. ft. $\times 10^2$	1.84	2.12	2.32
Weight, gm.	10.5	9.6	6.8

Table 2

Characteristics of Beds

Packing	Solid	Small Hole	Large Hole
Bed depth, ft.	2.0	2.0	2.0
No. of packing per cu. ft.	2900	3030	3430
Void fraction	0.447	0.462	0.526
Surface area of packing, ft.^{2}	53.3	64.2	79.3

The packing units used are also illustrated in Figure 1.

A vertical steel pipe with a 6-inch inside diameter was used as a column. The packed zone of the column was 2 feet long, which was held at both ends by rigid screens to the packings and also to prevent the expansion of the bed.

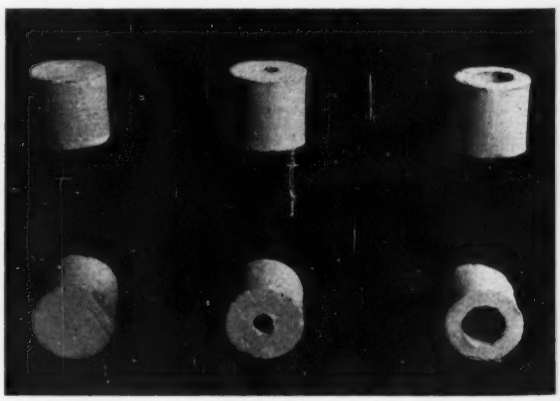

Solid ring $D_t = 0$ in. | **Ring with small hole $D_t = 0.197$ in.** | **Ring with large hole $D_t = 0.394$ in.**

Figure 1—Packing used in experiments

[1]*Manuscript received September 24, 1959; accepted July 4, 1960.*
[2]*Department of Chemical Engineering, Kansas State University, Manhattan, Kansas.*

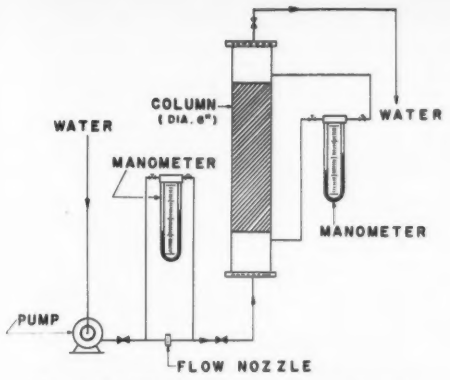

Figure 2—Flow diagram of experiment.

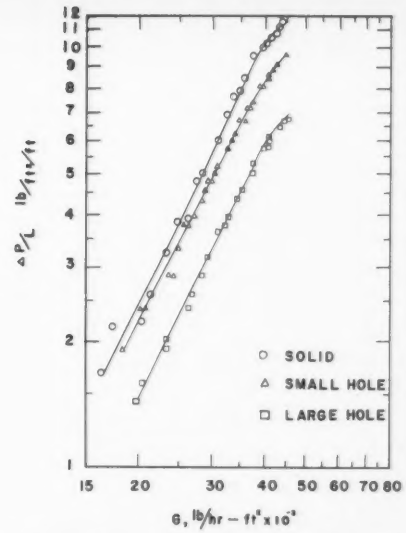

Figure 3—Experimental data: pressure drop gradient vs water flow rate.

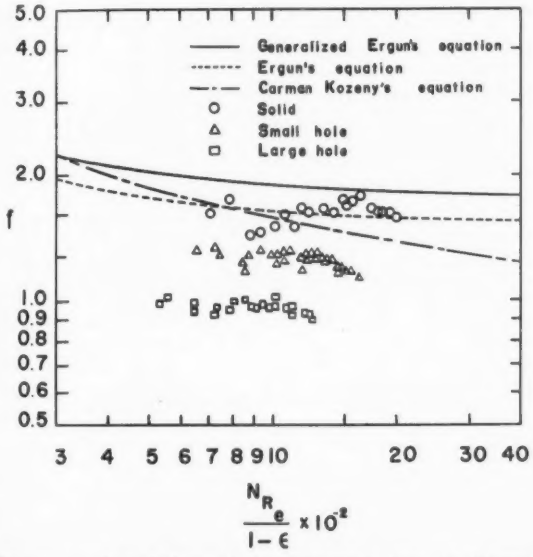

Figure 4—Correlation of experimental data by Ergun's equation.

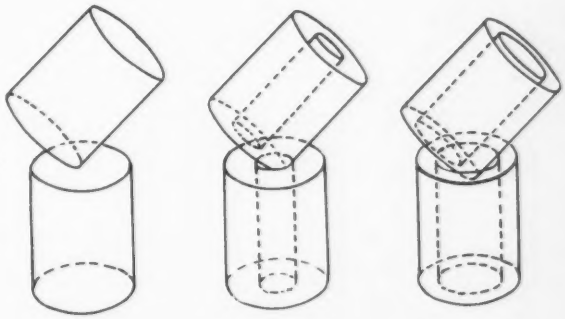

Solid **Small hole** **Large hole**

Figure 5—Interlocking of packing unit.

Precaution was taken in filling the column to assure that the clay packing would not be broken. This was accomplished by filling the column with water before putting in the packing. The water provided sufficient buoyancy to prevent the packing from being broken as well as to furnish a uniformly random-packed bed. The characteristics of the beds obtained are summarized in Table 2.

The fluid used in this experimental work was water. Its flow rates were measured by a flow nozzle and a mercury manometer.

Another manometer was connected to the pressure taps to measure the pressure difference of the extreme ends of the packed zone. The temperature of the water at the inlet and outlet was constant at 18.0° C.

Water was pumped through the flow nozzle, and the readings from the manometer were taken after a steady state condition was reached.

Records of pressure difference were taken from the manometer for various flow rates of water. A flow diagram of the entire experimental set-up is shown in Figure 2.

Results of Experiment

Altogether 74 runs were made. The pressure drop data are tabulated in Table 3*. They are also plotted in Figure 3, as a function of flow rates.

Correlations of the data by Carman and Kozeny's equation and Ergun's equations are illustrated in Figure 4. The results of these calculations are also summarized in Table 3. The deviations of these experimental data from the generalized correlations are expected[9]. It can definitely be observed from Figure 4 that Ergun's correlation follows the trend of the data much better than Carman and Kozeny's correlation does. In other words, Ergun's correlation is almost parallel to the trend established by the experimental data. In addition, Figure 4 shows that the hole size has profound effect on the correlation of pressure drop.

In order to simplify the analysis of the data obtained, the constants in Ergun's generalized equation were slightly adjusted to fit the data obtained from the solid rings as follows[9]:

*Table 3 of this paper has been deposited as Document No. 6389 with the ADI Auxiliary Publications Project, Photoduplication Service, Library of Congress, Washington 25, D.C. A copy may be obtained by citing the Document No. and by remitting $1.25 for photoprints, or $1.25 for 35 mm. microfilm. Advance payment is required. Make cheques or money orders payable to: Chief, Photoduplication Service, Library of Congress.

$$\frac{\triangle P}{L} = 131\,\frac{(1-\epsilon)^2}{g_c\epsilon^3}\,\frac{G}{\rho D_p{}^2} + 1.53\,\frac{1-\epsilon}{g_c\epsilon^3}\,\frac{G^2}{\rho D_p} \qquad \ldots\ldots\ldots\ldots (1)$$

$$f = \frac{\triangle P}{L}\,g_c\,\frac{D_p\rho}{G^2}\,\frac{\epsilon^3}{(1-\epsilon)} = 1.53 + 131\,\frac{1-\epsilon}{D_pG/\mu}$$

This equation is shown in Figure 4 by a dotted line.

Analysis of Data, Discussion, and Conclusion

Characteristics of bed as a function of hole size: As listed in Table 2, the effect of hole size to the number of packing units contained in a unit volume of the bed was appreciable. The increase in the number of packing with increase of the hole size may be explained as a result of overlapping or interlocking of the packing units as illustrated in Figure 5. The consequence of this increase in the number of the packing units is that the surface area in the bed increases more than the increase of the surface area of each individual unit. The overall void space of the bed increases, however, less than the increase of the void due to hole space as the diameter of hole increases. The number of packing units per cubic foot of the bed is represented empirically as a function of the ratio of inside diameter to outside diameter as:

$$\begin{aligned} n &= n_o + \triangle n \\ &= n_o + C\left(\frac{Di}{D_o}\right)^2 \qquad \ldots\ldots\ldots\ldots (2) \\ &= 2900 + 1955\left(\frac{Di}{D_o}\right)^2 \end{aligned}$$

Because of this increase in the number of packings, the surface area and porosity of the bed are expressed respectively as:

$$A = \frac{5}{2}\,n_o\,\pi\,D_o{}^2 + \pi\left(\frac{Ch}{D_o} - \frac{n_o}{2}\right)D_i{}^2 - \frac{C\pi}{2D_o{}^2}\,D_i{}^4 \ldots\ldots\ldots (3)$$

$$\epsilon = \left(1 - \frac{n_o\pi}{4}\,D_o{}^2h\right) + \frac{\pi h}{4}\,(n_o - C)\,D_i{}^2 - \frac{\pi}{4}\,\frac{Ch}{D_o{}^2}\,D_i{}^2 \ldots\ldots\ldots (4)$$

If it were assumed that there is no increase in the number of the packing units in the bed, total surface area in the bed and the porosity of the bed would increase parabolically as a function of D_i.

Effect of hole size on pressure drop: As already indicated in Figure 4, the effect of hole size on the friction factor correlation of pressure drop based on Equation (1) was appreciable and the experimental friction factors were always less than those calculated. Increase in the hole size increased this deviation. In the analysis of variance performed on the experimental data of friction factor with respect to the hole size of packing ring, F-test (the variance ratio) turned out to be highly significant. This indicates that the sample came from population with different means. Therefore, it can be concluded that the hole size of packing ring had a definite effect on the friction factor. Since F-test gave no clue as to how many differences there were, the test of Least Significant Difference on the data of friction factor was performed. The test showed that means of friction factors of each hole size were significantly different.

Since increase in the hole size in the packing unit increased the specific surface, the mean diameters of the packing units were reduced. According to Kramer[10] this would reduce the pressure drop due to the wall effect. Calculations according to the Kramer's equation, however, cannot account for more than 5% of deviation from the Ergun's correlation.

As already mentioned, it is believed that the characteristics of space or surface area with respect to the fluid flow inside the hole of the Raschig ring would be quite different from that of the outside area of the packing[1]. In his recent paper Greenaway[12] indicated that a bed's capacity to accept liquid into the ring interiors, which is called the "inlet availability", is inversely proportional to ring size. From the definition and the method of measurement, described in detail by Greenaway[12], of "inlet availability" the interlocking of the rings would definitely reduce the inlet availability of the rings over that of the rings with the same hole size when they are not interlocking. It may be expected that, when the hole size is small, this difference of characteristic is quite appreciable, but the fraction of the space occupied by the holes in the bed is small. The reverse is true when the hole size becomes large. Therefore, it is quite possible that when the hole size is larger this difference of characteristic appears more appreciably in an overall sense than when the hole size is small. This may be at least one of the reasons why the deviation from friction factor correlation increased as the hole size was increased. This, however, still does not explain the direction of deviation, which is consistently lower than the calculated values.

It can be seen that no provisions are made in Equation (1) to differentiate this difference of the characteristics of the spaces or areas inside and outside the hole in the packing units. As Equation (1) indicates, however, for a certain flow system at a fixed superficial flow rate, the porosity and the particle diameter are the two major factors affecting the pressure drop. Then, the fact that there are some differences between the effects of spaces or areas inside and outside the holes of the packing to the flow of fluid, would mean that either the effective and apparent porosities are different, or there is discrepancy between the effective and apparent diameters. These differences would be further enhanced by an interlocking of the particles as illustrated by Figure 4, to which the increase in packing holding capacity of the bed with the increase in hole size was attributed. As it can be observed, this interlocking of the packing units may not only block the passage of the fluid through the hole, but also hide the part of the outside surface of the packing units into the hole and, thus reduce the effectiveness of a part of the outside area. If it were considered that the interlocked particles are a single particle, the result would have been an increase in the particle volume. The effects of interlocking of the particles described above may never be clearly separated to allow an exact quantitative analysis because of the interaction between them. If it were assumed that the interlocking of the packing units would cause the reduction of the effective porosity, the result would have been a greater pressure drop than that which would be predicted by Equation (1). However, the results of the present investigation were completely reversed. The last two effects of the particle interlocking i.e. both the reduction in the effective surface area and the increase in the effective volume of the particle would result in the increase in the effective particle diameter over the apparent diameter according to the definitions of particle diameter, $D_p = 6/S_p = 6/S/_V$[7]. This increase in the effective diameter over the apparent diameter should result in reduction of pressure drop according to Equation (1).

Effect of hole size on mass transfer: If the analogy, $f \propto J_d$, were accepted, the results of this investigation will imply that the increase in mass-transfer rate due to the increases in hole size will not be as great as expected from the changes of apparent surface area, porosity and diameter. This reduction of J_d-factor may again be explained by the fact that effective surface area may be smaller than the apparent surface area which would be used in evaluating the mass-transfer coefficients.

Acknowledgment

The author wishes to thank S. L. Wang of Linde Company, who initiated this project.

Nomenclature

A = geometrical or apparent surface area of the packing units in one cubic ft. of the packed bed, sq. ft.
C = constant defined by equation (2).
D_t = diameter of hole, ft.
D_o = outside diameter of cylinder, ft.
D_p = diameter of packing unit, ft.
f = friction factor as defined by Ergun, dimensionless.
G = mass flow rate of fluid, lb./hr.-ft.^{2}
g_c = conversion factor, (lb. − mass) (ft.)/(lb. − force) (hr.^{2})
h = height of individual packing unit, ft.
J_d = mass transfer factor, dimensionless
L = depth of packed bed, ft.
n_o = number of the solid packing in one cubic ft. of the bed.
n = number of the packing unit in one cubic ft. of the bed.
$\triangle n$ = increase of the packing units over that of the solid ring, as defined by equation (2).
$\triangle p$ = pressure drop, lb./ft.^{2}
U = linear velocity of fluid, ft.
S = geometrical or apparent surface area of a single packing unit, sq. ft.
S_p = specific surface of the packing unit, ft.$^{-1}$
S_{po} = specific surface of the solid ring, ft.$^{-1}$
V = geometrical or apparent volume of a single packing unit, cu. ft.

Greek Letter

π = 3.1415 - - - -
ϵ = porosity of the packed beds.
ρ = density of fluid, lb./cu. ft.
μ = viscosity of fluid, lb./(ft.) (hr.)

References

(1) Badger, L. B., and Banchero, J. T., "Introduction to Chemical Engineering" p. 263, McGraw-Hill, New York (1955).
(2) Leva, M., "Tower Packings and Packed Tower Design" 1st ed., p. 17, The U.S. Stoneware Co., Akron (1951).
(3) Blake, C. F., Trans. Am. Inst. Chem. Engr. **14**: 415-421 (1921-22).
(4) Carman, P. E., Trans. Am. Inst. Chem. Engr. **15**: 150-166 (1937).
(5) Leva, M., et. al. U.S. Bur. Mines Bull. 504 (1951).
(6) Morcom, A. R., Trans. Am. Inst. Chem. Engr. **24**: 30-43 (1946).
(7) Ergun. S., Chem. Eng. Prog. **48**: 89-94 (1952).
(8) White, A. M., Trans. Am. Inst. Chem. Engrs. **31**: 390 (1935).
(9) Ergun, S., and Orning, A. A., Ind. Eng. Chem., **41**: 1179 (1949).
(10) Bird, R. B., et. al. "Notes on Transport Phenomena", p. 87, John Wiley & Sons, Inc., New York (1958).
(11) Leva, M., "Tower Packing and Packed Tower Design", 1st ed., p. 19, The U.S. Stoneware Co., Akron (1951).
(12) Greenaway. D., Chem. Eng. Science, **10**: 197 (1959).

★ ★ ★

Fundamental Aspects of Solids-Gas Flow

Part IV: The Effects of Particle Rotation, Roughness and Shape[1]

L. B. TOROBIN[2] and W. H. GAUVIN[2]

This paper examines the various complicating effects which rotation, surface roughness and shape impose on the motion and drag of single particles entrained in a fluid. In general, rotation appears to have little effect on the drag coefficient at low Reynolds Numbers, but influences the linearity of the motion and may thus play a part in the mechanism of particle entrainment in conveyed solids-gas systems. Negative lift has been observed in the critical Reynolds Number region as the result of asymmetry in the wake structure. Surface roughness will cause an early transition to a turbulent boundary layer at higher *Re* values, which will result in an appreciable decrease in drag coefficient, but it may increase the drag at low Reynolds Numbers.

The effect of particle shape is more complex than has been suggested by previously published analyses. The available empirical correlations are discussed and compared, and indicate a dependency on the particle-to-fluid density ratio.

The previous papers in this series[1,2,3] were concerned with studies related to the fluid dynamics of single spheres moving in steady or accelerated motion through a laminar fluid. It is now possible to consider the additional complexities which characterize actual solids-gas flows. The present paper will be devoted to an analysis of the literature dealing with the effects of particle rotation, roughness and shape. In most cases, the published studies have been confined to the behavior of a single particle contained in a laminar fluid. The discussion will first deal with macroscopic observations, i.e. the measurement of motion and drag, and then with the microscopic empirical and mathematical investigation of the fluid processes.

VI—THE EFFECT OF ROTATION

There has been a tendency among workers in the field of solids-gas flow to attribute the lowered values of the drag coefficient often measured in multiparticle systems to the fact that the particles are rotating[4,5]. Rotation of particles due to velocity gradients and collision with solid boundaries is particularly pronounced with non-spherical bodies. Gasterstadt[6] reported that wheat particles would at times rotate with a peripheral velocity of the same order as that of the air stream. However, observations by Pasternak with freely moving spheres[7] suggest the ratio of the peripheral velocity (hereafter referred to as U_p) to the mean relative velocity (U_o) to be of the order of 5 percent. Even if spherical particles have much smaller rotational velocities, it is important to know what effect they have on the drag coefficient.

[1]*Manuscript received April 7; accepted June 1, 1960.*
[2]*McGill University and Pulp and Paper Research Institute of Canada, Montreal, Que.*

The rotation can be resolved into directions perpendicular and parallel to the air flow direction. The rotation with the axis parallel to the flow is referred to as "screw motion", and it is a far less common occurrence than the second type, which has been called "top spin". The latter is brought about by collision with duct surfaces and particles going at different velocities, as well as the radial velocity gradients which predominate in the wall region. It includes rotation about all possible axes perpendicular to the air flow direction.

Top Spin Rotation

The aerodynamics of a spinning sphere have been little investigated. Most of the observations have been made on spheres mounted in air tunnels, and the Reynolds Number region involved has therefore been restricted to large values. These results are valuable, however, since they offer qualitative indications of the possible effect of rotation on the drag coefficients at lower Reynolds Numbers. Observations at lower Reynolds Numbers would have to be taken with freely moving bodies which would be extremely difficult since relatively small angular velocities would cause the particle to veer considerably from the rectilinear path necessary for the photographic measurement of the rotation.

One of the first and best instrumented measurements on sphere rotation was made in 1928 by Maccoll[8] who reported tests made in a 2-ft. × 2-ft. air duct on a 6-in. sphere spinning on an axis perpendicular to the air stream. These showed that at Reynolds Numbers of 6.15×10^4 to 10.70×10^4, C_D fell slightly from 0.52 to 0.48 as the ratio of the equatorial speed U_p to the wind speed U_o increased from 0 to 1 (see Figure 1). It then increased to 0.6 when the ratio reached a value of 2, and it remained fairly constant thereafter.

More recently, Davies[9], investigating the dynamics of golf balls, obtained results with smooth spinning spheres dropped into a wind-tunnel flow. Sufficient information was given to allow the authors of the present survey to calculate the drag coefficients, and these have been included in Figure 1. Although the drag values for the stationary case are lower than those given by Maccoll, they are well within the usual scatter reported in this Reynolds Number region. The results, although limited, seem to confirm that for large Reynolds Numbers top spin will have little effect on the drag coefficient for the spin velocities expected in most solids-gas systems.

More complete studies of the effect of top spin on drag are available for the simpler two-dimensional cylinder case. Experimental measurements of the effect of rotation were first obtained by Lafay[10,11,12] and then followed by those of Reid[13], Betz[14], Prandtl[15], Ackeret[16], Relf and Lavender[17], Thom[18,19,20,21,22,23], and Busemann[24]. The most recent study available was reported by Swanson[25] and the drag coefficients he obtained are shown in Figure 2. Although the rotation seems to have more of an influence on the drag of the cylinder than it did in the sphere studies, it still required rela-

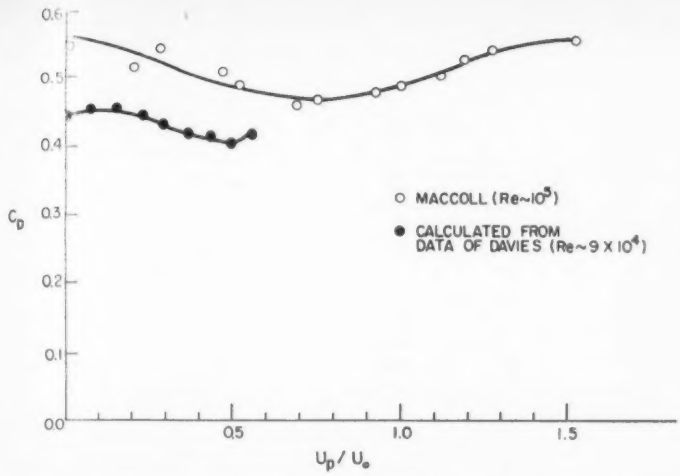

Figure 1—The effect of top spin rotation on the drag coefficients of spheres.

tively high spinning to have an appreciable effect in the subcritical Reynolds Number region. In the critical region, the rotation caused an earlier laminar-turbulent transition mainly by increasing the effective relative velocity between the surface of the cylinder and the free stream. This could become important in solids-gas systems if the upper critical Reynolds Number has been lowered because of the relative free stream turbulence, so that high rotation rates would in this case cause an even further drop in the Reynolds Number for transition.

The theoretical investigation of top spin rotation is again hampered by the presence of the non-linear terms in the Navier-Stokes equations which, as was previously shown[1], prevent solutions for the non-rotating system. Lamb[26] and Oseen[27] have provided solutions for stationary spinning spheres and cylinders respectively, by ignoring the inertia terms. Garstang[28] and later Drazin[29] using the Oseen approximation were able to prove that for low Reynolds Numbers and for systems in which the inertia terms are not of great significance the rotation would have no effect on the drag of a moving sphere or cylinder. Analysis at higher Reynolds Numbers have been attempted by Bickley[30], Gustafson[31] and Krahn[32], but the complete solution for this system cannot be expected until it has been accomplished for the non-rotating case.

Screw Motion

Although pure screw motion will rarely exist in solids-gas systems, it will probably occur as a component of the generalized rotation and its possible effects on the particle dynamics are therefore of interest.

Wieselsberger[33] studied the effect of rotation on fixed bodies spinning about an axis parallel to the air stream. These were performed with (a) a projectile shape 120 mm. in diameter and 526 mm. in length, (b) a cylinder 120 mm. in diameter and 364 mm. in length, and (c) a disk 150 mm. in diameter and 3-mm. thick. Wieselsberger was therefore able to investigate the effect of rotation on bodies in which either skin friction drag or form drag was predominant. He expressed his results as:

$$C_D = C_{DO} + \Phi C_D' (U_p/U_o) \quad \ldots\ldots\ldots\ldots\ldots\ldots (1)$$

Results are given for U_o = 28 m./sec., and for (U_p/U_o) ratios of from 0 to 3. He found that for shape (a) there was little change till $(U_p/U_o) = 0.5$, but at $(U_p/U_o) = 2$, C_D increased twofold. For (b) there was no increase until $(U_p/U_o) = 1.5$ and then there was a gradual increase of C_D from a value of $C_D = 0.84$ at $(U_p/U_o) = 1.5$ to a value of 0.92 at $(U_p/U_o) = 3$. For (c) the effect of rotation was negligible. Wieselsberger concluded that the influence of this type of rotation was of importance only with long slender bodies. It diminished as the form drag became predominant so that for a sphere it would cause only a slight increase of C_D at large values of (U_p/U_o).

Luthander[34] measured the drag coefficients for spheres under-going screw motion in the region of the critical Reynolds Number. Below transition, (U_p/U_o) ratios of up to 2 had very little effect on C_D, thus confirming the tendencies noted in Wieselsberger's work. There was a more noteworthy effect on the critical Reynolds Number only at high (U_p/U_o) values,

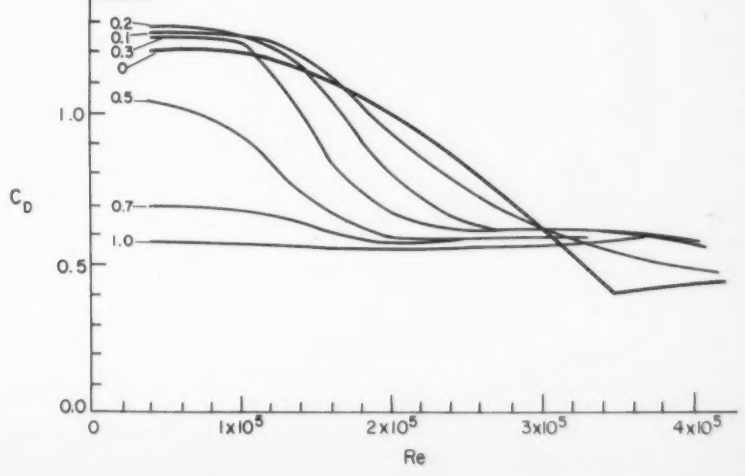

Figure 2—The effect of top spin rotation on the drag coefficients of cylinders (Swanson).

but it remained essentially unchanged up to values of 1.4.

Garstang[28] and Drazin[29] studied analytically the effects of screw motion for low Reynolds Number systems, and again found that the Stokesian drag would remain unaffected. Schlichting[35] provided an explanation of the very complex three-dimensional effects in the boundary layer of rotating bodies of revolution in axial flow for both laminar and turbulent boundary layers. In some cases, drag and torque were calculated, and these indicated increased drag as the rotational velocity was increased. The calculations could not give the entire drag evaluation because of the usual inability to deal with the wake region.

Howarth[36] discussed the laminar flow in the boundary layer about a sphere rotating in a fluid at rest. He found that the fluid was forced from the poles towards the equator, but the mathematical solution which he presented was invalidated by the interaction with the flow from the other hemisphere which made it impossible to use the boundary layer equations. Howarth showed mathematically that for an infinite cylinder rotating in a stream, the drag would be unaffected by rotation.

Burgers[37] considered the effect of centrifugal force on boundary layer flow. The considerations were limited, however, to the case where the motion outside of the boundary layer is free from separation effects and the application of this analysis to the case of a sphere is difficult.

Illingworth[38] recently calculated the skin friction force for a body of revolution in the early stages of suddenly-initiated (and subsequently constant) screw motion about the axis of symmetry. The dependence of the separation of the boundary layer of a sphere on such motion was determined as a function of time. The equations for the longitudinal and transverse components of the skin friction for the sphere are given as:

$$\tau_x = 0.84625\,(\mu\rho_o/\theta)^{1/2}U_o \sin(x/r)\,[1 + \{(2.3634 + 0.48451\beta\cos(x/r)\}\,\xi - \{-(0.17955 + 0.00759\beta)\sin^2(x/r) + (0.48844 + 0.32360\beta)\cos^2(x/r)\}\,\xi^2 + \ldots.]\ldots(2)$$

$$\tau_z = 0.56419\,(\mu\rho_o/\theta)^{1/2}\omega r \sin(x/r)\,[1 + \{1.2732\cos(x/r)\}\,\xi + \{(0.1077 - 0.01826\beta)\sin^2(x/r) + (8.2548 + 0.16698\beta)\cos^2(x/r)\}\,\xi^2 + \ldots.]\ldots(3)$$

Illingworth stated that rotation will impart a centrifugal acceleration to the fluid elements near the surface of the body, which in turn produces a favorable contribution to the pressure gradient upstream of the maximum section of the body, and an adverse contribution to the gradient downstream of this section. The effect of increasing the spin would seem to move the position of separation nearer to the maximum section of the body. Although this would increase the total drag value, this increase would be insignificant for low spin rates. The effects on the heat and mass transfer of the rotation may be more pronounced since they are more directly linked to the skin friction.

The Effect of Rotation on Linearity of Motion of a Particle

Although rotation may not be an important consideration for the drag coefficient, the question of its being a vital part in the mechanism of particle entrainment into a fluid stream is still in doubt. It is often felt that if the velocity field about a sphere is not uniform, there will be a tendency for the body to migrate from the low velocity to the high velocity region. This tendency has been observed by Tollert[39] who found that the concentration of spherical particles in laminar pipe flow was as much as 25% greater at the axis as compared with the wall section.

The difference in concentration may be due to the velocity gradient in the stream; it may also result from the rotation of the body. The friction force of the sphere rotating with top spin will cause entrainment of the fluid which adds to the flow on one side of the body and decreases it on the other. This phenomenon is referred to as the *Magnus effect*, and it would tend to exert a lift force on the body in the direction of the increased flow.

This problem had been discussed as early as 1672 by Newton[40] and later by Magnus[41]. Rayleigh[42] formulated a classical hydrodynamical approach in a paper dealing with the irregular flight of a tennis ball. This has been followed by the many studies of the rotating cylinder cited previously, but a comprehensive understanding of the Magnus effect is not yet at hand. Garstang[28] and Drazin[29] have also shown that the use of the Oseen approximation does not predict the expected lift.

Maccoll[8] pointed out that early mathematical approaches to this problem have visualized the spinning sphere as producing a swirl of air in its vicinity, modifying the stream lines so as to increase the pressure on one side, and decreasing it on the other. By exploring the pressure variations in the vicinity of the sphere, Maccoll found that this is only one result of the spinning, and that the actual flow which he measured did not correspond to the mathematical treatments. He found that the velocity of the fluid on one side of the sphere was very low, but the velocity on the opposite side was only slightly above the channel speed. This may be interpreted as an indication of considerable energy dissipation in the fluid around the sphere. The flow in the front of the sphere was hardly affected by the rotation. Maccoll established the presence of a single vortex behind the sphere below the axis of rotation of the body, and he found that the air velocity in the vortex was relatively low. The lift experienced by the sphere was expressed by the following equation:

$$\text{Lift force} = (1/2)\,C_L d\rho_o\,U_o^2 \ldots\ldots\ldots\ldots(4)$$

where C_L is the *coefficient of lift*. A plot of C_L versus the ratio of the equatorial speed to the wind speed shows C_L to have initially a negative value up to a ratio of 0.5. It then rises to a positive value of about 0.3 for a ratio value of 2. Maccoll felt that there was no satisfactory explanation for this negative lift, but that it could be due to the flow type actually encountered. Similar negative lifts at low (U_p/U_o) ratios had been reported with cylinders, and this would mean that rotation would tend to discourage rather than be the causative factor for solids entrainment. Measurements taken by Fauquet[43] on a rotating sphere in the Reynolds Number region of 2×10^5 to 6×10^5 did not show a negative lift region.

Satisfactory explanations for this phenomenon have resulted from the recent studies of Krahn[32], Taneda[44] and Swanson[25]. Taneda actually photographed the tracered boundary layer flow of a spinning sphere and he found that in the critical Reynolds Number region the rotation acted to delay transition on one part of the sphere and caused it to occur prematurely on the other. This causes an asymmetry of wake structure, as observed by Maccoll, which in turn produces the negative lift region, i.e. a limited Reynolds Number range in which the lift is negative. Taneda also performed some experiments in a turbulent fluid, and Figure 3 shows the marked effect of the free stream vorticity. If the effective turbulence is further increased by having low relative velocities between the particles and the stream in stream moving at high velocities or by the very large intensities occurring near the duct surface, it may very well be that the negative lift region would occur at even lower Reynolds Numbers. This would, in this case, prevent the Magnus effect from being a mechanism of entrainment.

VII — THE EFFECT OF SURFACE ROUGHNESS ON THE DRAG COEFFICIENT OF A SPHERE

Many solids-gas systems involve particles such as catalyst carriers whose surfaces are not smooth, and it is important to know to what extent this would affect their drag behavior.

In 1916 Pannell[45] found that the resistance to motion of a 6-in. sphere was very much reduced by roughening its surface. Similar results were reported by Jacobs[46] and Flachsbart[47]. It was suggested that the roughness of the surface had caused an early transition of the boundary layer flow so that it was turbulent at relatively lower Reynolds Numbers. Figure 4 shows the results of Fage and Warsap[48] on artificially rough-

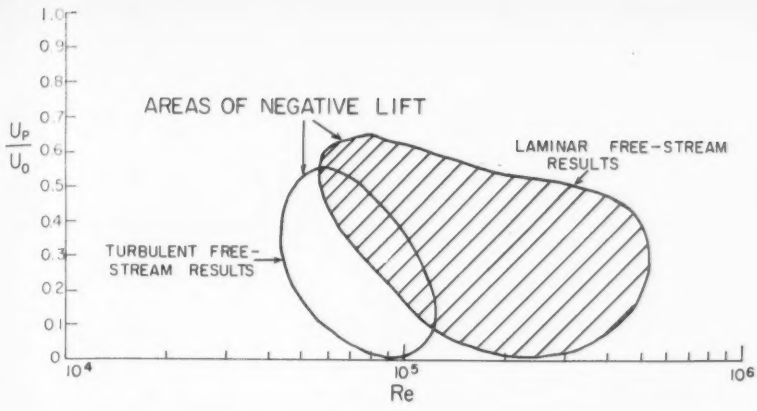

Figure 3—Regions of negative lift for spheres (Taneda).

ened cylinders, and this clearly indicates a systematic decrease of the upper critical Reynolds Number as the size of the sand grains used to produce the roughening is increased. Below a Reynolds Number of 2×10^4 there does not seem to be any roughness effect. Actually, if the grain size were increased further, it would be more proper to consider the bluff body as an irregular shape. Similar experiments were performed by Hoerner[49] with spheres, and very similar results were obtained.

Wadell[50] and Johnstone, Pigford and Chapin[51] instinctively felt that the influence of roughness on the drag coefficient was a minor one for subcritical Reynolds Numbers. Direct wind-tunnel measurement of the effects of roughness cannot be obtained for low particle Reynolds Numbers, but this view would seem to be upheld by the extrapolation of the available wind-tunnel data.

Miller and McInally[52], on the other hand, found that roughening of a sphere surface decreased its fall velocity at low Reynolds Numbers by as much as 90%, and its resistance behavior approached that of a cube. These results were therefore in direct contradiction with those previously mentioned, since they represented an increase in resistance.

The effect of surface irregularities may be dependent on the state of turbulence of the fluid. Flachsbart[47,53] found that for a very low turbulence stream, he could effect a drastic reduction in the critical Reynolds Number by mounting a fine (0.0008-in. diameter) wire ring on the surface of a sphere in front of its equator. He found surprisingly that if the air stream was made very turbulent by the use of screens, the ring would no longer cause a reduction in drag, but, on the contrary, would increase the overall resistance. Very high relative intensities may very well cause the roughness effects to become effective at the lower Reynolds Numbers. There is therefore a distinct need for the systematic investigation of the roughness effect in combination with the other complicating variables.

A quantitative treatment of the effect of roughness is made difficult by the lack of an adequate system to define roughness.

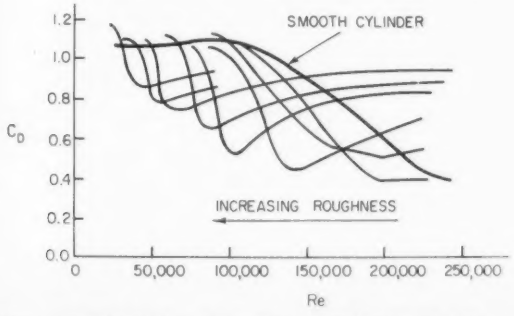

Figure 4—The effect of surface roughness on the drag coefficients of cylinders (Fage and Warsap).

Methods similar to those employed by Nikuradse[54] in his work on roughened pipe may be of value. Nemenyi[55] suggests a roughness "scale" which would depend on the shape and type of roughness protuberances in relation to the main dimensions of the body.

The possibility of a minimum value of protuberance which would affect the drag coefficient is suggested by Michelson[56]. He defines an "aerodynamically smooth" surface as one whose irregularities are completely submerged in the laminar boundary layer. He points out that since the boundary layer is very thin, an aerodynamically smooth surface is also smooth in the ordinary sense.

VIII—THE EFFECT OF PARTICLE SHAPE

The shape characteristics of a solid particle can exert a profound influence on its ability to absorb momentum from a moving fluid stream. It appears that the momentum transfer coefficients for freely moving non-spherical bodies cannot be obtained from fixed body wind-tunnel tests. In some cases the continual alterations in the body orientation can cause large changes in the boundary layer and wake structure. Discrepancies between fixed and moving drag results have also been observed with particles having a fixed orientation.

The Drag Coefficient of Regular Shapes

One of the earliest systematic studies of the fall rate of regularly shaped bodies in a fluid was recorded by Pernolet in 1851[57]. This was done with accurately machined lead shapes of equal mass consisting of spheres, cubes, discs, plates, and cylinders in a vessel six meters high. The results are inconclusive, however, because he included the period in which the particles accelerated to their terminal falling velocity. The non-spherical particles did not fall in a straight line, and their trajectories varied with their shape. This means that the drag values must vary continuously and unless accurate measurements are taken at very small distance intervals, the reported coefficients will represent gross averages only.

The advent of wind-tunnel facilities at the end of the First World War gave rise to a great many investigations in which all the drag of all manner of restrained shapes were and are still being determined. Summaries of the results are available[58,59] and a very thorough and intelligently prepared survey has recently been published by Hoerner[60]. Although these data cannot directly be applied to free movement, reference will be made to them for important pertinent information.

Burke and Plummer[61] supported lead cubes in a pipe in an upward current of turbulent air by means of a thread attached to the pan of a balance. The thread provided only partial restraint, so that the results are of some interest. Compared to a sphere of equal volume, the ratios of the resistance for cubes suspended from different points on their surface to that of the equivalent sphere were 1.7, 1.5, and 1.7 for suspension from the face, corner and edge, respectively.

Schmiedel[62] studied the settling velocities of thin circular discs moving with maximum area perpendicular to the fall. Subsequent workers recognized that the coefficient of resistance varied in a manner similar to that of a sphere, but found it difficult to assign a proper parameter to take the place of the diameter in the equations used in conjunction with the drag coefficients. Attempts were also made to reduce the coefficients to the curve obtained for spheres by the use of an appropriate *shape factor*. Towards this end Wadell[50,62] introduced the concept of *sphericity*, which he defined as the ratio ψ of the surface area of a sphere of equal volume to that of the actual particle. Since the surface of an irregular body is difficult to estimate for irregular particles, he developed another concept, the *degree of circularity* ϕ which is the ratio of the circumference of a circle having the same cross-sectional area as the irregular particle, to the actual perimeter of the latter's cross-section. He then proposed equations relating circularity to sphericity, which can be shown, however, to be only roughly approximate. Wadell was able to show that the data of Pernolet and of Schmiedel provided some evidence of the existence of a relationship between the drag coefficient and the sphericity.

Miller and McInally[52] contributed to the accumulating drag data, reporting the falling velocities of different plasticene shapes of equal volume. The trials were performed in a water tank ten feet in height and six inches square. They report little or no tendency for well-formed spheres to spin, whereas cubes would side-slip and would therefore depart from a vertical path. Rectangular prisms and long cylinders were found to fall with their axes normal to their path, and they generally maintained a more vertical motion than did the cubes. Miller and McInally obtained values for the drag coefficient, defining it by the equation:

$$\text{Resistance} = C_D L^2 \rho_o U_o^2 \quad \ldots\ldots\ldots\ldots\ldots\ldots (5)$$

where L = "wetted" diameter of the particle. The C_D values were consistently higher than those given for spheres and the data were of an exploratory nature only.

Squires and Squires[64] studied the settling of thin discs at very low Reynolds Numbers, and they confirmed an earlier Stokesian solution given by Oberbeck[65] that the resistance encountered by these shapes was given by:

(a) $8\mu U_o d$ for discs moving with the flat face perpendicular to the direction of the motion, and

(b) $5.34\mu U_o d$ for edgewise movement in the direction of motion.

This compares with a value of $3\pi\mu U_o d$ for a sphere.

Squires and Squires defined the Reynolds Number for non-spherical bodies to be given by:

$$\text{Re}_s = 4m\rho_o U_o/\mu \quad \ldots\ldots\ldots\ldots\ldots\ldots (6)$$

where m = mean hydraulic radius of particle = (projected area normal to the direction of motion/perimeter of the projected area).

At low values of the Reynolds Number it was found that bodies possessing three mutually perpendicular planes of symmetry would not change their initial orientation while falling, whatever it might be. This had previously been proved analytically by Gans[66] as a consequence of the linearity of the hydrodynamic equations of viscous flow when the inertia terms of the fluid are negligible.

Heywood[67,68] determined the settling velocities for four non-spherical shapes, for the range Re = 0.01 to Re = 1000. He proposed the following correlating factors to account for the departure from spherical behaviour:

(a) the volumetric shape factor k (sometimes referred to as the Heywood shape factor):

$$k = (\pi/6)d_s^3/d_c^3 \quad \ldots\ldots\ldots\ldots\ldots\ldots (7)$$

where d_s = diameter of a sphere with the same volume as the particle;

d_c = diameter of a circle of the same area as the projection of the particle lying in its most stable position;

(b) the area ratio = (projected area of the particle)/(area of the circumscribing circle);

(c) the prismoidal ratio = (mean thickness)/(maximum thickness).

Heywood presented his data as a plot of C_D versus Re, using k as a parameter. In the Reynolds Number region below 100, he obtained a family of parallel curves, with the highest value of C_D corresponding to the highest value of k. The curves converge and cross over at Re = 100 and then become parallel with the largest values of C_D corresponding to the lowest values of k.

The main objection to the Heywood factor is that it is not specific, so that a flat and an elongated particle can have the same shape factor. Furthermore, k cannot be justified on hydrodynamical grounds because there is no reason why, for example, a rod and a disc having the same k should give the same characteristic curve. More recently[69] Heywood stated that since minerals were mostly flat, it was the flattened value which should be applied. He did not feel that k could be employed without further modification to rod-like particles and other special shapes, and that further investigation of the correlating parameter was necessary.

Krumbein[70] investigated the fall velocity in water of seventeen forms in a 6-in. diameter lucite pipe, 6-ft. high. The particles were dropped in a random position and two feet were allowed for acceleration. The Reynolds Number region involved was above 500. Krumbein found that:

(a) sphericity is not the only factor involved in correlating the behaviour of non-spherical shapes

(b) it may be used as a first approximation as he was able to obtain a coefficient of correlation of 0.76 between the sphericity and the particle terminal fall velocity;

(c) particles falling at particle Reynolds Numbers in excess of 500 fell with their maximum cross-section perpendicular to the direction of flow.

Krumbein suggested an overall index of shape which he referred to as the "form coefficient" K, derived from the settling velocities of the particles concerned. It is given by:

K = (Actual settling velocity) / (Settling velocity of sphere of same volume) . . . (8)

This should not be confused with the *aerodynamic diameter* or *Stokes' diameter* suggested by Watson[71] and Walton[72], respectively. These are defined as the diameter of a sphere of the same density as that of the irregularly-shaped particle with a settling speed equal to that of the particle.

Particular difficulties arise in the selection of the characteristic dimension to be used in the Reynolds Number and of the area term in the drag equation. Unfortunately, there is insufficient fundamental information available to make the choice more than intuitive. Wind-tunnel data are generally correlated using the downstream length of the body for the characteristic dimension (except for flat shapes perpendicular to the flow), and the projected area perpendicular to the wind direction for the area term. The practice favoured with freely moving bodies is to use d_s for both the Reynolds Number and the drag coefficient.

Reynolds Number regions are conventionally classified into three crude groupings. A *viscous* or *Stokesian* region extends from zero to about 0.1, followed by an *intermediate* or *transition* region which extends up to about 1000. The regime above 1000 is called *Newtonian* or *turbulent*. The use of the latter term is regrettable since it often gives the impression that the particle finds itself in a turbulent stream, whereas the experiments are usually carefully confined to disturbance-free environments.

Pettyjohn and Christiansen[73] studied the free fall rates of isometric particles in all three regions of flow. Photographic methods were used to measure the settling rates in liquids of three different viscosities.

In the region Re < 0.5 there was no tendency for the particles to orient themselves in an equilibrium position. Also, the orienta-

tion did not affect the settling rates for these isometric particles. At Re ≃ 10, tetrahedrons and cubes assumed an orientation with their face in a horizontal plane. At Re ≃ 20, other particles tended to do the same, and orientation was maintained until a Reynolds Number region of 70 to 300 was attained, where particles, starting with tetrahedrons, wobbled, spun, and then followed a spiral vertical path. The drag coefficient increased abruptly with the onset of spinning, and it eventually became constant. It was noted that some particles started spinning at lower Reynolds values than did others of the same shape, and this produced a considerable scatter of data in the transition region.

Pettyjohn and Christiansen found that for Re < 0.05, Stokes' Law may be applied with an accuracy of ± 2% if the correction factor K was employed. K was found to be given as equal to $0.843\ ln\ \psi/(0.065)$. For the region Re = 2000 to Re = 200,000 the following equation was found to be valid within an accuracy of ± 4%:

$$U_o = \sqrt{(4/3)gd_p\,(\rho - \rho_o)\,/\,(C_D\rho_o)} \quad \ldots\ldots\ldots\ldots (9)$$

where $C_D = 5.31 - 4.88\psi$. Heywood's shape factor did not seem to be a good criterion of the effect of shape on C_D since no apparent relationship resulted between k and C_D, especially at high Reynolds Numbers. Pettyjohn and Christiansen concluded that sphericity is a good criterion of the effect of particle shape on resistance.

Very recently Chowdhury and Fritz[74] reported a study which seemed to repeat the work of Pettyjohn and Christiansen. Although they made no mention of the latter, they proposed a relationship for the viscous region which is in effect identical to that given by the earlier work. Their results for the high Reynolds Number region again agree closely with the Pettyjohn and Christiansen relationship except at the low sphericity values.

Barker[75], a student of Christiansen, sought to extend the particle spectrum investigated by the latter to encompass non-isometric shapes. He made use of a comparatively accurate photoelectric technique which utilized the light reflected from a particle as it passed the fields of view of two photomultiplier cells[76], and it was found to be superior to the photographic methods used by previous workers, which were said to be subject to error when the line of fall of the particles was not vertical. Referring to some of Christiansen's unpublished data, Barker showed that drag coefficients obtained for discs and cylinders having the same sphericities as cubes did not coincide as would be expected if sphericity were a good criterion. Furthermore, he felt that the work of Christiansen[77], Blizard[78] and Richards[79] had indicated a dependence on particle density other than that accounted for by the Reynolds Number. Barker decided, therefore, to study the effect of shape with bodies of varying density in liquids varying in density from 1.13 to 8.3 g./cc. in a region which was restricted to large Reynolds Numbers.

An interesting behavior of the particles in motion was noted. Spheres were found to wobble from side to side (1-in. maximum wobbling reported with a 1-in. sphere) and the deviation from the vertical path was random. Flat shapes fluttered but went straight down and only the heavier shapes spun about an axis in the plane of the flat surface. In one case, a particle would spin sometimes and flutter at others. The average velocity when fluttering occurred was found to be 5% higher than for spinning. Long shapes had the following characteristics: cylinders followed a vertical path except that their oscillation was of a greater amplitude than for shorter cylinders; the square, hexagonal and triangular prisms went down a wide spiral trajectory. Trials were also attempted in a 455-ft. smoke stack, but the major portion of the results had to be discarded because steady state conditions could not be attained.

The works cited previously did not attempt to relate the gyrations which the particle would perform during its movement to the momentum transfer, although it would be expected to exert an important influence. Barker assumed that the tendency for a particle to spin was directly proportional to the applied force couple, and inversely proportional to the moment of inertia and he felt that these were bound to affect the drag. This reasoning was incorporated into a dimensional analysis which produced the relationship:

$$C_{DB} = (\rho/\rho_o)^n\,(d_{min}/d_{max})^m\,\Phi\ \mathrm{Re} \quad \ldots\ldots\ldots\ldots (10)$$

where n, m and Φ are experimentally determined.

Barker initially employed the actual projected area of the solid as it fell, and the length of the body in the direction of motion, as his values for the area and diameter in the calculation of the drag coefficient. He found that the curve for $\psi = 0.67$ crossed over the curve for $\psi = 0.806$ at Re = 2,700 in the case of lucite, and at Re = 6,600 for the case of steel, although the intersection could be expected to occur at the same Re value if the Reynolds Number was properly defined. He then employed the length of the cylinder instead of the longest projected length in the direction of fall, and then the intersections did occur at the same Reynolds Number and this method was considered best for the purpose of correlation. The area term A, used for the calculation of C_D was the projected area of an equivalent sphere for the isometric particles, and the projected area of the particle perpendicular to flow for the non-isometric particles.

The results obtained for a wide variety of shapes are plotted in Figures 5, 6 and 7. The low scatter seems to confirm Barker's method of correlation for this Reynolds Number region. Figure 8 clearly shows the previously-overlooked influence of the density ratio on the drag coefficient. This complication is probably of little importance in the intermediate and low Reynolds Number regions where settling has been observed to be steady.

The drag results for non-isometric particles at low and intermediate Reynolds Numbers are of special interest since they are often of direct use in practical systems in which the fluid is laminar. McNown and Malaika[80,81] systematically studied the settling of non-isometric particles in these regions with axisymmetrical particles which were symmetrical about three mutually perpendicular planes. These included circular cylinders, double cones, square prisms and spheroids. Here again the particles were stable in any settling position below Re = 0.1 and in the region 0.1 < Re < 500 they settled with the largest cross-section in the three mutually perpendicular planes oriented perpendicular to the motion. The runs in the low Reynolds Number region were initiated with the particles oriented in their manner of settling for the intermediate runs. McNown and Malaika also evaluated the Oberbeck integrals for spheroids settling along a principal axis, and found close agreement between their experimental results at low Reynolds Numbers and the theoretically-derived ones by approximating the actual shapes with their spheroid counterpart. For the Stokesian regime, K (the ratio of the actual settling velocity to the velocity of a sphere of equal volume) was closely approximated by the relationship:

$$K_s = \frac{\alpha''\beta''}{(0.811/\xi^{1.50}) + 0.189\beta''} \quad \ldots\ldots\ldots\ldots (11)$$

For the entire range investigated, it was found that particles with the same a/s ratios had the same drag coefficient. (a is the particle length perpendicular to the largest circle or square cross-section and s is the diameter of the maximum cross-section or side of square base of a square prism). This indicates that sphericity cannot be used as an aerodynamic criterion with non-isometric particles for all regimes of flow.

Pramanik[82,83] extended the investigation to deal with triaxial particles, i.e. a, b, and c, the smallest, intermediate and largest semiaxes of the ellipsoids approximating the particles respectively are all different (in the previous study $b = c = s$). The results in the Stokesian range showed very good agreement with Equation 11. If a is the semiaxis in the direction of motion, it was found that the variation of K with the Reynolds Number

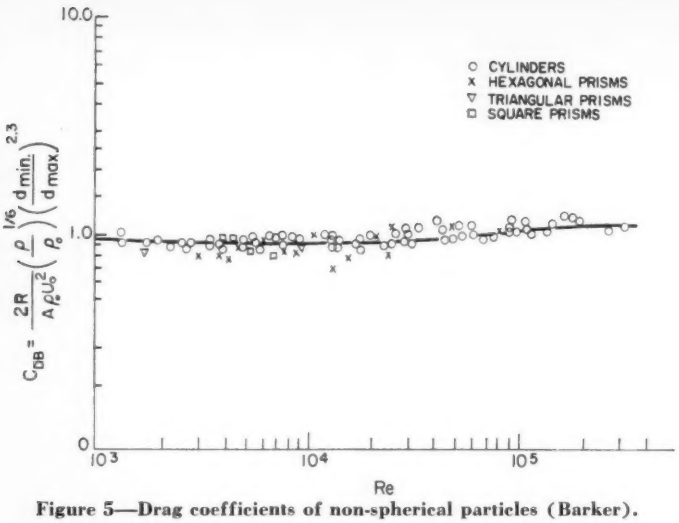

Figure 5—Drag coefficients of non-spherical particles (Barker).

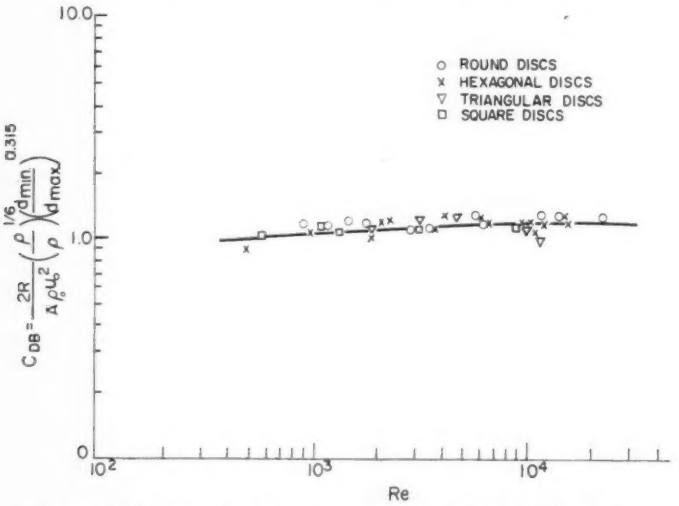

Figure 6—Drag coefficients of non-spherical particles (Barker).

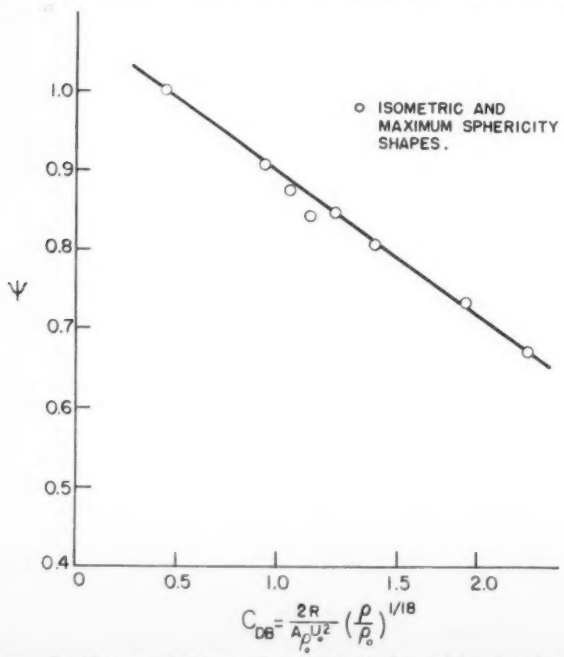

Figure 7—Drag coefficients of non-spherical particles (Barker).

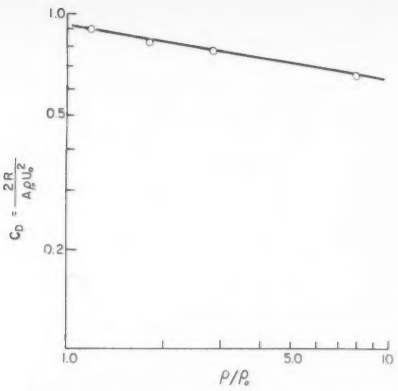

Figure 8—The effect of the fluid to solids density ratio on the drag coefficients of cylinders (Barker).

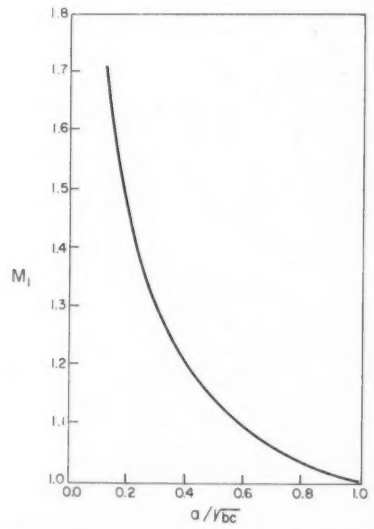

Figure 9—M_1 as a function of $a/\sqrt{bc}$ (Presler).

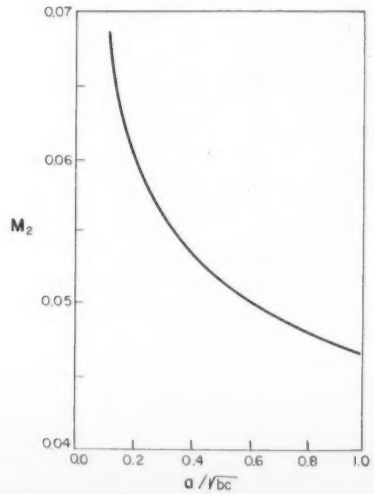

Figure 10—M_2 as a function of $a/\sqrt{bc}$ (Presler).

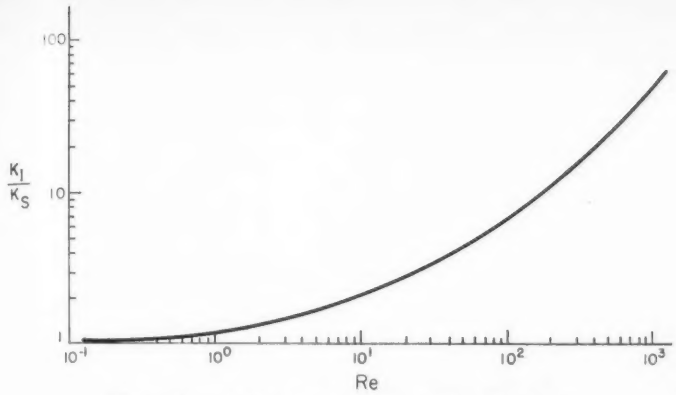

Figure 11—K_I/K_S as a function of *Re* (Presler).

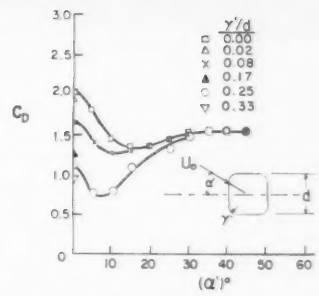

Figure 12—The effect of edge roundness and orientation on the drag coefficients of square cylinders (Polhamus).

was almost a unique function of $a/\sqrt{bc}$, with the b/c ratio being a noticeable but secondary effect.

Presler[84] using the experimental data of Malaika and Pramanik has developed a convenient generalized method for calculating particle drag coefficients for the Stokesian and intermediate range. Assuming that K_s can be determined by assuming the particle resistance is equal to the resistance of an ellipsoid of equal dimensions, he derived it theoretically for ellipses of full range of semiaxis values by using the Oberbeck integrals. K_s is obtained from the relation:

$$K_s = M_1 + M_2 (b/c - 1) \quad \ldots\ldots(12)$$

where M_1 and M_2 are analytical coefficients.

M_1 and M_2 are given graphically from the solutions as functions of the ratio $a/\sqrt{bc}$ and are shown in Figures 9 and 10. For the intermediate Reynolds Number region, Presler found it convenient to use an overall Stokes Law velocity correction factor K_I. He determined the ratios of K_I to K_s from the experimental data and these are given in Figure 11 as a function of

$$\mathrm{Re} = \frac{d_p U_o \rho_o}{\mu}.$$

The fact that the K_s values were calculated from the Oberbeck integrals by assuming the maximum particle area being perpendicular to the flow does not affect K_I, since they will settle with that orientation in the intermediate region. This is not necessarily the case in the Stokesian region, and the effect of orientation at very low Reynolds Numbers was investigated by Heiss and Coull[85] with particles which had one of the three mutually perpendicular axes equal in length. Their results compared favorably with solutions to the Oberbeck integrals given by Gans[66] for ellipsoids of revolution (i.e. spheroids since $b = c$). For orientations where the circularity of the projected area varies with different shape, their results were approximated by:

$$\log_{10}(K_s) = -0.25\left(\psi \frac{d_p}{d_n}\right)^{1/2}\left(\frac{d_p}{d_n} - 1\right) + \log_{10}\left(\frac{d_p}{d_n}(\psi)^{1/2}\right) \quad \ldots\ldots(13)$$

and in orientations where the circularity is constant and remains unaltered by changing shape:

$$\log_{10}(K_s) = \frac{-0.27}{(\psi)^{1/2}\left(\frac{d_p}{d_n}\right)^{0.348}}\left(\frac{d_p}{d_n} - 1\right) + \log_{10}\left(\frac{d_p}{d_n}\right)^{\psi^{1/2}} \quad \ldots(14)$$

where d_n = diameter of circle of area equal to projected area. Ludwig[86] investigated the fall of discs and cylinders and also found a marked dependency on $a/\sqrt{bc}$, but the simple relationships which he obtained are specific to his limited data.

Becker[87] has recently proposed an overall solution to the shape problem by developing what he terms a quadric resistance "law". In an analogue to Budryk's unsuccessful pseudo-theoretical treatment for spheres (as discussed in Reference 1), he feels that the total drag force on a particle, R, is made up of a viscous term R_V and an inertia term R_I (these are not to be confused with the skin friction drag and the form drag respectively). i.e.

$$R = R_V + R_I \quad \ldots\ldots(15)$$

Becker feels that this is a consequence of the Navier-Stokes equations containing both viscous and inertia terms, so that the solutions should contain additive viscous and inertia terms. At low Reynolds Numbers the inertia terms (which would be represented by R_I) are to be neglected and at high values the viscous terms, represented by R_V, are held to be ineffectual. Presumably, the intermediate region is found by adding the two terms. Although Equation (15) may have some use as a correlating device, the implied connotation is conceptually incorrect. Although it is true that the overall drag at a high Reynolds Number is proportional to the square of the velocity, it is incorrect to say that viscous forces play no part in determining the drag. Were it not for viscosity, then the inviscid flow equations would be valid, and these would of course predict zero drag. In the intermediate zone, the equation governing the drag at very low Re values would be altered by the inertial effects. For the particle "viscous drag force", Becker uses the equation:

$$R_V = \frac{\pi}{8} C_V \mu U_o d_a \quad \ldots\ldots(16)$$

where the coefficient C_V is a function of the form sphericity $\phi = \pi d_p^2/4A_n$, A_n being the area of the particle perpendicular to the motion. C_V is evaluated from the results at very low Re but is supposedly independent of the Reynolds Number. In the intermediate region, R_I is obtained by subtracting the value of R_V calculated from Equation (16) from the overall experimentally determined one. An *inertial drag coefficient*, C_I, is defined by the equation:

$$R_I = (1/2)\, C_I A_s \rho_o U_o^2 \quad \ldots\ldots(17)$$

where A_s is the area projected by a sphere with the same surface area as the shape. Plots of C_I versus Re for the region $10^{-1} <$ Re < 10 for isometric bodies show a large scatter (as compared to the good correlation for all shapes cited previously). Even more important, they point out the theoretical weakness of Becker's argument, since the inertia coefficients lie below the curve for spheres, whereas the effect of shape – particularly when the particles fall with their maximum cross-section perpendicular to the flow – must be to increase the inertial effects in the flow about the body.

At Reynolds Numbers greater than 1,000, C_I becomes

equivalent to $C_D\psi$, if the area term is the projected area of a sphere of equal volume. He suggests that C_I can be calculated from the sphericity ψ by the equation

$$C_I = 2.25 + 0.283\,(1 - e^{2\psi}) \quad \ldots\ldots\ldots\ldots\ldots\ldots (18)$$

Becker seems to have overlooked the works of Barker, Presler and Pramanik. The authors of the present survey have compared their experimental data with those predicted by Becker's correlations and have found the latter to be inappropriate for non-isometric bodies, particularly if they are prolate or oblate.

Particle Edge Effects

The edges of the particles used in most of the free-fall experiments were usually sharp, whereas the solids in multi-particle systems would often have their edges smoothed by attrition. There have been wind-tunnel studies made of the effect of edge roundness for large, but subcritical Reynolds Numbers and these may serve as a useful indication of what occurs in the free particle case. Polhamus[88] has recently studied the combined effect of body orientation and edge roundness with a two-dimensional square cylinder, and his results, which were presented together with pertinent data given by Wieselsberger[89] and Delany and Sorensen[58] are shown in Figure 12. It would appear that the edge roundness effect is most pronounced when the body is moving broadside-on, and in this case the drag is gradually reduced to that of a sphere, as the radius of edge roundness r' is increased. When the orientation angle α' approaches 45°, the effect of edge roundness becomes negligible. These results would have to be extended to three-dimensional shapes of different cross-section before any generalized conclusions can be drawn. Since the drag calculated for ellipsoids closely approximates the results obtained with their sharp-edged counterparts, it would seem that edge conditions would not affect the drag in the Stokesian region. This view is substantiated by Barth[90] who noted that the resistance of sharp-edged materials increased faster with increasing velocity than did that of rounded or spherical particles.

The Coefficient of Drag of Irregular Shapes

The correlation of the drag coefficients for irregular particles is difficult because of the variety of random geometric structures and surface characteristics involved. The work reported is therefore specific to the conditions and types of material studied, and only the most general qualitative behavior can be described.

Schulz[91] determined the constant settling velocity of marble, pyrite, sphalerite, quartz and coal particles, defining their shapes as roundish, longish and flat. The flat bodies have slightly higher C_D values than that given by the standard curve in the Reynolds Number region of 10 to 100. The data for cubical materials are below the standard curve at low values of the Reynolds Number, and then cross over at a value of about 60.

The resistance of coal particles was studied by Feret[92], Decaux[93], Audibert[94], Hirst[95], and Needham[96,97]. These values vary considerably, and the results seem to depend on whether the particles were balanced in an ascending fluid, or were descending through a fluid at rest.

Blizard[78] was able to correlate data for the fall rates of powdered coal and coke particles in hydrogen and air at Reynolds Numbers in excess of 1,000 by the following expression:

$$U_o = (d_p^{0.9})/(3.4\mu/\rho_o^{0.37})\,(\rho/\rho_o)^{0.44} \quad \ldots\ldots\ldots\ldots (19)$$

This expression indicates a dependence on density as did the work of Barker.

Burke and Plummer[61] suspended coke particles in a turbulent air stream and obtained the relationship:

$$U_o = 47.8\,[d_{av}(\rho - \rho_o)/\rho_o]^{0.6} \quad \ldots\ldots\ldots\ldots\ldots (20)$$

where d_{av} = particle mean diameter. The relationship obtained from the data of Martin[98] for air velocities required to support various sizes of crushed quartz grains is identical in form, but with a coefficient of 50.9. Both expressions are for Reynolds Numbers greater than 500.

TABLE 1

DRAG COEFFICIENTS FOR VARIOUS SHAPES

Re	Spheres	Coal, Anthracite, Sandstone and Pyrites	Shale
10	1.5	3.6	3.6
100	0.4	1.2	1.6
1,000	0.35	1.2	1.7
10,000	0.35	1.3	1.8

Miller and McInally[52] found that the data for coal, anthracite, sandstone and pyrite particles all fell (within the experimental error) on the same curve. The values for shale followed the same curve up to a Reynolds Number of about 100 and then C_D became larger for the flat shale particles than it did for the rounded-off or cubical particles, and it seemed to increase slightly with increased Reynolds Numbers, as shown in Table 1.

The data of Prockat and Linsel[99] and also Rosin and Kaiser[100] for various types of coal, show the C_D values for these irregular particles to be lower than that given for spheres, for Reynolds Numbers less than 100, in contradiction to the above results.

The proper definition of the diameter of an irregular particle which should be used in the definition of the Reynolds group in the drag coefficient relationship is difficult to establish. Eirich[101] has shown that porous or indented spheres carry along some of the fluid through which they pass. This led him to believe that the outer outline of an irregular particle is the one which has the most hydrodynamic significance, because the retained fluid acts as part of the particle. Hawksley[102] feels that the drag of non-spherical and rough particles is governed by the size of the enveloping surface and he suggests as a convenient approximation the use of a *drag diameter* which would be the diameter of a sphere having the same external surface area as the particle. He feels that the drag diameter would be the more fundamental quantity when compared with *Stokes' diameter* discussed earlier.

Guruswamy and Roy[103] have defined the Reynolds Number of irregularly shaped particles as:

$$\mathrm{Re} = (V^{1/3}U_o\rho_o)/(\mu) \quad \ldots\ldots\ldots\ldots\ldots\ldots (21)$$

where V is the volume of the irregular particle. They were able to correlate the settling rates of irregular coal particles with a plot of K versus ψ.

Brownell, Dombrowski and Dickey[104] have prepared a plot of sphericity versus bulk porosity to facilitate the measurement of the *effective* particle area and volume for complex particle shapes. Nichols and Gauvin[105], however, have shown this plot to be very inaccurate.

The problem of classifying irregular particles with an aerodynamically meaningful shape parameter must be overcome before any order can be brought into the determination of the drag coefficients of naturally-occurring particles. Sedimentary petrologists are immediately concerned with shape characterization since it is closely related to many geological phenomena, and pertinent information from this field of specialization has been discussed by Marchildon[106]. Wadell[107] had, in addition to his sphericity and circularity concepts, defined several others which may be of some use. He described a laborious but significant method of classifying the "roundness" of a particle by reproducing it as a camera lucida drawing and measuring the various radii of curvature of the plane cross sections. The roundness would be quantitatively obtained from maximum plane cross-section by measuring the average corner radius and dividing it by the radius of the largest inscribable circle. Wadell also defined an operational sphericity ψ_{op} to be used in approximating the difficulty measured ψ, and it is given by:

$$\psi_{op} = \left(\frac{\text{Particle Volume}}{\text{Volume of smallest circumscribing sphere}}\right)^{1/3} \quad \ldots\ldots (22)$$

TABLE 2

b/c	a/b	Shape Classification
> 2/3	> 2/3	Sphere-like
> 2/3	< 2/3	Disc-like
< 2/3	> 2/3	Rod-like
< 2/3	< 2/3	Blade-like

Nichols[105] found that ψ_{op} cannot be considered equivalent to ψ. An approximation ϕ to the previously described circularity ϵ was defined as the ratio of the diameter of a circle of equal area to the diameter of the smallest circumscribing circle. Wadell felt that ϕ would be a good approximation to ψ_{op} for roughly equi-axial particles only, and Pye and Pye[108] confirmed it to be a poor approximation for other particles, since it is impossible to get a three-dimensional evaluation of an object from a two-dimensional measurement.

Zingg[109] proposed a rough shape classification, using the three mutually-perpendicular axes a, b and c (as previously defined for the ellipsoid) and these are employed as in Table 2. From the results cited previously with regular shapes, this may prove to be a valuable supplement to the ψ characterization. Cailleux[110] defined a *flatness factor* F, given by:

$$F = \frac{b + c}{2a} \qquad (23)$$

and a *roundness ratio* R_c, given by:

$$R_c = \frac{2\,(\text{Radius of sharpest corner})}{\text{Longest diameter}} \qquad (24)$$

Von Andel, Wiggers and Maarleveld[111] feel that ψ, the Wadell roundness and the Zingg critera are as easy to measure and more relevant than F and R_c. Plots of ψ_{op} as a function of a/b and b/c have been calculated by Krumbein[113] who assumed ellipsoid shapes.

Recently Aschenbrenner[112] obtained an approximation to ψ (which he called the *working sphericity* ψ_A) in terms of a, b and c by assuming the particles to have the shape of a tetrakaidecahedron. It is defined as 0.955 times the ratio of the surface area of an orthotetrakaidecahedron having the same volume as a tetrakaidecahedron, used for the approximation to the surface area of the tetrakaidecahedron. He found ψ_A to be a better approximation to ψ than was ψ_{op}, especially at low ψ values.

Krumbein[113], Powers[114] and Rittenhouse[115] have each offered very approximate visual means of characterizing particles by publishing illustrations of solids having various roundness and sphericity values.

The significance of the various shape parameters discussed cannot be properly assessed until systematic drag experiments are performed with the many varieties of irregular shape which occur. It may very well be that some of the parameters which are extremely difficult to measure may not exert a noticeable influence in the overall momentum transfer.

In all the investigations reported with freely moving bodies, the particles assumed an orientation which was dictated by the aerodynamical processes occurring in its boundary layer and wake. In actual multiparticle systems, frequent collisions with adjacent particles would discourage the establishment of preferred orientation, and it would most likely become random. The same may be expected to result from free-stream velocity gradients or turbulence, this being supported by high-speed motion studies by Pasternak[7,116]. Although it would require subtle experimental techniques, it is vitally important that drag determinations be made with single shapes under conditions which are more closely associated with the fluid parameters which are characteristic of multiparticle systems. This is presently being attempted in these laboratories by Marchildon[106].

Acknowledgments

The authors wish to express their appreciation for the continued assistance given to them by Librarians A. Finnemore and L. Lefebvre of the Pulp and Paper Research Institute of Canada, and P. Keir of McGill University, in obtaining the many papers reviewed in this series. L. B. Torobin is indebted to the Scientific Research Bureau, Trade and Commerce Department, Province of Quebec for three consecutive fellowships in support of his research program.

Nomenclature

Any consistent set of units may be employed. Those listed are merely illustrative.

a = particle length perpendicular to largest circle or square cross-section, ft.
a,b,c = shortest, intermediate and longest axis respectively of a triaxial particle, ft.
A = projected area of sphere of volume equal to that of the particle, ft.^{2}
A_n = normal projected area relative to motion, ft.^{2}
A_r = area projected by a sphere with same surface area as particle, ft.^{2}
A_t = tangential area of particle relative to motion, ft.^{2}
C_D = total particle drag coefficient, dimensionless.
C_{D_R} = total particle drag coefficient, dimensionless, Equation (10).
C_D' = empirical rotation drag coefficient, dimensionless, Equation (1).
C_{DO} = drag coefficient for zero rotation, dimensionless.
C_L = coefficient of lift, dimensionless, Equation (4).
C_I = Becker "inertial drag" coefficient, dimensionless, Equation (18).
C_V = Becker "viscous drag" coefficient, dimensionless, Equation (16).
d = cylinder or sphere diameter, ft.
d_{ap} = arithmetic mean diameter, ft.
d_a = diameter of sphere of equivalent surface area, ft.
d_c = diameter of circle of same area as projection of particle lying in its most stable position, ft.
d_{min} = minimum body length, ft.
d_{max} = maximum body length, ft.
d_n = diameter of circle of area equal to projected area of particle, ft.
d_p = diameter of sphere of equivalent volume, ft.
F = flatness factor = $(b + c)/(2a)$, dimensionless.
k = Heywood spape factor = $(\pi/6)d_p^2/d_c^2$, dimensionless.
K = U_o/U_{os}, dimensionless.
K_I = Presler empirical velocity correction factor, dimensionless.
K_s = U_o/U_{os}, for Stokesian region only, dimensionless.
L = wetted diameter of particle, ft.
m = mean hydraulic radius, ft.
M_1 = analytical coefficient, dimensionless.
M_2 = analytical coefficient, dimensionless.
r = sphere radius, ft.
r' = radius of edge roundness, ft.
R = total drag force, lb. force.
R_c = roundness ratio = $\dfrac{2\,(\text{Radius of sharpest corner})}{\text{longest diameter}}$, dimensionless.
Re = Reynolds Number, dimensionless.
Re_s = $4m\rho_o U_o/\mu$, dimensionless.
R_I = Becker "inertial drag", dimensionless.
R_V = Becker "viscous drag", dimensionless.
s = diameter of maximum cross-section or side of base of a square prism, ft.
U_o = mean velocity of particle relative to fluid, ft./sec.
U_{os} = velocity of sphere of equivalent volume calculated from Stokes' Law, ft./sec.
U_p = peripheral velocity of particle surface relative to fluid, ft./sec.
V = volume of irregular particle, ft.^{3}
x = downstream distance, ft.
α' = angle of incidence of flow, degrees.
α'' = "normal factor" = A_n/A, dimensionless.
β = $\omega^2 r^2/U_{os}$, dimensionless.
β'' = tangential factor, Equation (11), dimensionless.
θ = time from beginning of motion, seconds.
μ = fluid viscosity, lb./(sec.) (ft.).
ρ_o = fluid density, lb./ft.^{3}
ρ = particle density, lb./ft.^{3}
τ_x = longitudinal component of skin friction, lb. force/ft.^{2}
τ_t = transverse component of skin friction, lb. force/ft.^{2}
ϕ = form sphericity = $\pi d_p^2/4A_n$, dimensionless.
ϵ = circularity = (circumference of circle having the same cross-sectional area as irregular particle)/(perimeter of particle cross-section).
ω = angular velocity, radians/sec.
Φ = functional operator.

ξ = $U_t\theta/r$, dimensionless.
ψ = sphericity = (surface area of sphere of equal volume)/(surface area of actual particle).
ψ_A = (0.955) (surface area of an orthotetrakaidecahedron having the same volume as a tetrakaidecahedron used for approximation)/(surface area of tetrakaidecahedron), dimensionless.
ψ_{ob} = $[(V)/(\text{volume of smallest circumscribing sphere})]^{1/3}$.

References

(1) Torobin, L. B., and Gauvin, W. H., Can. J. Chem. Eng., **37:** 129 (1959).
(2) Torobin, L. B., and Gauvin, W. H., Can. J. Chem. Eng., **37:** 167 (1959).
(3) Torobin, L. B., and Gauvin, W. H., Can. J. Chem. Eng., **37:** 224 (1959).
(4) Khudyakov, G. N., and Chukhanov, Z. F., Doklady Akad. Nauk. S.S.S.R. **78:** 681-684 (1951).
(5) Khudiakow, G. N., Izvest. Akad. Nauk. S.S.S.R., Ordel. Tekh. Nauk., **7:** 1022-1034 (1953)
(6) Gasterstadt, J., Diss. Techn. Hochsch. Dresden (1922).
(7) Pasternak, I. S., Ph.D. Thesis, McGill University (1959).
(8) Maccoll, J. W., J. Royal Aeronaut. Soc. **32:** 777 (1928).
(9) Davies, J. M., J. Appl. Phys., **20:** 821 (1949).
(10) Lafay, A., Comptes Rendus, **151:** (1910).
(11) Lafay, A., Revue de Mecanique, **30:** 417 (1912).
(12) Lafay, A., Pub. Scientifique et Tech. du Min. de L'Air, No. 78 (1935).
(13) Reid, E. G., N.A.C.A. T.N. 209 (1924).
(14) Betz, A., N.A.C.A. T.M. 310 (1925).
(15) Prandtl, L., N.A.C.A. T.M. 367 (1926).
(16) Ackeret, J., Zeits. f. Flugtech. Motorluftschiffahrt, **16:** 45 (1925).
(17) Relf, E. F., and Lavender, T., A.R.C. R. and M. 1009 (1927).
(18) Thom, A., Ph.D. Thesis, University of Glasgow (1926).
(19) Thom, A., A.R.C. R. and M. 1018 (1925).
(20) Thom, A., A.R.C. R. and M. 1082 (1926).
(21) Thom, A., A.R.C. R. and M. 1410 (1931).
(22) Thom, A., A.R.C. R. and M. 1520 (1932).
(23) Thom, A., A.R.C. R. and M. 1623 (1934).
(24) Busemann, A., Ergibnisse der Aerodynamik Versuchsanstalt zu Gottingen **4:** 101 (1932).
(25) Swanson, W. M., Ph.D. Thesis, Case Institute of Technology (1957).
(26) Lamb, H., Hydrodynamics, Cambridge University Press, London (1932).
(27) Oseen, C. W., Hydrodynamik. Leipzig (1927).
(28) Garstang, T. E., Proc. Roy. Soc., **142A:** 491 (1933).
(29) Drazin, M. P., Proc. Camb. Phil. Soc., **47:** 142 (1951).
(30) Bickley, W. G., Proc. Roy. Soc., **119A:** 146 (1925).
(31) Gustafson, T., N.A.C.A. Transl. N-25921 (1954).
(32) Krahn, E., J. Aeronaut. Sci., **23:** 337 (1956).
(33) Wieselsberger, C., Physik. Z., **28:** 84 (1927).
(34) Luthander, S., and Rydberg, A., Physik. Z., **36:** 552 (1935).
(35) Schlichting, H., N.A.C.A. T.M. 1217 (1949).
(36) Howarth, L., Phil. Mag. (7), **42:** 1308 (1951).
(37) Burgers, J. M., Proc. Koninkl. Acad. Wetenschap. Amsterdam, **45:** 13 (1941).
(38) Illingworth, C. R., Phil. Mag. **45:** 1 (1954).
(39) Tollert, H., Chem.-Ing.-Tech., **26,** No. 3, 5: 141 (1954).
(40) Newton, Sir I., Phil. Trans., **6:** 3078 (1672).
(41) Magnus, G., Abh. der Akad. der Wissensh., Berlin (1852).
(42) Rayleigh, Lord, Scientific Papers, **1:** 344 (1857).
(43) Fauquet, M. A., Comptes Rendus du Congrès des Sociétés Savantes de Paris et des Départments, Section des Sciences, 80ième Congrès, **17:** (1955).
(44) Taneda, S., Reports of Research Institute for Applied Mechanics, **5:** 123 (1957).
(45) Pannell, J. R., Adv. Comm. for Aeronautics Rep. and M. No. 190 (1916).
(46) Jacobs, E. N., N.A.C.A. T.N. 312 (1929).
(47) Flachsbart, O., Physik. Z., **28:** 461 (1927).
(48) Fage, A., and Warsap, J. H., A.R.C. R. and M. 1283 (1929).
(49) Hoerner, S., N.A.C.A. T.M. 777 (1935).
(50) Wadell, H., J. Frank. Inst., **217:** 459 (1934).
(51) Johnstone, H. F., Pigford, R. L. and Chapin, J. H., Trans. Am. Inst. Chem. Engrs., **37:** 95 (1941).
(52) Miller, W., and McInally, T. W., J. Royal Tech. College Glasgow, **3,** Part 4: 682 (1936).
(53) Flachsbart, O., N.A.C.A. T.M. 475 (1925).
(54) Nikuradse, J., Petroleum Engr., **11:** 124 (1940).
(55) Nemenyi, P., Trans. Am. Geophys. Union, **21:** 633 (1940).
(56) Michelson, I., Report No. N-71, Calif. Inst. Tech. (1950).
(57) Pernolet, V., Ann. Mines, IVème Ser., **20:** 379, 535 (1851).
(58) Delany, N. K. and Sorensen, N. E., N.A.C.A. T.N. 3038 (1959).
(59) Heddleson, C. F., Brown, D. C. and Cliffe, R. T., A.P.E.X. 299, General Electric Co. Aircraft Nuclear Propulsion Dept., Cincinnati (1957).
(60) Hoerner, S. F., Fluid Dynamic Drag, by the Author, New Jersey (1958).
(61) Burke, S. P. and Plummer, W. S., Ind. Eng. Chem., **20:** 1200 (1928).
(62) Schmiedel, J., Physik. Z., **29:** 594 (1928).
(63) Wadell, H., Physics, **5:** 281 (1934).
(64) Squires, L. and Squires, W., Trans. Am. Inst. Chem. Engrs., **33:** 1 (1938).
(65) Oberbeck, A., Crelles Jour., **81:** 62 (1876).
(66) Gans, R., Ann. Phys., **80:** 657 (1928).
(67) Heywood, H., Proc. Inst. Mech. Engrs. (London), **140:** 257 (1938).
(68) Heywood, H., Chemistry and Industry, **56:** 149 (1937).
(69) Richardson, J. E. and Zaki, W. M., Trans. Inst. Chem. Engrs. (London), **32:** 35 (1954), Discussion.
(70) Krumbein, W. C., Am. Geophys. Union, 621 (1942).
(71) Watson, H. H., Brit. J. Ind. Med., **10:** 93 (1953).
(72) Walton, W H., Brit. J. Appl. Phys. Supp., 3 (1952).
(73) Pettyjohn, E. S., and Christiansen, E. B., Chem. Eng. Progr., **44:** 157 (1948).
(74) Chowdhury, K. C. R., and Fritz, W., Chem. Eng. Sci., **11:** 92 (1959).
(75) Barker, D. H., Ph.D. Thesis, University of Utah (1951).
(76) Christiansen, E. B., and Barker, D. H., Rev. Sci. Instr., **23:** 427 (1952).
(77) Christiansen, E. B., Ph.D. Thesis, University of Michigan (1943).
(78) Blizard, J., J. Franklin Inst., **197:** 199 (1924).
(79) Richards, M., Physics Review, **22:** 122 (1921).
(80) McNown, J. S., and Malaika, J., Trans. Am. Geophys. Union, **31:** 74 (1950).
(81) Malaika, J., Ph.D. Thesis, State University of Iowa (1949).
(82) Pramanik, H. R., M.S. Thesis, Iowa State University, Iowa (1950).
(83) McNown, J. S., Malaika, J., and Pramanik, H. R., Proc. 4th Int. Assoc. for Hydraulic Research, 511 (1951).
(84) Presler, A. F., Ph.D. Thesis, Iowa State College, Iowa (1956).
(85) Heiss, J. F., and Coull, J., Chem. Eng. Progr., **48:** 133 (1952).
(86) Ludwig, J., Chemikerztg., **79:** 774 (1955).
(87) Becker, H. A., Can. J. Chem. Eng., **37:** 85 (1959).
(88) Polhamus, E. C., N.A.C.A. T.N. 4176 (1958).
(89) Wieselsberger, C., Ergb. Aerod. Versuchsanstalt zu Gottingen, Munich (1923).
(90) Barth, W., Chem.-Ing.-Tech., **26:** 29 (1954).
(91) Schulz, P., Ph.D. Thesis, Dresden-Freiburg (1914).
(92) Feret, R., Compt. rend., **172:** 575 (1921).
(93) Decaux, J., Ann. Mines Belg., **22:** 1089 (1921).
(94) Audibert, E., Ann. Mines, **1:** 153 (1922).
(95) Hirst, A. A., Trans. Inst. Mining and Met. Engrs. (London), **85:** 236 (1932-3).
(96) Needham, L. W., and Lynch, S., Trans. Inst. Chem. Engrs. (London), **23:** 93 (1945).
(97) Needham, L. W., and Hill, N. W., Fuel, **26,** No. 4: 101 (1951).
(98) Martin, G., Trans. Inst. Chem. Engrs. (London), **4:** 164 (1926).

(99) Prockat, F., and Linsel, H., Zeitschr. f.d. Berg-, Hutten-u. Salinenwes. im Preuss. Staate, 327 (1932).
(100) Rosin, P. O., Trans. Inst. Chem. Engrs., **15**: 167 (1937).
(101) Eirich, F., Repts. Progr. Phys., **7**: 329 (1940).
(102) Hawksley, P. G. W., Brit. J. Appl. Phys. Nottingham (1954).
(103) Guruswamy, S., and Roy, L. C., J. Sci. Ind. Research (India), **12B**: 270 (1953).
(104) Brownell, L. E., Dombrowski, H. S., and Dickey, C. A., Chem. Eng. Progr. **46**, No. 8: 415 (1950).
(105) Nichols, I. O., M. Eng. Thesis, McGill University (1956).
(106) Marchildon, E. K., Private Communication (1959).
(107) Wadell, H., J. Geology, **43**: 250 (1935).
(108) Pye, W. D., and Pye, M. H., J. Sed. Petr., **13**: 28 (1943).
(109) Zingg, T., Schweizer min. pet. Mitt., **15**: 39 (1935).
(110) Cailleux, A., Soc. Geol. France, Comptes Rend. (1947).
(111) von Andel, T. J. H., Wiggers, A. J., and Maarleveld, G., J. Sed. Petr., **24**: 100 (1954).
(112) Aschenbrenner, B. C., J. Sed. Petr., **26**: 15 (1956).
(113) Krumbein, W. C., J. Sed. Petr., **11**: 64 (1941).
(114) Powers, M. C., J. Sed. Petr., **23**: 117 (1953).
(115) Rittenhouse, G., J. Sed. Petr., **13**: 79 (1943).
(116) Westwater, J. W., C.E.P., **55**: 49 (1959).

★ ★ ★

Graphical-Numerical Determination of Variable Diffusion Coefficient in Solids[1]

RAYMOND C. HALL[2]

Considerable gain in information in characteristics of diffusion coefficient may be obtained if data are analysed for variable diffusion coefficient instead of for a constant value of diffusivity. This paper presents a simple method for graphical analysis of concentration gradients in solids to determine the diffusion coefficient as a function of concentration.

Consideration is given to problems encountered in extrapolation of data. It is shown that, if relative values of diffusion coefficient is the objects of consideration, no great need exists for exacting extrapolation. Two extrapolations are employed on any given functional model; the results of one extrapolation are greater, while those of the other are less than the results predicted by the model.

In many papers dealing with diffusion coefficient the calculation of this coefficient involves at first an experimental determination of a concentration gradient.[1,2,3,4] This gradient, usually shown as a graphical curve, is then analyzed for the proportionality constant in Ficks' law. In most real cases, especially as related to movements through solids, this proportionality factor or coefficient of diffusion is not a constant; frequently it varies with concentration. It is, however, common practice to assume this coefficient as a constant and to evaluate it, from the concentration gradient, on this basis.

Considerable information may be lost by such practice and one may wonder why data are not more commonly analyzed for variable coefficient of diffusion. It may be that many investigators have not followed through on methods of treatment of data in order to analyze for variable diffusivity. Crank[5] and Jost[6] present the basic equations by which a concentration gradient may be analyzed to calculate $D = f(c)$. Frequently the algebraic equation of $C = f(x)$ is rather complex and difficult to write. In such a case, graphical, numerical or mechanical methods for integrations and differentiations may be employed.

The objects of this paper are threefold: (a) to demonstrate the use of such graphical, numerical, and mechanical methods on an actual concentration gradient under conditions where D varies appreciably with concentration, (b) to point out and discuss several of the practical problems which were encountered in this solution, and (c) to demonstrate how these problems were handled.

Although a specific solid, neat portland cement, and a specific moving material, solium, were used for this work, the methods employed can be applied to any suitable curve of concentration as a function of depth. Although the concentration gradient used in this work was established by means of radioactive tracer techniques, any method by which a suitable gradient can be determined may be employed. Recent developments in techniques of use with radioactive materials have made these methods efficient and practical for experimental determination of concentration gradients in solids; hence this paper deals with a curve which was so established.

In general, experimental procedures for studies on movement of materials in cement or concrete consist of preparing a test specimen having dimensions such that it can, for mathematical treatment, be considered as an infinite or semi-infinite volume. Actual dimensions of cement and similiar materials to meet this condition need not, in general, exceed about 1″ square by 2″ long with all the 1″ × 2″ plane faces sealed with an impermeable coating. After sizing and sealing, the specimen is submerged in a prepared solution. The solvent of this solution is the material whose diffusion characteristics are under investigation and to which an appropriate activity of radioactive solvent has been added. After a suitable holding period the block is removed and activities at given depths are determined. From these data the geometric curve of concentration — depth is established; it is then analyzed for the diffusion coefficient.

Prager[7] developed equations by which the diffusion coefficient can be approximated as a function of concentration. For this method the total quantity of material moving into a semi-infinite film as a function of time is observed for a series of different driving potentials. Data are analyzed with a step by step method which requires a trial and error method on successive steps. This procedure has the advantage of being a non-destructive method of obtaining data but does require data at several solution concentrations. The method presented below has the advantage of employing much simpler mathematics as well as requiring data at only one concentration of the solution phase.

Recent advances in high speed mechanical computers and in programming for these computers have made the application of these devices to problems of this type very practical. As an initial step in writing a program for a digital computer, an analysis of a problem in a manner similar to the treatment given in this paper is frequently desirable. Hence this paper could serve as a basis upon which to write such a program.

If only a few curves are to be analyzed — such as might be the case for a preliminary or for a feasibility study — it would be impractical to write a program. In this case the method outlined herein could be applied directly.

Preparation of Concentration—Depth Curve

It is assumed that the data of concentration as a function of depth is established. Normal variability in experimental data, inherent to all physical measurements, may be smoothed out by one of several methods.

One method — readily adaptable to work in cement — was to plot the concentration on a logarithmic scale against depth on a linear scale. The best curve "by eye" was then drawn or, if suitable, a least squares line as described by Wylie[8], could have been drawn. (Other approaches are suggested by Davis[9] and Snedecor[10].) The data of this best line were then re-plotted

[1]*Manuscript received August 24, 1959; accepted, July 12, 1960.*
[2]*Department of Chemical Engineering, Kansas State University, Manhattan, Kansas.*

on rectangular co-ordinate paper. A typical curve is shown in Figure 1a.

Evaluation of Diffusion Coefficient As a Function of Concentration

Jost[6] and Crank[5] suggest comparable methods for treatment of experimental data in order to evaluate a variable diffusion coefficient where the coefficient varies with concentration. The method involves integration and differentiation of the experimentally established gradient of concentration — depth. If the algebraic equation of this curve is difficult to write, methods of graphical or mechanical integration and differentiation may be employed.

Using the equation, from either Crank or Jost,

$$D = \frac{1}{2t}\frac{dx}{dc}\int_{C_i}^{C_o} x\,dc \qquad \ldots\ldots(1)$$

C_o is generally assumed to be homogeneous throughout the block and usually is zero.

It is assumed that concentration in the solution phase remains substantially constant and that all material which enters the block (the solid phase) does so by leaving the solution. This is comparable to providing a large quantity of dissolved solvent in solution relative to the total quantity of solvent which enters the test block. Equation (1) is comparable to

$$D_i = \frac{1}{2t}\left(\frac{\triangle X}{\triangle C}\right)_i \left[\sum_{C=C_o}^{C=C_i} (X \triangle C)\right] \qquad \ldots\ldots(2)$$

where D_i is evaluated at concentration C_i on an actual concentration gradient curve. The evaluation of $(\triangle X/\triangle C)_i$ is shown in Figure 1a.

A highly satisfactory means of establishing the perpendicular to the curve at depth x_i is to employ the mirror method as described by Dana and Hillyard[11]. A front surfaced mirror, as provided by a polished metal surface, rather than a rear-surfaced glass mirror is required for this application.

To draw the perpendicular to the curve at depth x_i, the mirror is placed on the pivot C_i, x_i in such a manner that one face of the mirror is on a line which passes, perpendicular to the surface of the paper, through the pivot point and with the greatest length of the mirror approximately perpendicular to the curve. The mirror is then rotated on this vertical line which passes through the pivot point until the visual reflection of the curve and the curve on the paper join so as to form a smooth and continuous curve. The position of the ends of the mirror are then marked on the paper. The procedure is next repeated, about this same point, on the other segment of the curve. The perpendicular to the curve is then drawn through C_i, x_i such that it passes (as best possible) through the points where the ends of the mirror were marked and the perpendicular to this line is then drawn. The slope of the last line which is parallel to the tangent is taken, after proper scaling as $\triangle C/\triangle X$. Or the points which marked the ends of the mirror may be employed directly, with attention to signs and scaling, to make this calculation.

One method for evaluating

$$\sum_{C_i}^{C_o} X \triangle C$$

is illustrated in Figure 1b.

In this case the trapezoid rule is followed.

$$\sum_{C=C_o}^{C=C_i} X \triangle C = \left(C_1 - C_o\right)\left(\frac{X_0 + X_1}{2}\right) + \left(C_2 - C_1\right)\left(\frac{X_1 + X_2}{2}\right) + \ldots$$

$$\left(C_i - C_{i-1}\right)\left(\frac{X_{i-1} + X_i}{2}\right) \qquad \ldots\ldots(3)$$

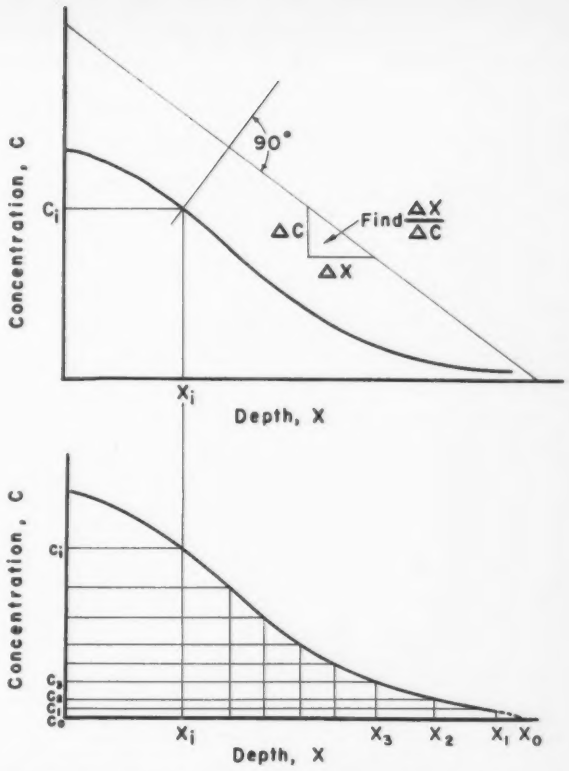

Figure 1a—Use of mechanical and graphical methods to evaluate $\Delta X/\Delta C$ at X_i. A front surfaced mirror is employed to establish the perpendicular to the concentration gradient curve at point X_i, C_i.

Figure 1b—Use of the trapezoidal rule to evaluate Equation (3). Region of questionable extrapolation, under dotted curve $= (C_1 - C_0)(X_0 - X_1)(\frac{1}{2})$.

If greater accuracy is required, methods such as Simpson's rule[12], or improvements by extrapolation as outlined by Salvadori and Baron[13], may be employed.

The evaluation of $1/2t$ is straightforward.

Thus, by repeating this procedure at various X, and calculating the corresponding D_i, the plot of D_i against C may be prepared.

Sources of Difficulty

It is observed that the first term in the graphical integration by the trapezoidal rule necessitates an evaluation of X_o where the curve converges to C_o. Various algebraic expressions which may serve to fit experimental data in a satisfactory manner, such as equilateral hyperbola or reciprocal exponential type, may not converge to $C = 0$ for $X < \infty$. This, however, presents no real problem in obtaining suitable accuracy in evaluating

$$\sum_{C=C_o}^{C=C_i} X \triangle C$$

The effective value for X_o may be set at any value for C sufficiently small and the $\triangle C = (C_1 - C_o)$ taken to any practical degree of smallness. Such procedure is justifiable because, by the nature of the system and the treatment to which it may have been subjected for any finite t, the actual curve must and does converge to C_o at finite x. Failure of an algebraic equation to converge to zero is merely an example of how an idealized algebraic equation can fail to adequately describe the real physical situation. Thus, two major problems develop; the

first is the evaluation of the concentration gradient at depths beyond which measurements were made and the second is the evaluation of the initial concentration of the moving material in the solid.

In order to demonstrate these, as well as other practical problems which were encountered in evaluating the integral and the differential at various points, some data of Chang[14] were analyzed. The techniques applied are presented here.

The Problem of Extrapolation

The depth — concentration data were assembled in Table 1*. The block of concrete (2″ diameter cylinder, 4″ long, and having all surfaces except the ends covered with wax) was held submerged in a radioactive solution for a period of 273 days.

The two ends of the block, Ends I and II, were analyzed 192 days and 635 days respectively after removal of the block from the radioactive solution. It was reasonable to assume that both ends of the block were of similar physical and chemical characteristics, so that diffusion characteristics should have been very similar. It is obvious that the concentration — depth curves for the two ends do not coincide. Although it is not the purpose of this paper to discuss the reasons for this discrepancy, it may be noted that the total sodium in the block (i.e. the integrated area under the curve) was greater for the measurements which were made on End II than for those made on End I. Since the block was not exposed to any external source of sodium during this time it appears as if a violation of the material balance was obtained. Since this may be taken as an error the question was naturally raised as to which curve was representative of the true situation. One suggestion was that both curves, used together, were the most representative of the true data.

Data were plotted on semi-log paper as shown in Figure 2 where plots for counts, as made on Ends I and II, 92 days and 635 days respectively after removal of the block from the solution, are plotted as separate curves and the least squares curve for both sets of data combined together is also shown as one straight line. It was noted that the best curves by eye tended toward an S shape which was distinctly different from a straight line. Data from each of these three curves were plotted on rectangular coordinates. The plot from the resulting "best by eye" curve for the data of End II is shown in Figure 3; it is generally representative of the other two curves.

Steps 1, 2, and 3 on Figure 3 illustrate the application of the mirror method to the evaluation of $\triangle X/\triangle C$.

The problem of extrapolation of the curve in Figure 3 was considered; this extension was necessary in order to effect the integration of $(X\triangle C)$ from C_o to C_1. The extrapolation of the curve on Figure 2 was made. Extrapolation of the least squares line on this plot was easy; however, the question of how closely this line came to true values was raised. It was decided to graphically extrapolate the "best by eye" curve.

The practice of using extrapolations is usually considered as hazardous. Even if a suitable plot or mathematical model can be found which will give "best fit" over reasonable ranges of data there is no guarantee that this straight line or this set of evaluated constants will remain valid over appreciable extrapolations. Obviously it is desirable to obtain data on concentrations at appreciable depths in order that the severity of this source of errors may be reduced to a minimum. Accurate evaluation of concentrations at low values is often difficult and frequently is costly to make. Hence, some method of extrapolation will normally be required.

A common type of study involves consideration of a large number of specimens all having essentially the same fundamental characteristics. As an example, one may be concerned with the influence of density of material on the D values. A series of specimens would be prepared, all having different densities. If suitable evidence is available, or may be established, to indicate that the general characteristics of the concentration gradients are independent of density (even though slopes or constants of a mathematical model may vary between densities), one would be justified in expending great effort and expense to obtain data at low concentrations on one speciman in order to establish the general mathematical model. Data on the remaining specimens would then be obtained at only enough points to evaluate the constants of the model and these would then be used to extrapolate to low C.

In other cases sufficient information, either experimental or based on postulated mechanisms, may be available to aid in writing the mathematical model.

In the event that no information is available and expense or other restrictions prohibit its establishment, an extrapolation will be necessary. This paper suggests that it is not necessary to obtain an exacting extrapolation: rather it proposes that the two extrapolations be made; one having values greater than and one having values less than the apparent true value. The resulting calculations will provide two sets of values (of $\sum_{C=o}^{C=n} xdc$), one of which may be assured to be less than true and one greater than true. The range of these values of D may then be considered. If the range is too great for the desired use, an improved means of extrapolation must be found. If, on the other hand, the range is within reasonable limits for the immediate purpose at hand, the extrapolation method used may be considered as satisfactory.

The curve of Figure 2 is one which must be extrapolated. The data were taken several years ago by another investigator and no method was available by which data at greater depths could be obtained. The specimens were several years old at the time they were submerged and they remained in solution for nearly a year; it would take a long treatment time to reproduce the work. No information was available on which to base a hypothetical mathematical model.

A first method of extrapolation is demonstrated in Figure 4. Data had initially been smoothed on a plot of log $C = f(x)$, (Figure 2). The end of this curve, on the semi-log paper, was plotted on Figure 4. On this plot it appeared as if the end of the concentration gradient was approaching a straight line. Two extrapolations, both straight lines, were made. Extrapolation A was made with slope appreciably greater and extrapolation B was made with a slope appreciably less than the apparent slope of the end of the data curve.

A second approach to extrapolation is demonstrated in Figure 5. In this case the $\triangle C/\triangle X$ was plotted against depth. The resulting plot indicates that the slope is approaching a constant value at the greater depths. From this curve two values of slope were chosen for extrapolation, one greater and one less than the apparent final slope.

In a third method, demonstrated in Figure 6, a model of the form $C = A^{x^{-b}}$ was assumed. For depths in excess of 0.07 inches it appeared as if the values of A and b were constant. The resulting straight line was extended to depths of 30 inches. Only one line was employed in this case although two, one a maximum and one a minimum, could have been used.

Calculations and results of the extrapolations A and B from Figure 4 a in conjunction with the curves from Figure 2 are shown in Tables 2 and 3* and are plotted in Figure 7. Comparisons of the values of D as obtained from the various extrapolations of Figures 4, 5 and 6 are tabulated in Table 4a* and plotted in Figure 8.

In as much as the extrapolation of Figure 6 extends the C to very low values and, at higher x values, causes the curve to be nearly parallel to the x axis, the need for adequate evaluation of C_o was brought into focus. This is demonstrated by considering three different values for C_o.

*Tables 1, 2, 3, and 4a of this paper have been deposited as Document No. 6394 with the ADI Auxiliary Publications Project, Photoduplication Service, Library of Congress, Washington 25, D.C. A copy may be obtained by citing the Document No. and by remitting $1.25 for photoprints, or $1.25 for 35 mm. microfilm. Advance payment is required. Make cheques or money orders payable to: Chief, Photoduplication Service, Library of Congress.

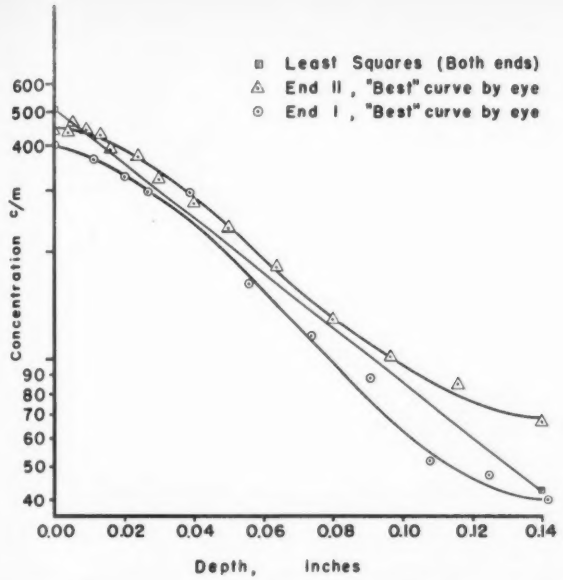

Figure 2—Concentration gradient of sodium in concrete specimen.

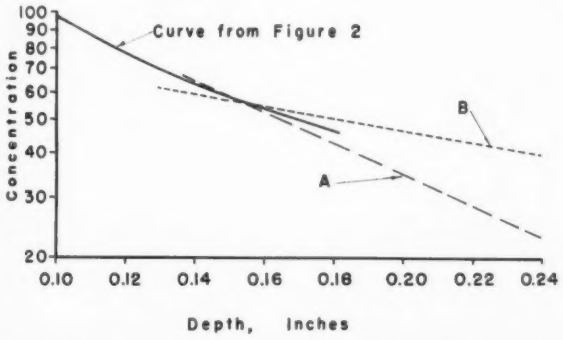

Figure 4—Extrapolations (for End II of curve by eye from Figure 2) to $C = C_o$. Extrapolation B at slope less than apparent slope of data curve and extrapolation A at slope greater than apparent slope of the curve from data.

The Problem of Initial Concentration

The importance of reasonable evaluation of C_o is involved in the evaluation of $\sum_{C_n}^{C_o} X\triangle C$ where

$$\sum_{C_i}^{C_o} X\triangle C = \sum_{C_i}^{C_n} X\triangle C + \sum_{C_n}^{C_o} X\triangle C \quad \ldots\ldots\ldots\ldots (4)$$

when x_n is the deepest point where $\triangle X/\triangle C$ is measured and x_i is the point where D_i is being evaluated. Thus if

$$\sum_{C_n}^{C_o} X\triangle C = K \quad \ldots\ldots\ldots\ldots\ldots\ldots\ldots\ldots\ldots\ldots (5)$$

then

$$\sum_{C_i}^{C_o} X\triangle C = \sum_{C_i}^{C_n} X\triangle C + K \quad \ldots\ldots\ldots\ldots\ldots\ldots\ldots (6)$$

and the problem is essentially that of evaluating K where the magnitude of K depends on the value of C_o. In actual practice many natural materials may contain a measureable degree of radioactivity which may be of importance in the evaluation of

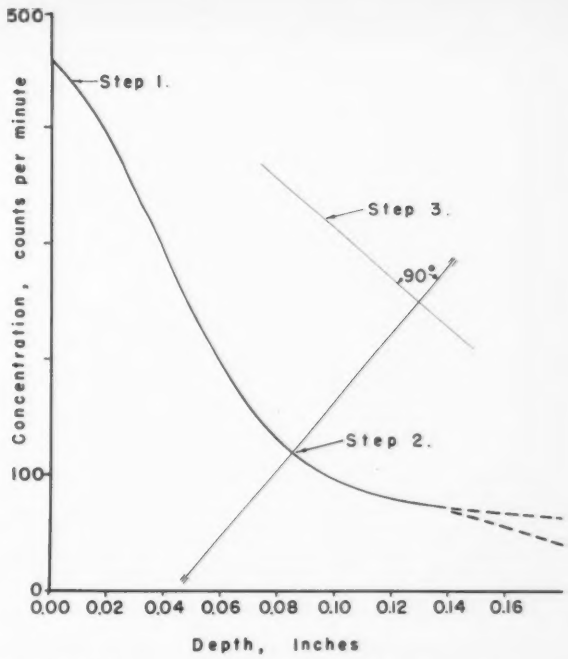

Figure 3—Concentration gradient for End II. "Best" curve by eye from Figure 2 replotted on rectangular coordinates and analysed for $(\Delta X/\Delta C_i)$. Extrapolations with constant slopes of 300 and 800 (Figure 5) also shown in dotted lines.

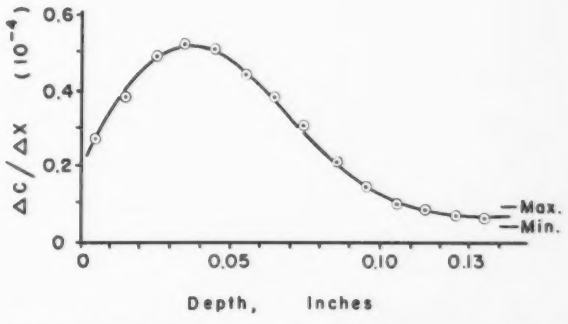

Figure 5—Plot of slope at various depths (for End II of curve by eye from Figure 2). Assume extrapolated curve holds constant slope of between 800 and 300 counts per minute/inch.

$\sum_{C_o}^{C_i} X\triangle C$, especially if introduced activities are relatively low or if extrapolations, as mentioned above, are critical. In this particular study the evaluation of C_o was inadvertently neglected. The potential seriousness of this error was further considered by assuming a natural background of $C_o = 20$ *c/m* on data obtained 92 days after removal of the block from solution. These calculated values were compared with those which were determined on the basis of no natural background. Results are summarized in Figure 9 (extrapolation of the curve by eye was made by assuming a slope the same as for extrapolation B of the data obtained 635 days after removal of the block from the solution).

Conclusions

Results of the application of the proposed method of analyzing for variable diffusion coefficient to the system sodium-

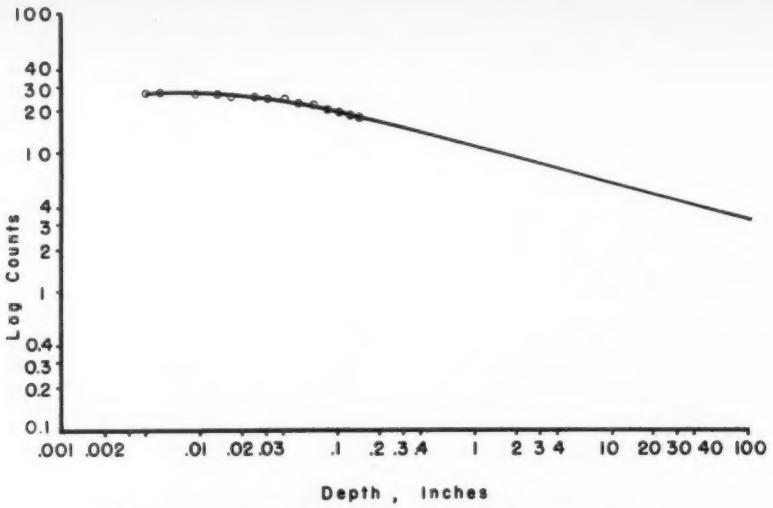

Figure 6—Assume data is represented by equation of form $C = A^{x^{-b}}$ with A and b constant for depths greater than 0.05 inches. Use these values of A and b for extrapolation of concentration gradient data to $C = C_0$.

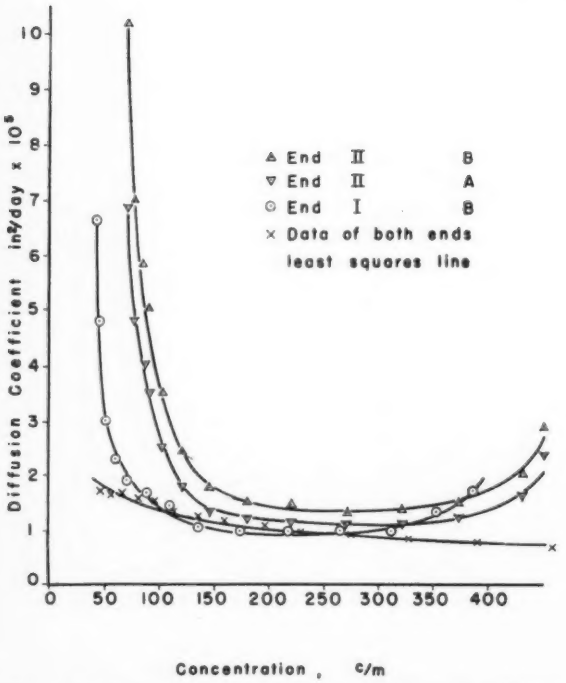

Figure 7—Comparison of D values based on extrapolation of least squares line and extrapolations A and B (Figure 4) of data from Figure 2.

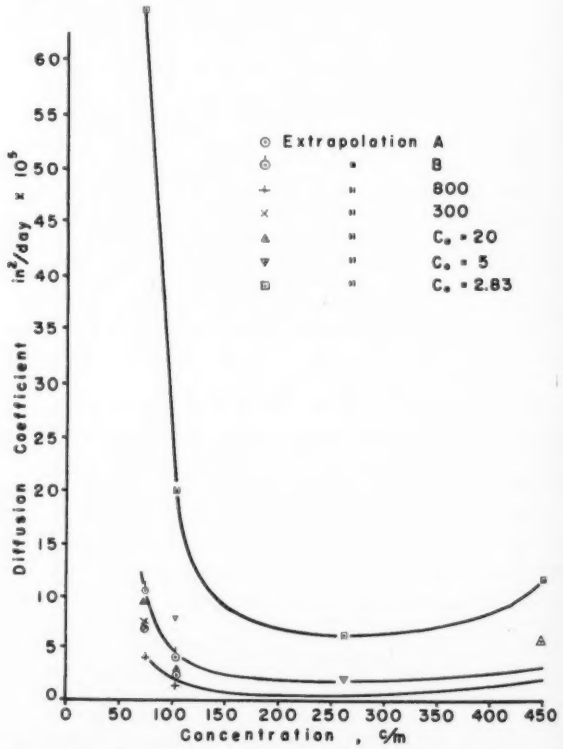

Figure 8—Comparison of D values from Table 4a. Extrapolations A and B from Figure 4. Extrapolations 800 and 300 from max. and min. of Figure 5. Extrapolations $C_0 = 20$, 5 and 2.83 from Figure 6.

cement, clearly demonstrated that the coefficient is not a constant but varies appreciably with concentration, especially over the lower ranges.

Results of various methods of extrapolation demonstrated that, if information on only relative values of D be needed, no great concern need be given to the method of extrapolation (Table 4b). If, however, exacting values of D are required, a method must be found which will predict the shape of the concentration gradient to considerable depth with considerable accuracy. If no other means are available upon a graphical or a mathematical model can be built to accomplish this extrapolation, it is suggested: that data necessary to construct a complete curve be gathered on at least one representative specimen, that the mathematical model be built from this information and that this model be used for extrapolation of fewer data on brother specimens.

In the problem considered there was no alternative to making an extrapolation. The model, $C = A^{x^{-b}}$, gave D values having order of magnitude comparable to D values which were calcu-

lated by assuming a constant coefficient. It was felt that this method was superior to others, if true values of D were desired.

Need for evaluation of inherent concentration was demonstrated, if true value of D is needed.

Wider use of a method such as this is suggested as a means of obtaining more and better information on D values by analysis of concentration gradients.

Nomenclature

C = concentration, convenient units.
C_o = initial concentration in block
C_i = concentration in block after time t and at depth X_i.
D = coefficient of diffusion, length squared per time
D_i = coefficient of diffusion at a given C_i.
t = time interval during which block was submerged.
X = length (depth into block, measured from and perpendicular to exposed surface)

References

(1) Barrer, R. M., Diffusion in and Through Solids. The MacMillan Company, New York (1941).

(2) Gevantman, L. H., and D. San., **33**: 122 (1955).

(3) Spinks, J. W. T., H. W. Baldwin and T. Thorwaldson., **30**: 20-28 (1952).

(4) Swanson, V. A., Diffusion of Sodium in Various Types of Concrete. Unpublished M. S. thesis, Kansas State University, Manhattan, Kansas (1956).

(5) Crank, J., The Mathematics of Diffusion. Oxford University Press, Amen House, London. E. C. 4 (1956).

(6) Jost, W., Diffusion in Solids, Liquids, Gases (Translation edited by Eric Hutchinson). Academic Press, Inc., New York (1952).

(7) Prager, Stephen., J. Chem. Phys. **19**: p. 537 (1951).

(8) Wylie, C. R., Jr. Advanced Engineering Mathematics. McGraw-Hill (1957).

(9) Davis, D. S., Nomography and Empirical Equations. Reinhold (1955).

(10) Snedecor, G. W., Statistical Methods. The Iowa State College Press, Ames, Iowa.

(11) Dana, Forest C., and L. R. Hillyard. Engineering Problems Manual. McGraw-Hill (1947).

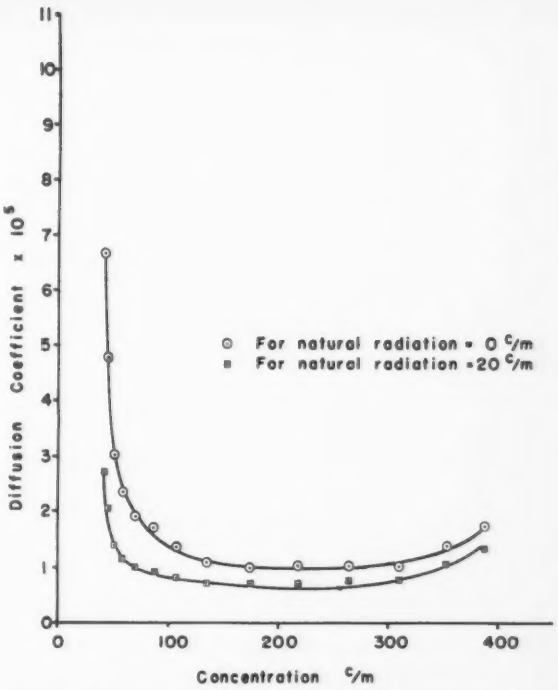

Figure 9—Influence of natural radiation (concentration on magnitude of *D*. Treatment of data from Figure 3 with extrapolation *B*.

(12) Mickley, H. S., T. K. Sherwood, and C. E. Reed. Applied Mathematics in Chemical Engineering. McGraw-Hill (1957).

(13) Salvadori, M. G. and M. L. Baron. Numerical Methods in Engineering. Prentice-Hall (1955).

(14) Chang, S. C., Diffusion of Sodium into Concrete. Unpublished M. S. thesis, Kansas State University, Manhattan, Kansas (1958).

★ ★ ★

Concentration Distribution in Two-Phase Pipe Flow[1]

S. L. SOO[2] and J. A. REGALBUTO[3]

Concentration distribution of solid particles in two-phase turbulent pipe flow was studied. Due to the inertia of solid particles, transport of solid particles across the velocity field of the turbulent stream by turbulent diffusion results in deceleration of particles in the region near the wall by the stream and acceleration of particles transported toward the high velocity core. In the core, the particles have lower mean velocity than the stream while near the wall the mean particle velocity is higher. This gives rise to a non-uniform distribution of solid particles in fully developed turbulent pipe flow. Experimental determination of concentration distribution was made with an impact disk particle counter system.

Consideration of wall interference in two-phase (solid particle-gas system) turbulent motion indicates that the presence of the wall such as in fully developed pipe flow affects considerably the mean stream condition[1,2]. The presence of the wall increases significantly the intensity of particle motion above that in free turbulence due to continuous transport of momentum from the wall to the core. It is reasonable to question the effect of momentum transport from the wall on the concentration distribution over the duct.

A knowledge of the distribution of the solid particles is significant, considering its effect on heat and mass transfer processes usually encountered in the applications of two-phase turbulent motion. In References [3] and [4] uniform distribution of the concentration of solid particles was assumed. The experimental results of Reference [5] considers basically the gravity effect on two-phase streams of large weight ratio (loading) of solid particles to gas, and when there is no apparent gravity effect, the concentration of solid particles was taken to be uniform. This paper concerns the concentration distribution in the case of small loading, where gravity effect is measured to be small.

At present, very little is known about pipe turbulence of a single phase fluid. Various conjectures were made as a matter of qualitative explanation of experimental results of mean velocity distribution, turbulence intensities, shear stresses, eddy viscosities, turbulence dissipation, energy balances, and energy spectra. A plausible explanation is that there is a flow of kinetic energy by turbulent diffusion down the gradient of turbulent energy toward the center of the pipe where eddies are dissipated, while turbulence diffusion of pressure energy is directed from the core region toward the wall. There is continuous transport and diffusion of small energy-rich eddies from the wall region toward the center. At the same time there is a flow of energy-poor fluid lumps back toward the wall, where mean motion shears these lumps into small high-intensity eddies. The phenomenon is extremely complicated and comprehensive analytical treatment is rendered difficult[6]. The net situation is that there is turbulent transport of momentum through accelerating the fluid from the wall toward the core region.

It might even be said that our knowledge of the one-phase pipe turbulence has not yet readied us for studying a two-phase solid-gas suspension. The significance of the problem itself, however, calls for some immediate attention. Due to transport of fluid momentum toward the core region, as explained in the above, the solid particles are transported by the fluid, opposing the diffusion mechanism due to concentration (number density of solid particles) gradient. It can be expected that the distribution of solid particles in fully developed two-phase turbulent motion will not be uniform over the cross-section of a pipe.

In addition, the inertia of the solid particles play an important part in the transport process. Solid particles transported from the center to near the wall is decelerated to the local mean stream velocity. The mean velocity of solid particles u_p in this region is therefore higher than that of the stream u. Based on the local static number density or concentration, C_s (number of particles per unit volume of fluid when both are at rest or both moving at the same speed), the local number density C is then

$$C = C_s \frac{u}{u_p} \qquad (1)$$

A higher particle velocity than the stream velocity shows up as a decrease in particle concentration.

On the other hand, the solid particles transported from near the wall (which are already decelerated) to the core region is accelerated by the stream to the mean velocity of the core region. The average particle velocity u_p in the core region is lower than that of the fluid, u. Based on Equation (1), this shows up as an increase in particle concentration above the local static value.

The net effect of transport of momentum and inertia of solid particles (especially the latter) can be visualized, without going into the details of particle motion itself, as acceleration of solid particles transported by turbulent diffusion from the wall toward the center of the pipe and deceleration of solid particles transported from the center toward the wall. The direction of acceleration is therefore radially inward toward raising the particle concentration in the core, opposing the diffusion mechanism due to concentration gradient. It should be noted that one cannot account for the effect of particle inertia by considering any special distribution of turbulent diffusivity

[1]*Manuscript received December 27, 1959; accepted July 15, 1960.*
[2]*Professor of Mechanical Engineering, University of Illinois, Urbana, Ill.*
[3]*Textile Research Fellow, Princeton University, Princeton, N.J. His contribution on the experimental program was in partial fulfillment of requirements of M.S. degree.*
Based on a paper presented to the C.I.C. Chemical Engineering Conference, November 9-11, 1959.

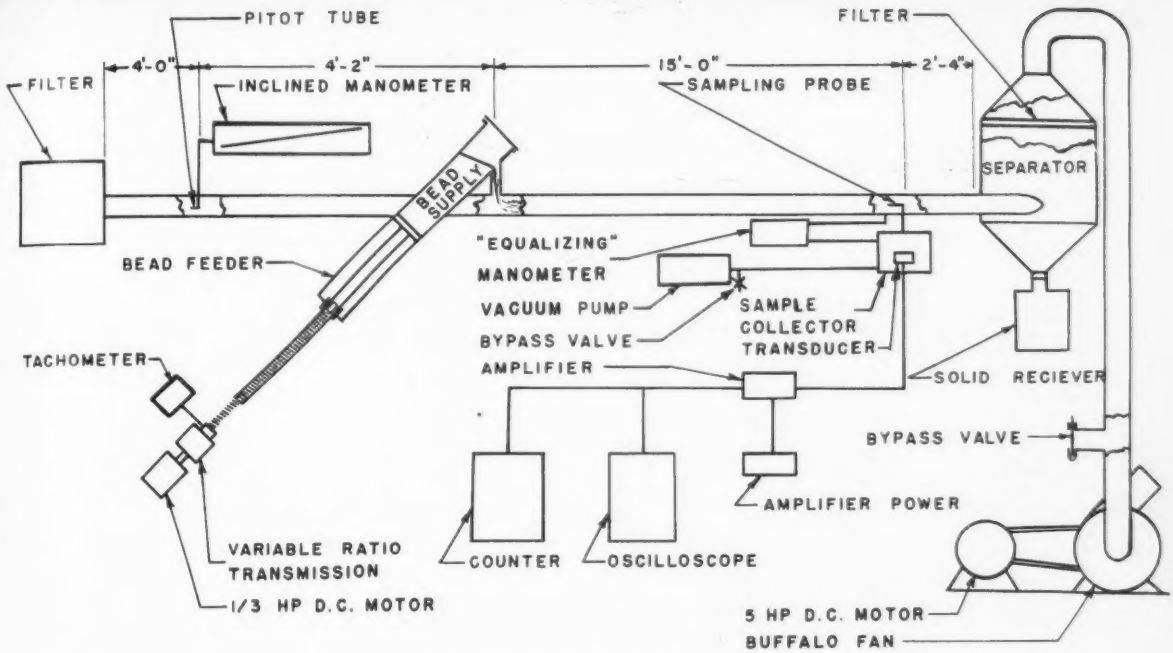

Figure 1—Schematic diagram of apparatus.

of particles alone; it would give uniform distribution of solid particles when fully developed turbulence is achieved.

The above phenomenon can be formulated in the following manner as a first approximation.

The rate of radial motion of solid particles due to concentration gradient is given by:

$$\dot{n} = -D\frac{dC}{dr} \quad \ldots\ldots(2)$$

where r is the radial coordinate, D the particle diffusivity (due to stream diffusivity)[1], C the particle concentration.

Neglecting gravity effect, the change of particle concentration by diffusion, or the total variation of $\dot{n}$ with respect to time is:[6]

$$\frac{d\dot{n}}{dt} = \frac{u}{r}\frac{\partial}{\partial r}(r\dot{n}) = \frac{-u}{r}\frac{\partial}{\partial r}\left(r\,D\,\frac{\partial C}{\partial r}\right) \quad \ldots\ldots(3)$$

for steady motion ($\partial/\partial t = 0$) at mean axial flow velocity u. When a steady concentration profile is maintained, the rate $d\dot{n}/dt$ is due to transport of particles across the fluid velocity field and is proportional to the drag force acting on the particles. Hence as an approximation, $d\dot{n}/dt$ is proportional to the concentration C at radius r, or

$$\frac{d\dot{n}}{dt} = fC, \quad \ldots\ldots(4)$$

f is the acceleration of solid particles transported by turbulent diffusion from the wall toward the center of the pipe and deceleration of solid particles transported from the center toward the wall. f relates fluid drag and inertia of solid particles as a solid particle moves across the distributed velocity field of the turbulent stream.

Combining Equations (3) and (4), we get, for constant particle diffusivity,

$$\frac{D}{r}\frac{\partial}{\partial r}\left(r\frac{\partial C}{\partial r}\right) + \frac{fC}{u} = 0 \quad \ldots\ldots(5)$$

f, in general, is a function of state parameters of the system and radius r.

If an average value of f is taken, the solution of Equation (5) is then:

$$C = C_o J_o(r\sqrt{f/Du}), \quad \ldots\ldots(6)$$

where C_o is the concentration at the center of the pipe or the reference concentration, and J_o is the zero order Bessel's function. The above relation gives a concentration profile somewhat similar to that of mean velocity. The parameter affecting concentration distribution fR^2/Du (where R is the pipe radius) can be determined from measured concentration distribution.

An impact disk particle counter was developed for the purpose of measuring the distribution of solid particles in two-phase turbulent pipe flow (glass beads in air). Measurements were made on a two-phase flow facility. Figure 1 shows the duct, the solid particle sampling system and the particle counting system schematically.

Two Phase Flow Facility

The measurements of concentration distribution were made along a vertical diameter of a three-inch inside diameter pipe. Air is induced through the pipe by a Buffalo Volume Fan driven by a 5 hp. shunt-wound D.C. motor. Changes in the air stream velocity are facilitated by field control of the motor or manipulation of a bypass valve immediately preceding the blower intake. The dimension as shown in Figure 1 is such that fully developed pipe flow exists at the points of sampling[1].

Foreign particles are excluded from the air stream by approximately 15 sq. ft. of 5 micron filter paper surrounding the pipe intake. A pitot-static tube located 10 diameters downstream is used to report the mean stream velocity via an inclined draft gage.

The solid phase (spherical glass beads) is metered into the air stream 20 diameters downstream from the air inlet by an inclined piston and cylinder arrangement. The uppermost end of the cylinder is connected to the main pipe by a short vertical tube. Beads loaded into the cylinder are forced upward by the piston over a shallow V-notch weir, thence down the vertical tube into the air stream. Linear motion of the piston is accomplished by a power screw and nut mechanism. The nut is secured to the piston and constrained from rotating while the screw is powered by a 1/3 hp. D.C. motor driving through a

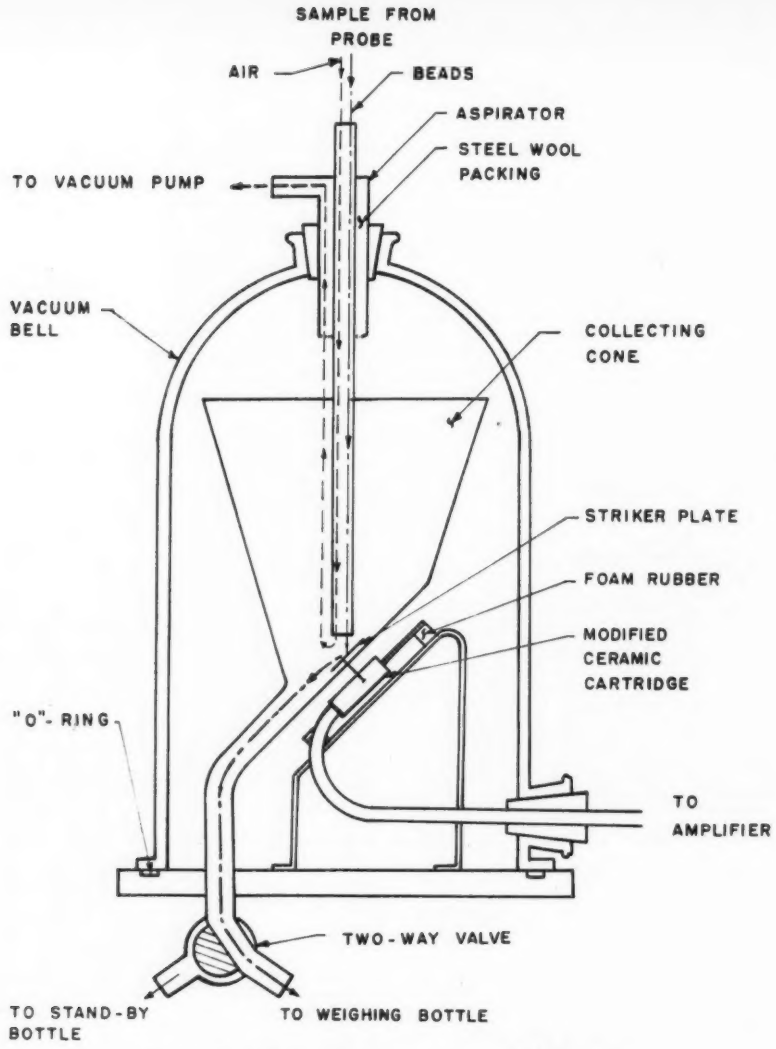

Figure 2—Schematic diagram of sampling system.

Zero-Max variable speed transmission. This combination provides both the torque necessary to rotate the screw and the means by which to regulate the screw r.p.m., and hence the bead feed rate.

A theoretical feed rate, calculated from power screw r.p.m., thread pitch and the cylinder diameter compared favorably with that obtained by weighing a sample collected by the separator over a measured time interval. Further calibration was deemed unnecessary and the tachometer indicating the screw r.p.m. was calibrated to give the feed rate directly in lb./hr.

At the downstream end of the pipe, the glass beads are divorced from the air by diffusing the stream into a cyclone-type separator. The air exits through 3 sq. ft. of 5 micron paper at the top of the separator while at the bottom, a double door device allows collection of the beads without unduly disturbing the equilibrium of the flow system.

Sampling of the Solid Phase

The solid phase distribution is sampled by a probe fabricated from .062″ inside diameter, .016″ wall tubing. The probe is mounted on a vernier depth gage which allows easy traverse in the duct and further, locates the probe precisely (to within .001 inch).

A 90°, 1/2 inch radius bend in the tube collects the bead sample downward out of the main duct into a vacuum bell housing the transducer of the counting system. A collecting cone then funnels the sample into either of a pair of weighing bottles, after the beads have collided with the transducer. (Figure 2)

To insure that the sampling is truly representative of the actual particle distribution, the vacuum bell is kept at a pressure low enough to induce, through the probe, an airflow whose velocity at the probe inlet is the same as the air stream velocity in the immediate vicinity. In the line between the vacuum pump and the bell, a bypass valve (opening to the atmosphere) controls the air flow through the probe. Thus the velocity within the probe can be matched not only to different average air velocities but, more important, to the velocity profile encountered as the probe traverses the duct.

A static pressure tap, located 8 diameters back from the probe inlet in a horizontal plane, is connected by a 1/32 inch inside diameter tube to one leg of a U-tube manometer. The other leg of the manometer is connected to a second static tap in the wall of the main duct at the same station as the probe inlet. Since, for the least disturbance to the flow field, the velocities within and without the probe are desired to be equal, it is

necessary that the static pressures measured by the manometer be identical. Thus the velocities can be matched simply by adjusting the vacuum bell bypass valve until the legs of the U-tube manometer are equal. An added feature of the manometer is its adjustable inclination which allows matching of the velocities to any resonable degree of accuracy.

Finally, added protection is given the vacuum pump against ingesting glass beads by the design of the aspirator shown in Figure 2. Particle inertia is utilized to separate the solid and gas phases as the air stream must reverse direction 180° and then pass through a closely packed steel wool filter before reaching the vacuum pump.

Substantiation of the velocity matching capability of the induction was first attempted by photographing the two-phase flow in the vicinity of the probe. The photographic technique and equipment used in this test is described in Reference[1]. A series of pictures was taken at various values of the difference in static pressure ($\triangle p_s$) within and without the probe. Checks were made with flow conditions at 40 ft./sec., 115 micron beads (more susceptible to suction of probe than 230 micron particles) and average loading of .025 lb. of beads per lb. of air. Photographs* show that the bead flow pattern in general was not changed significantly by the presence of the probe. The gas flow pattern might be affected locally, but we are only concerned with motion of the beads. This is shown by the near straight line trajectories in all the photographs referred to above.

However, the photographs could not give enough detail about the effect of $\triangle p_s$ on the quantity of beads ingested by the probe. To this end a second test was made which resulted in a plot of beads ingested (in terms of the count recorded per second) versus $\triangle p_s$ (Figure 3).

The shallow slope at $\triangle p_s = 0$, indicates that the number of beads ingested is relatively constant if the manometer legs are equalized within 0.1 inch total.

Actually no accurate adjustment for $\triangle p_s$ is necessary as long as it is constant for a given set of traverse. As shown in Figure 3, within the range where $\triangle p_s$ vs. counts per second is linear, when the number is directly proportional to $\triangle p_s$, subsequent normalization rather than actual number of count determines the concentration distribution. This normalizing procedure is necessary also because variation in particle sizes within the range of 210 to 250 microns for 230-micron particle diameter and 105 to 125 microns for 115-micron particle diameter.

To insure that samplings were made at points of fully developed pipe flow, checks were made at locations 3 feet apart along the pipe. The concentration distribution was shown to be steady.

Solid Phase Counting System

An ordinary Sonotone 3T ceramic cartridge, intended primarily for use in high fidelity phonographs, is the transducer of the "counting" system. The cartridge is modified by replacing the needle with an elliptical plate connected to the ceramic crystal by a short stem. The axis of the stem is oriented in such a way that beads impacting on the plate excite the crystal in exactly the same manner as the original needle. (Figure 2)

Anticipation of a low signal level from the crystal dictated the use of a low-noise, high-gain, battery-powered amplifier. Chosen was a Tektronix Model 122 with a maximum gain of 1000 and a maximum noise level of 20 microvolts r.m.s.

After amplification, the signal is fed into a Hewlett-Packard Model 521A electronic counter and an oscilloscope. A useful feature of the counter provides control of the input voltage level to the counting circuit. Thus, given a favorable signal-to-noise

*Figures 3a, 3b, 3c, 5b, 5c, 5d, 6b, 6c, 7b, 7c, 7d, and 7e, of this paper have been deposited as Document No. 6393 with the ADI Auxiliary Publications Project, Photoduplication Service, Library of Congress, Washington 25, D.C. A copy may be obtained by citing the Document No. and by remitting $1.25 for photoprints, or $1.25 for 35 mm. microfilm. Advance payment is required. Make cheques or money orders payable to: Chief, Photoduplication Service, Library of Congress.

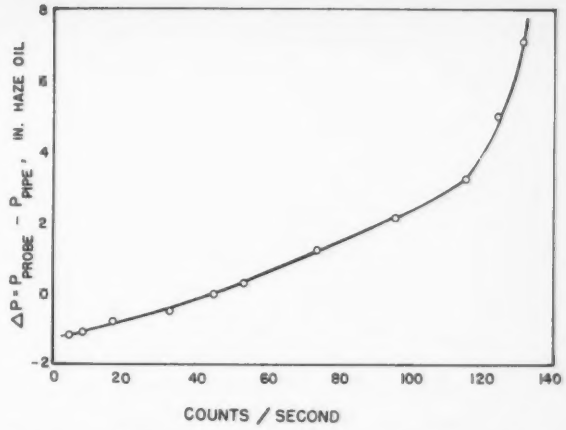

Figure 3—Counting system response to variation in $\triangle p_s$.

ratio, unwanted noise and random vibrations can be excluded from the count. Precise time gates of one-tenth second and one second are provided along with a manual gate for counting over an extended period of time.

General information about signal-to-noise ratio, signal wave form, presence of a signal, etc., is checked by an oscilloscope.

Undesirable interference from mechanical or electrical sources is eliminated insofar as possible. The transducer is isolated from mechanical vibration by extensive foam rubber mounting. Connecting tubes and cables are as flexible as possible. To prevent stray electrical pickup, the cases of the various components were connected and the system grounded at a single point to prevent circulating currents. Another important item in this system is a wire mesh cage enveloping the transducer.

Transducer Calibration

The response of the modified cartridge was investigated by subjecting the impact plate to sinusoidal air pressure variations and viewing the output on an oscilloscope. To obtain the pressure variations, the output from a variable frequency oscillator, suitably amplified, was broadcast from a high fidelity speaker system. Varying the oscillator frequency showed resonances at 400 c.p.s. and 800 c.p.s. in addition to a response limit of approximately 8000 c.p.s. The resonance amplitudes were small enough in comparison to the bead signal and the frequency response high enough in comparison to the anticipated average number of counts per second, so that further modifications were deemed unnecessary.

An initial calibration to allow conversion from counts per second to pounds of beads per second was made by weighing a "counted" sample collected under operating conditions. The count was manually started at the instant the two-way valve in the collecting system was switched from the stand-by bottle to the weighing bottle.

Weighing inconsistencies, while not unduly large, resulted from the extremely small samples obtained over a long time period. Thus an alternate method utilizing the average bead flow was used. Plotting each solid phase distribution profile (in terms of counts per second), a mean effective figure of counts per second was obtained. Comparing this average figure with the known average bead flow indicates the necessary magnitude of the desired conversion factor in pounds per count. This latter method is preferred because of the larger quantities involved and the greater accuracy to which these quantities are known.

Due to the lack of a precise time gate longer than one second in this particular counter, it became necessary to determine the number of intermittent digit displays to be averaged for a representative bead flow figure in counts per second.

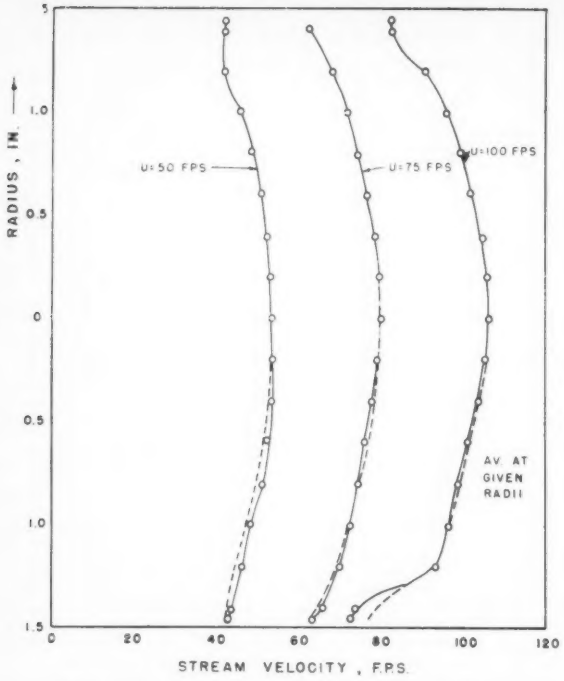

Figure 4—Velocity profiles at probe location.

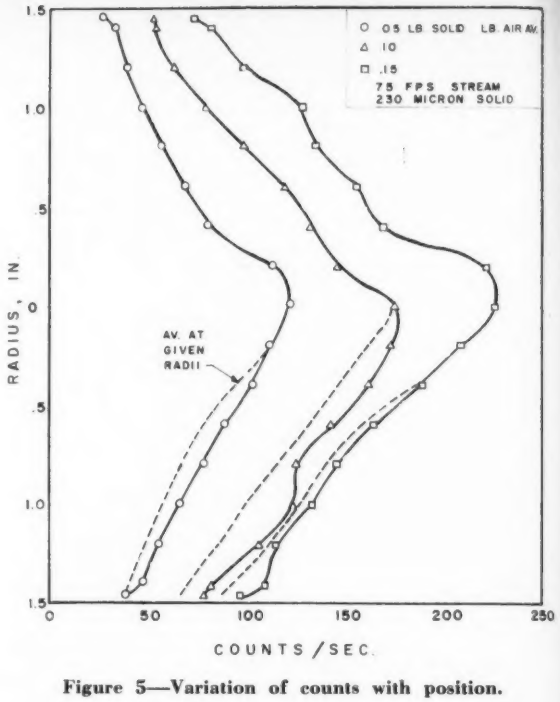

Figure 5—Variation of counts with position.

Averaging a 60 second sample after every 10 displays showed that the average of approximately 20 displays resulted in a figure only 1% different from the overall average.

Determination of Concentration Distribution of the Solid Phase

At each combination of average stream velocity, bead size and loading, bead flows were measured in one-tenth inch increments from wall to wall. Before recording any data the flow was allowed to equilibrate and final equilibrium was considered attained only after maximum and consistent counts per second were observed.

Prior to recording the 20 consecutive displays at each point in the traverse, the only adjustment necessary was that of matching velocities within and without the probe. However, the feed rate and average stream velocity were checked and adjusted if necessary.

In this manner fluctuations were minimized to approximately 0.1% in the feed rate and 2% in average stream velocities.

Results

The original data used to obtain the concentration distribution is itself of interest and is presented graphically. The velocity profiles, from which the air flow at a discrete point is determined, are given in Figure 4 at average air (at room temperature and atmospheric pressure) velocities of 50, 75 and 100 feet per second.

Solid particles of two mean diameters 230 microns and 115 microns were used. The loading chosen were .05, .10, and .15 lb. of solid per lb. of air.

Figure 5, 5(b), 5(c) and 5(d) give the counts per second (N) obtained by the solid particle counter. The mass flow is obtained by determining a normalizing constant K, in such a way that

$$K\,2\pi\int_o^R N\,rdr = \frac{\text{Total solid flow rate}}{} \qquad \ldots\ldots\ldots\ldots (7)$$

and the mass flow of solid particles is obtained from the product NK, where K may be expressed in the unit lb./in.^{2} per sec. per (c.p.s.), giving the mass flow in the unit of lb./in.^{2} sec. or lb./hr. in.^{2}. Figure 6, 6(b) and 6(c) show results calculated for the case of 230 micron glass beads in air.

The concentration of solid particles is obtained by dividing the local rate of mass flow of solids by the local mass flow rate of air based on Figure 4. Figure 7, 7(b) and 7(c) give the concentration distributions in the case of 230-micron glass beads. Figure 7(d) and 7(e) give the mass flow and concentration distribution of 115-micron glass beads in air.

The parameter fR^2/Du can be determined from these measured data. Since, from Equation (6),

$$2\pi\int_o^R Crdr = 2\pi C_o\int_o^R J_o\left(\alpha\frac{r}{R}\right)rdr \qquad \ldots\ldots\ldots\ldots (8)$$

where $\alpha = \sqrt{fR^2/Du}$

if we let $\alpha\, r/R = X$

$$\frac{1}{\alpha^2}\int_o^\alpha J_o(X)\,XdX = \frac{1}{C_oR^2}\int_o^R Crdr \qquad \ldots\ldots\ldots\ldots (9)$$

The right-hand side of the above equation can be calculated from experimental data. The integral on the left hand side is given in Figure 8, from which α or fR^2/Du can be determined by curve fitting as shown in Figure 7.

The calculated results are summarized in Table 1.

Discussion

It is evident that an interesting regime in two phase turbulent flow has been encountered by the combinations of particle size, average velocity, and loading chosen for this investigation. The concentration profiles clearly indicate that the effect of gravity on the particles becomes negligible (1) as average stream velocity increases (average loading remaining constant) and (2) as the bead size decreases. However, the concentration profiles at 100 f.p.s. indicate that increasing the loading at this higher velocity makes the gravity effect less significant. This suggests the existence of particle interaction[9] even though the mean distance between spheres at a loading of 0.15 lb. of 230 micron beads per lb. of air is approximately 20 diameters.

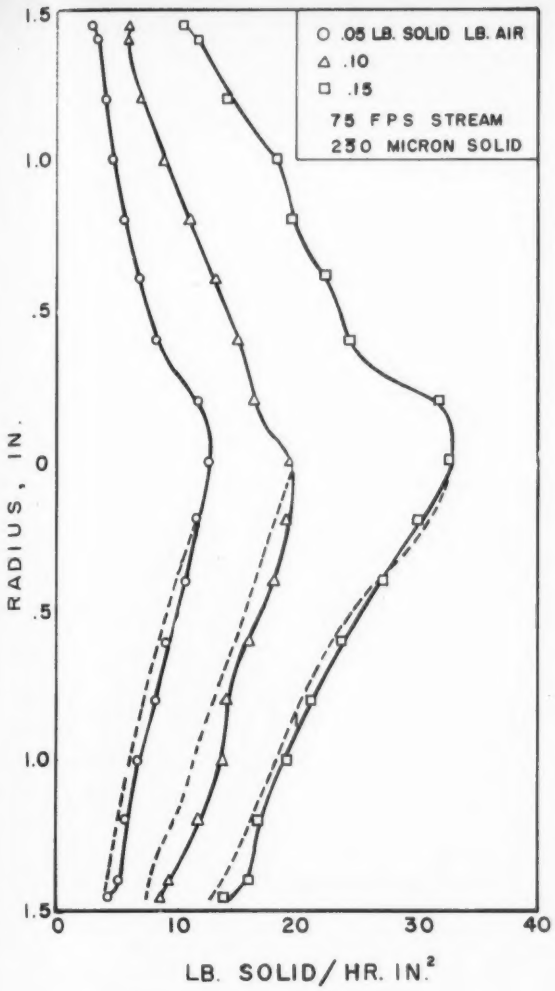

Figure 6—Solid phase distribution.

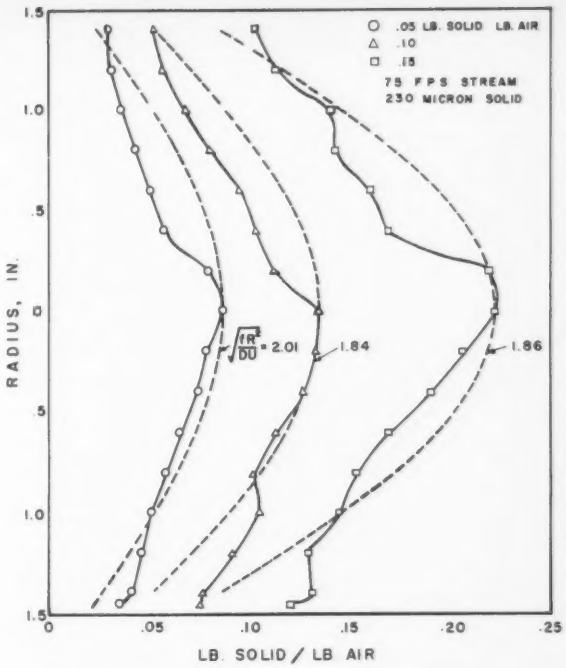

Figure 7—Concentration profile.

The most striking common feature of the concentration profiles is the maximum which occurs (in some cases, spectacularly) at the center of the duct.

The investigation stopped at an average stream velocity of 50 f.p.s. and 115 micron beads because beyond this point (higher velocities and smaller bead sizes) the signal-to-noise ratio rapidly approached one. That is, the pressure fluctuations of the turbulent air stream impinging on the transducer plate produced signals indistinguishable, except by form, from the bead signals.

Any further investigation would necessitate the addition of a discriminating circuit between the transducer and the counter. This circuit would be designed to pass the short rise time bead signals while rejecting the approximately sinusoidal noise signals[7].

Obviously, the value of f should decrease to zero toward the center of the pipe and u increases toward the center of the pipe. Table 1 shows the average values of fR^2/Du and f of various cases. Rather than making detailed inferences regarding the trend of variation, it can be said that the measurements, within its range of accuracy, suggest a value of the order of 2 for the wall effect parameter fR^2/Du in the case of 230 micron particles and 4 for 115 micron particles. This is for a pipe flow Reynolds number range of 80,000 to 140,000 and particle diffusivity, D, at the ratio of density of solid to density of gas of 1780. (density of glass/density of air). The acceleration f is naturally smaller for lower stream velocity. However, for

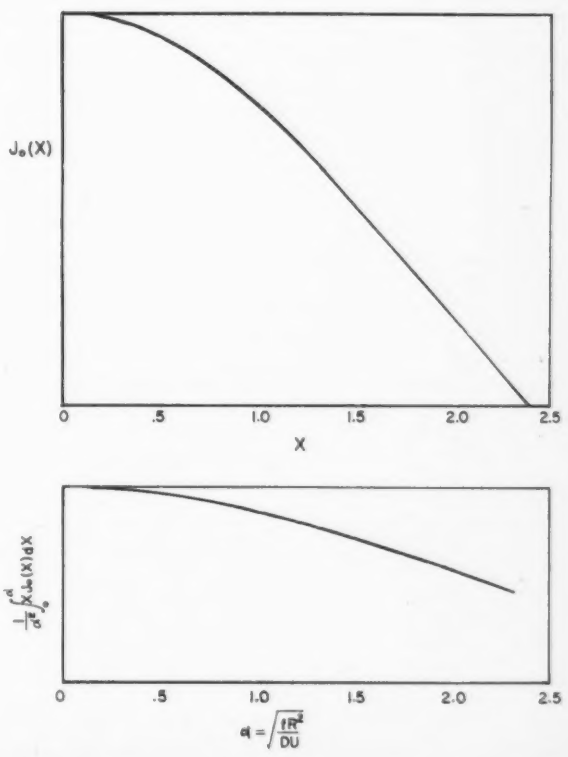

Figure 8—Diagrams for the determination of concentration distribution.

TABLE I
Summary of Results

Solid particle diameter, micron	Mean stream velocity f.p.s.	Diffusivity of solid particles[1] ft.²/sec.	Loading lb. solid per lb. air	Solid flow rate lb./hr.	fR^2/Du	f f.p.s.²	f/u 1/sec.
230	100	2.7×10^{-3}	.15	98.4	2.19	38.0	.380
			.10	65.5	4.16	72.1	.721
			.05	32.8	4.36	75.7	.757
	75	2.4×10^{-3}	.15	147.3	3.45	39.7	.529
			.10	98.2	3.38	39.0	.520
			.05	49.1	4.03	46.5	.620
	50	2.0×10^{-3}	.15	196.5	3.67	23.5	.470
			.10	131.0	4.00	25.6	.512
			.05	65.5	1.69	10.8	.216
115	50	1.4×10^{-3}	.15	98.4	4.16	18.0	.360
			.10	65.5	4.94	21.4	.428
			.05	32.8	4.40	19.0	.380

different particle sizes involved, no significant difference was found for the same mean stream velocity. Therefore, the value of fR^2/Du depends to a large extent on the value of D. The larger the value of D (very small particles, high mean stream velocity, small density ratio of solid and gas, etc.)[1], the more uniform is the distribution of solid particles.

The gravity effect has been neglected in the above consideration. In some of the results, however, its effect is quite obvious. Assymmetry of concentration profiles actually indicates superposition of the gravitational acceleration on the acceleration due to transport of momentum from the wall. The greater the value of f when compared to the gravitation of acceleration, the more symmetrical is the concentration distribution (compare Figures 7(c) to 7(b)).

Conclusions

The above results suggest that in a two-phase turbulent stream of high average stream velocity, low loading (within the carrying capacity of the stream[10]) and with small particles (hence small gravity effect[10]), the concentration profile of solid particles in steady fully developed turbulence would approximate the turbulent velocity profile due to the similarity of these transport processes.

The assumption of a constant concentration distribution appears to be valid for the conditions of low loading, high average stream velocity and small solid particle size.

The above analytical consideration of mass transport in two-phase turbulent pipe flow is a simple way of visualizing the problem of concentration distribution in that case. The parameter fR^2/Du is a simple measure of the distribution; a smaller parameter means a more uniform distribution.

Acknowledgement

This work was sponsored by Project SQUID which is supported by the Office of Naval Research, Department of the Navy, under contract Nonr 1858 (25) NR-098-038. Reproduction in full or in part is permitted for any use of the United States Government.

The experimental work was performed when the senior author was connected with Princeton University, Princeton, New Jersey.

We wish to thank J. B. Fenn, Director, Project SQUID, for his suggestions.

Nomenclature

- C = Concentration or number density of solid particles (or mass of solid per unit volume)
- C_s = Static concentration or number density of solid particles
- C_o = Concentration at the center of pipe
- D = Particle diffusivity
- f = Acceleration due to transport of particles across the turbulent velocity field of the stream
- J_o = Zero order Bessel's function
- K = A normalizing constant
- N = Counts per second
- $\dot{n}$ = Rate of motion of solid particles per unit area
- R = Pipe radius
- r = radial coordinate
- u = Mean stream velocity
- u_p = Mean particle velocity
- a = $\sqrt{fR^2/Du}$, parameter of concentration distribution

References

(1) S. L. Soo, H. K. Ihrig, Jr., and A. Z. El Kouh, "Experimental Determination of Statistical Properties of Two-phase Turbulent Motion." Proj. SQUID Report PR-82-P, Sept. 1958. To be published in Trans. A.S.M.E., Basic Engineering. Sept., 1960.

(2) S. L. Soo, C. L. Tien, Trans. A.S.M.E., J. of Appl. Mechanics, V. 27, Ser. E, n. 1, Mar. 1960. pp. 5 to 15.

(3) C. L. Tien. "Transport Processes in Two-phase Turbulent Flow," Proj. SQUID Report PR-91-T-R, June 1959. To be published in Trans. A.S.M.E., Heat Transfer.

(4) S. L. Soo, "Gas Dynamic Processes Involving Suspended Solids," Proj. SQUID Report PR-97-P, Aug. 1959. To be published in J. of A.I.Ch.E. ASME paper No. 60-HT-23.

(5) C. Y. Wen and H. P. Simons, A.I.Ch.E. Jour. June, 1959. p. 263.

(6) J. O. Hinze, "Turbulence," McGraw-Hill Book Co., Inc., 1959, p. 300.

(7) W. W. Wilmarth, NACA TN 4139, Mar. 1958.

(8) S. L. Soo, C. L. Tien, V. Kadambi, Rev. of Sci. Inst., V. 30, n. 9, Sept. 1959, p. 821.

(9) R. L. Peskin, "Statistical Effects Resulting from the Presence of Many Particles in Motion in an Ideal Fluid." Proj. SQUID Report PR-92-P, June 1959, to be published in Journal of Fluid Mechanics.

(10) S. L. Soo, Chemical Engineering Science, 1956, Vol. 5, pp. 57 to 67.

★ ★ ★

The Corrosion Behavior of Aluminum in Natural Waters[1]

HUGH P. GODARD[2]

This paper reviews the behavior of aluminum in contact with natural waters. The influence of water composition and service factors on corrosivity to aluminum are discussed. Laboratory pitting test methods are described and data are presented to support the existence of a cube root (in time) rate curve for the pitting of aluminum in water. Information on the pitting of aluminum in 17 Canadian waters is given and mention is also made of the pitting of aluminum in seawater and oil field brines. A statistical treatment of pitting data is presented. Finally, measures for extending the life of aluminum equipment subject to pitting by water are suggested.

While the corrosion behavior of aluminum in contact with various waters has been studied as far back as 1920[1], the new metal has not been much used for handling natural waters until recent years. Some waters tend to pit aluminum and this may have discouraged its application. A 10 year research program in these laboratories on the pitting corrosion behavior of aluminum alloys has led to a better understanding of the mechanism and of the environmental factors that influence pitting and particularly of the corrosion rates. This together with the application of statistics to pitting data now enables the prediction of performance from laboratory test results and from early service experience. Further, it is becoming apparent that for many applications pitting can be tolerated providing perforation does not occur and equipment is therefore being designed to contain the pitting for the desired life period.

A glossary of water and pitting terms used in this paper is appended.

General Corrosion Behavior of Aluminum in Surface Waters

In general, the corrosion behavior of aluminum in surface waters is good, but it can vary from excellent to poor depending on the composition of the water and the conditions of service. Conditions of service include such factors as water velocity, temperature and oxygen content, which are often as important as the actual composition of the water.

If aluminum is corroded by water the attack takes the form of pitting. There is no general corrosion or gradual thinning as occurs with steel. The number of pits formed and their rate of penetration depend on the composition of the water and on the conditions of service. Pitting that would occur in stagnant water is often prevented completely if the water is in constant motion, either by flowing or by turbulence due to agitation[2]. The rate of penetration of pits decreases rapidly, and if the metal thickness is adequate, perforation will not occur for a very long time even though an appreciable pit depth may be reached after a short period of service. For example, although a piece of aluminum sheet 0.020 in. thick, pre-etched to render it active, will perforate in Kingston tap water in only a week, a sheet only 0.125 in. thick is not expected to perforate in less than 25 years. In a long term experiment still under way the maximum pit after five years was only 46 mils.

Influence of Water Composition

In general, soft waters are the least aggressive, and most can be safely handled in aluminum[1,3]. This is in contrast to black iron, galvanized iron and copper to which soft waters are more aggressive than hard waters.

The factors which are believed to influence both the occurrence and rate of pitting of aluminum in stationary waters are:[4,5,6]

pH
total hardness
chloride
oxygen
copper

The effects of the various compositional factors are interrelated, and it is not yet possible on the basis of the limited data available to weigh the importance of each, or to predict from a table of water composition alone, the influence of the water on aluminum. The copper content is believed to be important, but as copper in most surface waters is less than 0.2 p.p.m. it is rarely determined and is thus usually unavailable. The influence of copper is dependent on *pH*, and is less pronounced in alkaline waters[7]. More copper can be tolerated in a soft water than in a hard one. Traces of mercury which are present in a few instances in some ground waters and in industrially polluted streams have a strong detrimental influence on aluminum. Mercury also is not determined in conventional water analysis.

Determination of the Pitting Tendency of a Water To Aluminum

(1) *General*

The pitting tendency of a given water to aluminum under stagnant conditions can be determined in the laboratory in a fairly short time with a five gallon sample of water. A pitting rate curve is determined which can be related to curves for other waters for which there is service experience. A reasonable prediction can then be made as to the corrosivity of such waters and the probable life of a piece of aluminum equipment with a given wall thickness in it. Velocity tests can also be made to establish the influence of steady flow.

[1]*Manuscript received November 12, 1959; accepted June 15, 1960.*
[2]*Head, Chemical Division, Aluminium Laboratories Limited, Kingston, Ont.*
Based on a talk delivered to the Detroit Section, National Association of Corrosion Engineers, March 20, 1959.

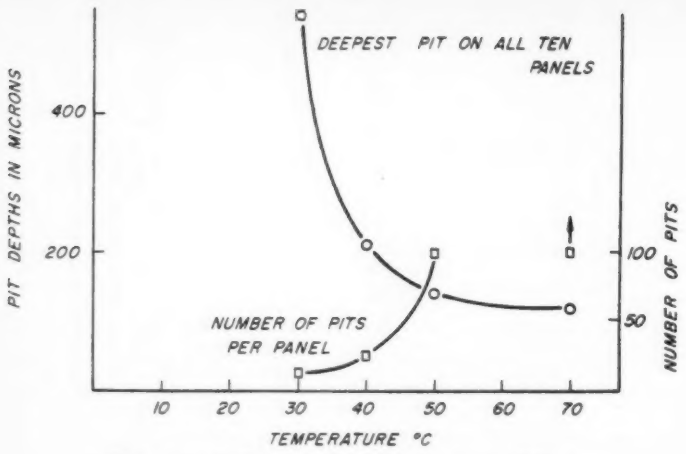

Figure 1—Influence of temperature on pitting.

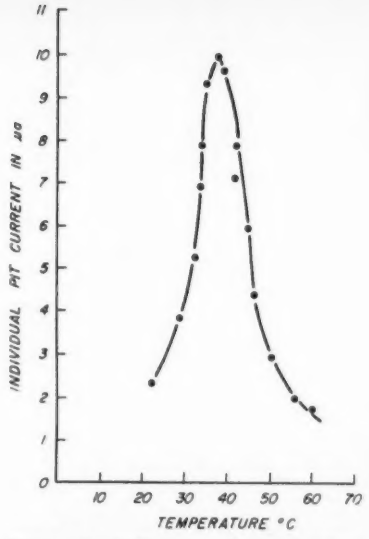

Figure 2—Influence of temperature on individual pit current.

(2) *Laboratory Pitting Tests*

(a) Stationary water. The determination of pitting rate curves for aluminum in stationary water in the laboratory has been described by Aziz and Godard[8]. Strings of 10 coupons are immersed for several time periods. Experience has shown that values taken at one week, one month and three months give an approximate pitting rate curve and a good idea of the aggressivity of a given water to aluminum.

By rough estimate, in the eight years since this technique was developed in these laboratories, several hundred pitting rate curves have been determined. The early work was done on Kingston tap water in a 300 gallon tank. The water was adjusted to 25°C. and a low rate of input and overflow was maintained to avoid bacterial growth. The water changed continuously about once a day so that there was no appreciable water movement.

It has been found that pitting tests can be run in smaller containers and common household plastic pails have been used to test waters brought to the laboratory from other locations. It has been shown that the same values are obtained in Kingston tap water whether in a pail or in the large tank. It has also been shown that the pitting of aluminum in laboratory tap water was the same as its behavoir in Lake Ontario water taken directly from the lake at a point remote from the city[2].

(b) Moving water. In work on the pitting of aluminum in Lake Ontario water, samples were put directly into the lake, near the shore. These did not pit at all. As the water was fairly rough at the test location it was reasoned that perhaps the constant motion of the water had prevented the initiation of pitting.

A laboratory test was devised which showed that the number of pits and their depth after a given time was greatly reduced with increased rate of flow, and that at 8 f.p.m., a rather low rate of motion, no pitting occurred at all while the coupons in the adjacent stationary water pitted normally[2].

More recently a new apparatus to test aluminum in moving water has been developed that can be applied to volumes of water as small as two gallons. It is thus applicable to the five gallon water samples commonly brought to the laboratory. The test is being applied to lengths of tubing as well as to elongated sheet samples.

The apparatus consists of a simple re-circulating system in which the water is drawn up out of an inert polyethylene container by means of a stainless steel gear pump equipped with Teflon plastic gears and pumped through a vertical stand of the tubing under study and then returned to the container. The pump is driven by a variable speed drive (0 to 400 r.p.m.) which in turn is driven by an electric motor. All connections are made with Tygon plastic tubings secured with hose clamps. Two marks are placed five feet apart on the lower and upper short sections of connecting Tygon tubing, and at water velocities of up to 1 foot per second the flow rate is determined by measuring with a stop-watch the time it takes water to pass between these two marks. At high rates of flow the velocity is determined by measuring the time it takes to discharge a known volume of water through tubing of known internal diameter. Using this apparatus and 1/2 inch diameter tubing, water velocities of 7 feet per second have been obtained.

This work has shown that extruded aluminum is more susceptible to pitting than sheet surfaces.

Field experience has shown that at much higher velocities, in the order of 20 f.p.s., turbulence occurs especially at fittings which cause pitting of aluminum.

(c) Influence of temperature. It has been found that as the temperature rises the pitting probability increases and the pitting rate decreases (See Figure 1). The pitting of 2S aluminum in Kingston tap water has been studied up to 70°C. using an individual pit current technique[9]. For this purpose a pit is machined from a disc of metal and re-inserted in the hole using a plastic insert to insulate the pit electrically from the sheet. Electrical leads fitted to the back of the disc containing the pit, and to the sheet are connected to a microammeter. This enables measurement of the actual current flow from the pit. Some pits develop a maximum current at about 40°C. at which point the rate is five times that at room temperature (See Figure 2). Above 40°C. the pit current drops sharply and, at 70°C., becomes less than at room temperature. Other pits have no such maxima and the pit current decreases linearly over the whole temperature range. Thus, above 40°C., the higher the temperature the longer is the life. This is the reason for the recent use of aluminum in domestic hot water tanks.

Shape of Pitting Rate Curve in Fresh Waters

An examination of the laboratory pitting data suggested that the maximum pit depth (d) was proportional to the cube root of time (t)[10]. Thus the rate of penetration may be expressed by the equation:

$$d = Kt^{1/3}$$

It is believed that the constant (K) will be a function of the

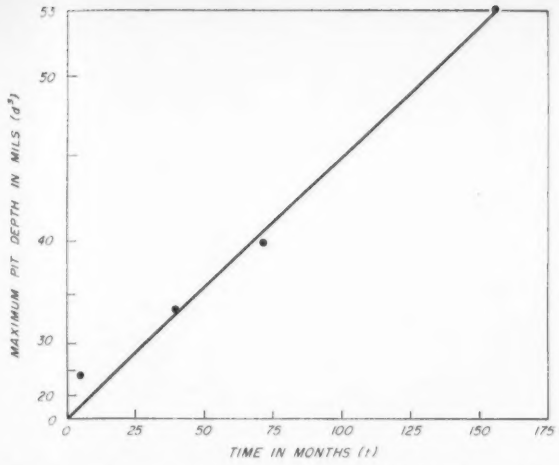

Figure 3—Pitting rate curve for Arvida 57S aluminum pipe.

alloy and of the water conditions (composition, temperature, movement, etc.). A plot of maximum pit depth against the cube root of time gives a straight line. The equation has been found to fit data obtained on many alloys in Kingston tap water and on Alcan 3S sheet in some 24 other Canadian waters.

The cube root equation assumes that pitting initiates at the time of immersion which is the case in laboratory tests where the specimens are etched to render the surface active. In service however, an induction period (t_o) may occur, which will introduce an error in the cube root plot. Because time is measured from the start of service, the value t will be in error by $t - t_o$. The value for $t^{1/3}$ which more accurately, should be $(t - t_o)^{1/3}$ will be distorted and a comparison of values at two periods such as

$$d_2 - d_1 = K[(t_2 - t_o)^{1/3} - (t_1 - t_o)^{1/3}]$$

will be incorrect to an extent depending on the value of t_o. The error will increase as t_o becomes larger and will decrease as the period of observation (t) increases ($t - t_o$ will then approach t). The error can be avoided by plotting the cube of the maximum pit depth (d^3) against t since this is the same relation. A comparison of data at two time periods then becomes:

$$d_2^3 - d_1^3 = K\,[(t_2 - t_o) - (t_1 - t_o)]$$
$$= K\,(t_2 - t_1)$$

In this case t_o disappears.

The most convincing data in support of the cube root relation has come from the examination of sections taken at intervals from a 2000 ft. line of 4 inch Alcan 57S water pipe at Arvida, Que., now 13 years old. The maximum pit depths found are shown in Table 1.

A cube plot of these data is shown in Figure 3.

Taking the $d^3 = Kt$ equation, and calculating the expected maximum pit depth for 13 years from the 3.3 and 6 year results

TABLE 1

MAX. PIT DEPTHS IN ALCAN 57S WATER LINE AT ARVIDA, QUE.

Period of Service	Max. Depth
Years	(mils)
0.4	25
3.3	31
6.0	40
13.0	53

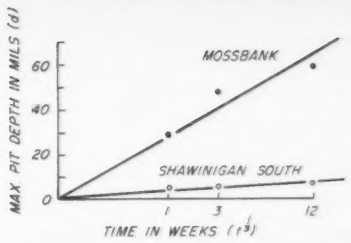

Figure 4—Pitting rate curves for 3S alloy sheet in Canadian waters—the extremes.

one obtains a value of 56 mils, in excellent agreement with a maximum depth of 53 mils which was actually found on a 60 foot length of pipe. This is cited to emphasize the value of knowing the pitting rate curve and as an example of what can be done with pitting data.

Typical Pitting Curves in Canadian Fresh Waters

Figure 4 shows the pitting rate curves for 3S alloy in the least aggressive and the most aggressive of 17 Canadian fresh waters tested to date in this laboratory together with one from an English source. The least aggressive water was taken from the municipal supply at Shawinigan (South) Que., while the most aggressive water was found to be that from Mossbank, Sask. As all specimens were etched before immersion pitting started at the time of immersion.

The partial composition of these waters as determined on the samples is shown in Table 2.

To obtain a pitting rate parameter that can be visualized, the time in weeks to obtain a 40 mil pit in 3S alloy has been taken. On this basis the 17 fresh waters tested vary from 2.6 weeks for Mossbank, Sask., to 953 weeks for Shawinigan South, Que. The data for the waters tested are given in Table 3.

No simple correlations appear in these data. The pitting aggressiveness of these waters is not related simply to *pH*, total hardness or copper content or to any obvious combinations of these. In general, however, the softer waters tend to be at the top of the table while the harder waters tend to be at the bottom. If pitting aggressiveness to aluminum is to be related to water compositions more detailed water analyses will be required, but comparisons will be difficult owing to the wide variation in compositional factors in waters.

Shape of the Pitting Rate Curve in Seawater

Tests on many aluminum alloys immersed in the sea at three locations, (Esquimalt, B.C., Halifax, N.S. and Harbor Island, N.C.) for periods of up to five years have shown that in sea water also the rate of penetration of pits decreases with time. However, the number of samples per time point has been smaller and control over the tests much less, with the result that there has been considerable scatter in the results and an accurate determination of the rate curve has not been possible.

In one test made in Halifax harbour, with the co-operation of Naval Research Establishment, Dartmouth, a pitting rate

TABLE 2

PARTIAL COMPOSITIONS OF WATERS FROM SHAWINIGAN (SOUTH), QUE., AND MOSSBANK, SASK.

	Least Aggressive	Most Aggressive
	Shawinigan, Que.	Mossbank, Sask.
pH	7.1	7.8
total solids	140 p.p.m.	1038 p.p.m.
total hardness	73 "	555 "
copper	0.04 "	0.005 "
chloride	–	20 "
sulphate	–	417

TABLE 3

PARTIAL COMPOSITIONS AND PITTING DATA FOR SEVENTEEN FRESH WATERS
(In increasing order of pitting corrosivity)

Order	Test No.	Wks. to 40 Mils.	Location	pH	Hardness p.p.m.	Copper p.p.m.
1	8	953	Shawinigan South, Que.	7.1	73	0.04
2	7	453	Shawinigan, Que.	7.4	18	0.04
3	12	207	Crofton, B.C.	6.7	27	0.021
4	6	205	Hamilton Bay, Ont.	7.1	205	0.003
5	6	–	Kingston, Ont.	7.9	160	0.005
6	5	175	Credit Valley, Ont.	7.1	0	0.028
7	4	147	Columbia River, B.C.	7.5	72	0.017
8	16	83	Canyon Meadows, Alta.	7.9	169	0.005
9	14	46	Regal Golf Course, Calgary, Alta.	8.1	331	0.007
10	1	25	N. Sask. River, Drayton Valley, Alta.	8.1	267	0.11
11	13	23	Peterborough, Ont.	7.5	86	0.012
12	15	17	R. G. May Golf Course, Calgary, Alta.	7.9	218	0.002
13	22	8	Billingham Beck, England	8.7	443	0.011
14	24	6	Jasper, Alta.	8.2	196	0.007
15	2	6	Lethbridge, Alta.	7.9	228	0.017
16	9	4.4	South Saskatchewan River, Sask.	7.6	206	0.04
17	10	2.6	Mossbank, Sask.	7.8	555	0.005

curve was established for Alcan 65S-T6 sheet immersed in seawater for periods up to 14 months. For etched coupons the cube root plot is shown in Figure 5.

Shape of Pitting Rate Curve in Oilfield Brines

This is a subject of considerable current interest in this laboratory. Although only five brines have been tested to date, several others are now under investigation, while samples of still others are being obtained.

It should be pointed out at once that oil field brines differ very considerably from sea water. Sea water has a uniform composition and while the salinity or salt content varies from one ocean to another and also with the season the ratio of salts is constant and is accurately known. An average solids content for sea water is about 40,000 p.p.m. Oil field brines may contain six or more times this amount of solids and the individual components vary widely. For example, the compositions of the five brines tested to date are given in Table 4.

Oilfield brines may contain hydrogen sulphide, in which case they are designated "sour", or not, in which case they are termed "sweet". The presence of H_2S in brines has a very strong influence on their corrosiveness to steel. Its influence on the corrosivity of brines to aluminum is not yet known although H_2S by itself is not aggressive to aluminum.

Oilfield brines are believed to contain variable and sometimes appreciable amounts of heavy metals although analyses are lacking. It is expected that heavy metals, if present, would have marked influence on the pitting behavior of aluminum.

All five brines tested to date tended to pit aluminum and decreasing rate curves were obtained. Two of the five showed rates of the order found in fresh water and seawater while the other three showed much higher pitting rates, and are considered too aggressive to be handled in aluminum.

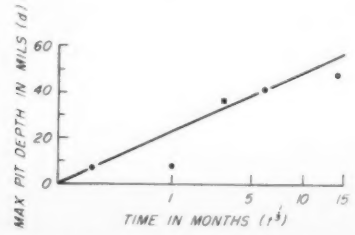

Figure 5—Pitting rate curve for 65S aluminum in seawater.

TABLE 4

PARTIAL COMPOSITIONS OF SEVERAL OILFIELD BRINES

Series No.	Test No.	pH	Total solids p.p.m.	Cl p.p.m.	SO_4 p.p.m.	H_2S
1	3	5.3	155,700	—	—	absent
2	11	6.6	127,000	68,600	9,500	present
3	17	7.5	15,000	8,300	4	absent
4	18	7.7	16,000	7,700	1,800	present
5	23	8.9	94,800	50,900	4,000	present

By coincidence, the three more aggressive brines all contained hydrogen sulphide while the two less aggressive brines did not. The three aggressive brines also differed from the other two, and from all the fresh waters tested, in that no pitting developed for the first week even on etched coupons.

Treatment of Pitting Data

(1) *Theory of Extreme Values*

A theory of extreme values was developed by Gumbel[11] to predict probable weather and flood excesses from limited data. The Gaussian probability curve for samples of data with random distribution is generally known.

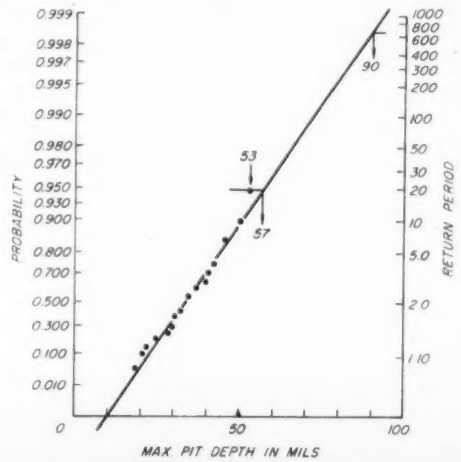

Figure 6—Extreme value plot of Arvida pipe data.

The "extreme value" is the last point on the tail of the curve to the right. Gumbel showed that under certain very general conditions in a series of data the maxima themselves followed a distribution curve, according to the formula:

$$N = e^{-e^{-y}}$$

Analysis of a large volume of data involving the counting and measuring of tens of thousands of pits has shown that the pitting of aluminum in fresh water follows Gumbel's equation, and thus extreme value statistics can be applied to aluminum pitting data[12].

A special type of extreme value probability graph paper has been devised to permit direct plotting and extrapolation of the results. Treatment of data can be illustrated by taking the example of one of the pitting strings of 10 coupons tested in this laboratory. The deepest pit on each coupon is found and measured. These measurements (n) are arranged in order of depth, then are numbered from one to ten and the probability of occurrence (ϕ) of each determined from the equation:

$$\phi = \frac{n}{N+1}$$

The maximum pit depth on each coupon is now plotted on the special paper with depth as abscissa and probability as ordinate. If a straight line can be drawn through the points, conformance of the data with the theory can be assumed. Obviously the more data available the better the chance of obtaining a good straight line and thus the maximum depths from 20 samples will be better than 10 and so on.

The use of an extreme value probability plot is illustrated by the pitting data from a 60 foot length of Alcan 57S water pipe after 13 years' service at Arvida, Que. This example was cited earlier to support the cube root pitting equation. The pipe was cut into 20 lengths three feet long and the deepest pit in each determined. After placing in order of increasing depth, and determination of probability, the data were plotted on the extreme value graph paper (See Figure 6). The first thing to be noticed is that a good straight line can be drawn through the points. This proves that the data can be treated by extreme value statistics. It will be recalled that the deepest pit by actual measurement was 53 mils. However, the line indicates that the predicted maximum pit depth for the 60 feet, based on the other 19 sections and as defined in the appendix is 57 mils.

The right hand ordinate of the paper carries a scale designated "return period". The "return period" for any given pit depth is the number of observations that must be made to find a pit of that depth. Conversely for any given number of samples the predicted maximum pit depth can be determined.

Now the pipe was 2000 feet long and the unit section length was 3 feet. There were thus 667 such lengths in the entire line, and for a return period of 667 the predicted maximum pit depth is 90 mils. In other words, if the entire 2000 feet of line had been examined this should be the deepest pit.

Thus an extreme value plot will give several valuable pieces of information.

(1) If a straight line is obtained the data fit the theory and can be treated by it.
(2) Data which lie well away from the line are spurious and can be discarded.
(3) The predicted maximum pit depth for the area examined can be calculated.
(4) The data can be extrapolated to predict the maximum pit depth for any selected larger area of surface.

Another recent application of the extreme value plotting technique has been to determine the degree of uniformity of pitting rate for 50 consecutive lots of Alcan 2S sheet produced in one plant over a period of one year using the maximum pit depth found in Kingston tap water on a string of 10 coupons per lot after three months' immersion. Although the deepest of the maxima was double the shallowest maximum, an extreme value plot gave a straight line and thus it was concluded all the material was part of one population and there was no real difference among the lots.

Eldredge has applied the method with success to the treatment of pitting data obtained by caliper surveys on steel oil well piping[13].

(2) *Calculation of Probable Life*

If the predicted maximum pit depth is calculated and the cube root pitting rate law assumed, the time to initial perforation can easily be computed. In the case of the Arvida pipe, 36 years would be required to reach the pipe wall thickness of 125 mils, or 23 more years' service could be expected. From somewhat limited experience the author's present view is that there is a factor of safety in such predictions, and that an even longer life will probably be realized.

Case Histories

(1) *Water Pipelines*

The data in Table 5 were compiled during regular examinations of actual aluminum pipelines.

(2) *Water Storage Tanks*

At Shawinigan, Que., two large (50,000 gallon) aluminum overhead water storage tanks were built in 1948, one for an industrial plant, and one for the municipality. When inspected in 1957 after 9 years' service the maximum pit in the first mentioned was found to be 90 mils and in the other 184 mils. Calculations of probable life predicts a long forward life free of maintenance — at least 100 years for the industrial plant tank, and 25 years for the other.

(3) *Heat Exchangers*

(a) Wall board factory installation. In a large mill near Ottawa an all-aluminum heat exchanger is used to recover waste heat expelled as steam during the pressing of a waste-wood type of wall board. The steam is drawn by a fan into a hood and then through a bank of water sprays (Ottawa River water) to warm up the incoming plant water supply. The spray chamber is about 4 × 5 × 10 feet, and there is a series of baffles to remove entrained water droplets. The exchanger was placed

TABLE 5

ALUMINUM PIPELINE CASE HISTORIES
(Maximum pit depths found in service)

Description	Location	Years Service	Length Feet	Diameter Inches	Pipe Wall Mils	Maximum Pit Depth Mils	Length Examined Feet
Plant Water Supply	Arvida, Que.	13	2000	4	125	53	60
Golf Course Supply	Kingston, Ont.	11	300	1½ to 2½	125	0	60
Golf Course Supply	Calgary, Alta.	7	–	2	55	37	40
Golf Course Supply	Peterborough, Ont.	6	–	3	55	15	20
Golf Course Supply	Joliette, Que.	5	–	2,3,4	57	Perforation	10
Steam Condensate Return	Kingston, Ont.	12	500	1¼	133	0	24
Water Injection Line	Drayton Valley, Alta.	1	39,500	4,6	188 and up	6	3

in service in 1949 to replace a similar unit of galvanized steel that had lasted only two years. When examined one month later it was in excellent condition, and it is still in use after 9 years service without maintenance.

(b) Air conditioning system. In a large Canadian manufacturing plant an all-aluminum heat exchanger is used to de-humidify incoming air to the main air-conditioning system. The air is drawn through a bank of water sprays by a large fan. The spray chamber is about 12 × 12 × 12 feet. A series of baffles removes entrained spray. The unit was placed in service in 1950. When examined in 1951 it was in excellent condition. It is still in use after 8 years service.

The only corrosion problem encountered was perforation of a horizontal sheet in the fan plenum where water which had not been removed by the baffles settled in stagnant pools. The violent agitation in the main chamber apparently prevented such pitting.

Prevention of Perforation of Aluminum Equipment

The following means are available for extending the life of aluminum equipment handling a water which tends to cause pitting: (1) Increase the wall thickness. The value of increased wall thickness is apparent from the nature of the pitting rate curve. Twice the wall thickness will give eight times the life. (2) Use Alclad aluminum. This consists of a duplex material the core alloy of which is protected by a thin cladding layer of another aluminum alloy selected to be anodic to the core so that when a pit reaches the core it will spread laterally. Further penetration will be arrested until the area of core exposed is such that the cladding will no longer protect the center due to the increased resistance of the electrolyte patch. Experience indicates that this delaying action will increase the time to perforation of a given thickness of metal from five to ten times. (3) Increase the movement of the water, i.e. avoid stagnant conditions. This has already been dealt with. (4) Deaerate the water. It has been shown that deaeration of Kingston tap water prevents the initiation of pitting that would otherwise occur and it seems reasonable to assume that deaeration will have a similar influence in other waters. (5) Use inhibitors. In a circulating system an inhibitor such as sodium dichromate at 500 p.p.m. and *pH* 8 should completely prevent pitting. There is some evidence that polyphosphate and silicate inhibitors also inhibit the pitting of aluminum in water. (6) Apply cathodic protection. It has been shown that the pitting of aluminum in Kingston tap water can be prevented by the initial application of a protective current density of about 2 Ma/ft^2 at a potential of about 1.0 volts negative to a copper-copper sulphate electrode, which is the value necessary for the prevention of pitting of aluminum in seawater. (7) Avoid undesirable dissimilar metal couples. Aluminum in contact with dissimilar metals other than zinc and cadmium tends to corrode galvanically, the severity depending on the conductivity of the water, and on the other metal. In fresh waters the tendency is small but in brines and seawater it is large. The most aggressive metals are copper, brass and bronze, followed by lead and then steel. Stainless steel can be safely used with aluminum in all but brines and seawater.

Conclusion

It has been shown that while some waters tend to pit aluminum, the rate of penetration follows a rapidly decreasing rate curve that approximates a cube root function. In many cases such pitting can be tolerated since in water handling equipment perforation is the main criterion of performance. It has also been shown that statistical treatment of pitting data is possible, and is, in fact, a valuable tool in predicting the life of equipment from early service experience. The amount of aluminum equipment in water handling service is increasing rapidly and should continue to grow as the performance of aluminum becomes more widely known.

Nomenclature

d = maximum pit depth
K = constant
t = time of service
t_o = time to initiation of pitting
d_1 = maximum pit depth at time t_1
d_2 = maximum pit depth at time t_2
ϕ = probability
n = ordered number of the pit depth (1 to 10)
N = Total number of maxima (10)

References

(1) Seligman, R., and Williams, P., J. Inst. Met. **23,** 159-192 (1920).
(2) Wright, T. E., and Godard, H. P., Corrosion **10,** 195-198 (1954).
(3) Sawyer, D. W., and Brown, R. H., Corrosion **3,** 443-456 (1947).
(4) Porter, F. C., and Hadden, S. E., J. Appl. Chem. **3,** 385-409 (1953).
(5) Sverepa, O., Werkstoffe und Korrosion **9,** 533-535 (1958).
(6) Davies, D. E. J. Appl. Chem. **9,** 651-659 (1959).
(7) Haygood, A. J., Minford, J. D. Corrosion **15,** 20-24 (1959).
(8) Aziz, P. M., and Godard, H. P., Ind. Eng. Chem. **44,** 1791-1795 (1952).
(9) Aziz, P. M., Corrosion **13,** 536-538 (1957).
(10) Marchand, G., and Hone, A., Aluminum Laboratories Limited, unpublished work (1950).
(11) Gumbel, E. J., U.S. Dept. Commerce report (1954) Applied Mathematics, Series 33.
(12) Aziz, P. M., Corrosion **12,** 495-506 (1956).
(13) Eldredge, G. G., Corrosion **13,** 51-60 (1951).

APPENDIX

Glossary of Terms

(1) *Water Technology*

Natural waters. The term "natural water" refers to rain water, surface water and ground water. These are usually fresh waters, as opposed to seawater. The term "surface water" describes waters in creeks, rivers, ponds and lakes, while the term "ground waters" denotes sub-surface waters from springs and wells, some of which are brines. Any of these waters which have been processed for consumption or industrial use are termed "treated waters".

The purest water found in nature is dew, hoarfrost and rainwater. However, many rain waters are far from pure because rain drops falling through the atmosphere absorb matter in amounts depending on the purity of the air. Above large manufacturing areas the air is often laden with dust, soot, silica, silicates, sulphates, chlorides and carbonates, oxides of sulphur and nitrogen, hydrogen sulphide, ammonia, organic matter and other impurities. These are absorbed in the falling rain or snow and give rise to very inferior water. Near the seacoast, rain carries salt absorbed from particles of salt or sea spray blown inland by on-shore breezes. This may reach 15 p.p.m. but decreases rapidly with distance from the sea.

Surface waters dissolve salts from the soils with which they are in contact and thus have varying composition depending on the soil and the length of contact.

Water composition units. No standard method of reporting the results of water analyses has been adoped in Canada or elsewhere. Several systems are in vogue necessitating the use of conversion factors when comparing analyses.

Constituents may be reported as grains per gallon, (Imperial or American) in parts per hundred thousand, or in parts per million. In Europe results are sometimes reported as milligrams per litre (identical with parts per million).

Some laboratories report the bases as basic radicals, others as oxides, and the acids may be reported similarly or as hypos thetical combinations. The system used by the United State-Geological Service is widely used, has been adopted by the

Canadian Department of Mines and Technical Surveys, and is used at Aluminium Laboratories. The unit in this system is parts per million. The following items are commonly reported:

pH	iron
residue on evaporation	silica
total hardness	bicarbonate
calcium	sulphate
magnesium	nitrate
alkalis (sodium and potassium)	chloride

Suspended matter, turbidity and color are sometimes recorded. Analyses may also be made for dissolved oxygen and free carbon dioxide, but these require determination at the time of sampling.

Hardness in fresh water. Originally "hardness" was defined as the capacity of a water for precipitating soap. The fatty esters such as sodium oleate, stearate, etc., instead of remaining in solution and forming a lather are precipitated by calcium and magnesium (present as the bicarbonates, sulphates and chlorides) as an insoluble curd. Other salts such as those of iron, aluminum, manganese, strontium, barium, heavy metals, brines and free acids precipitate soap in a similar manner. Normally, these salts are present in insignificant amounts and the hardness reported is due only to the calcium and magnesium salts. This is known as "carbonate hardness" or "temporary hardness". The hardness due to sulphates and chlorides is known as "non-carbonate" or "permanent" hardness.

Today, hardness can be titrated quickly with a visual color change end-point using reagents based on EDTA (ethylene diamine tetra acetate). In this method small amounts of the salts producing permanent hardness are reported as calcium, an insignificant error in most cases.

The simplest general compositional classification of fresh waters is by hardness, which is expressed in terms of calcium carbonate in parts per million. Waters are classed as soft or hard according to the following table:

very soft	1– 30 p.p.m. ($CaCO_3$)
soft	31– 60
medium hard	61–120
hard	121–180
very hard	> 181

Other hardness units, and their conversion factors to p.p.m. are given in the table below:

Unit	X Factor to p.p.m.
parts per 100,000	10.0
grains per U.S. gallon	17.1
grains per Imp. gallon	14.3
English (Clark) Degrees	14.3
French degrees	10.0
German degrees	17.9
Equivalents per million	50.0

1 English Degree = 1 grain $CaCO_3$ per Imp. Gal.
1 French Degree = 10 p.p.m. $CaCO_3$
1 German Degree = 10 p.p.m. CaO

(2) *Pitting Terminology*

Pitting rate. The rate of deepening of a pit, which follows a decreasing rate curve in the case of aluminum.

Maximum pit depth. The depth of the deepest pit found on the surface examined. Not necessarily the deepest pit on the entire surface of the equipment.

Predicted maximum pit depth. The most probable value for the deepest pit on the area being considered, predicted by extreme value statistics from actual pitting data from the same or similar samples.

Pitting probability. The tendency to initiate pitting. May be expressed as a percentage from test data[6,7].

Pitting density. The number of pits per unit area.

Severity of pitting; Intensity of pitting. Ambiguous terms which should not be employed since it is not clear whether they refer to pitting density or pit depth.

Average pit depth. Frequently the five or ten deepest pit depths are measured and averaged. Such numbers have little practical value since only the deepest pit is of concern. Much less useful than predicted maximum pit depth.

★ ★ ★